Mathematical modelling and 3-D computer simulation of Neogene carbonates (S. Spain): Unravelling the controlling factors of carbonate platform evolution

Dissertation
zur Erlangung des Doktorgrades
der Naturwissenschaften im Fachbereich
Geowissenschaften
der Universität Hamburg

vorgelegt von

José Manuel Cuevas Castell

aus Spanien

Hamburg
2005

Als Dissertation angenommen vom Fachbereich Geowissenschaften
der Universität Hamburg
auf Grund der Gutachten von Prof. Dr. C. Betzler
und Prof. J.C. Braga

Hamburg, den 16. Dezember 2005

Prof. Dr. H. Schleicher
Dekan des Fachbereichs Geowissenschaften

Table of contents

Abstract

Geological mapping, mapping of facies distribution, and reconstruction of platform-interior growth geometries of several Messinian carbonate platforms located in SE Spain (Province of Almería) were carried out to reveal the controlling factors involved in the evolution of these platforms. Growth of the carbonate platforms has been simulated using "REPRO", a FORTRAN program which was developed for the modeling of carbonate environments, especially for systems with coral reefs, and which provides 3-D computer models. The different platform environments and depths were calculated with several zoning subroutines. Simulation of the six platform-related facies was done using various routines. The Reef Framework Facies was modeled by the numerical solution of a Fisher-equation, which is a generally accepted model for growth and proliferation of populations in biology and ecology. The Lagoon Facies was simulated by a function of water depth-dependant carbonate production. The distribution of reef-debris (Breccia and Block Facies, and Middle Slope Calcarenite Facies) were modeled by using a routine which simulates gravity-driven particle export from the reef crest. Pelagic deposits were modeled using a routine for simulating a constant pelagic rain with a diffusion factor. Finally, the entry of a fan delta conglomeratic system in one of the carbonate platforms was simulated by a siliciclastic point source and gravity-driven particle redistribution.

The best fits between the modeling results and the real platform geometries were achieved under the assumption that platform growth geometries were controlled by short-term sea-level fluctuations superimposed onto a longer term sea-level drop. The sea-level curve used for the modeling of the platforms is based stable oxygen isotope record at ODP Site 926. In the study region, the curve suggests a maximum sea-level drop of 70 m that results from a 50 m eustatic sea-level drop and 20 m of tectonic uplift. This curve compares well with relative sea-level curves based on the fluctuations in the reef crest position during the growth of the platforms. The sea-level fluctuations were governed by orbital forcing. The periods of short-term sea-level fluctuations coincide with precession, but a certain modulation of the precessional cycles by obliquity is recognizable during the early stages of evolution. The period of the long-term sea-level drop was approximately 100 ka, corresponding with short eccentricity.

The validity of the modeling results are demonstrated by using three independent methods. Firstly, the outer morphologies of the real carbonate platforms coincide with the shapes and dimensions of the simulated platforms. Secondly, several synthetic geological sections were compared with modeled sections located in equivalent positions showing good match between the real and the modeled sections. Finally, the coral growth rates provided by the Fisher-equation subroutine compare well to the coral growth rates in Recent fringing reefs, which are approximately 2 to 8 mm/y.

The modeling results allow to understand the internal complexities of the carbonate platforms, as well as the lateral variations of the sedimentary packages and facies. REPRO provides a separate visualization of the different facies bodies as a function of time and space, showing the intrinsic pattern of facies distribution in the platforms. On a local to regional scale, the modeling results also permit to distinguish between relative and global sea-level signals in the western Mediterranean Messinian sedimentary sequences and reveal that the sedimentary cycles were produced by sea-level fluctuations with different periodicities. Moreover, the number of sedimentary cycles recorded in the neritic deposits differs of the number recorded in the pelagic deposits, which demonstrate that neritic and pelagic depositional realms record environmental oscillations in a distinct way.

Zusammenfassung

Gegenstand der durchgeführten Untersuchungen sind mehrere Karbonatplattformen messinischen Alters im SE Spaniens (Provinz Almería). Neben einer Kartierung der Faziesverteilungen wurde insbesondere versucht, die Geometrien des Plattform-Inneren zu rekonstruieren, um die kontrollierenden Faktoren in der Entwicklung dieser Plattformen aufzuzeigen. Die Evolution der Plattformen wurde mit Hilfe des FORTRAN Programms "REPRO" simuliert, welches für die 3D-Modellierung von Karbonatsystemen, insbesondere von Korallenriffen, entwickelt wurde. Verschiedene Plattform-Milieus und unterschiedliche Wassertiefen wurden hierbei unter Anwendung mehrerer Subroutinen berechnet. Die Simulation von sechs verschiedenen Faziesbereichen, die mit der Plattformentwicklung einhergehen, wurde durch die Benutzung mehrerer Routinen ermöglicht. Die Fazies des Riffgerüstes (Reef Framework Facies) wurde mit Hilfe einer numerischen Lösung der Fisher-Gleichung simuliert, ein in der Biologie und Ökologie allgemein akzeptiertes Modell des Wachstums und der Vermehrung von Populationen. Die lagunäre Fazies (Lagoon Facies) wurde als Funktion einer von der Wassertiefe abhängigen Karbonatproduktion. Die Verteilung der Faziesbereiche des proximalen und mittleren Riffhangs (Breccia and Block Facies, bzw. Middle Slope Calcarenite Facies) wurden mittels einer Routine errechnet, die den Schwerkraft gesteuerten Export von Riffschutt aus dem Randbereich des Riffes simuliert. Pelagische Ablagerungen wurden mit einer Routine modelliert, die einen konstanten pelagischen Partikelregen unter Berücksichtigung eines Diffusionsfaktors simuliert. Zudem wurde der Eintrag eines konglomeratischen Fandelta-Systems in eine der Karbonatplattformen durch Ansetzen einer siliziklastischen Punktquelle und einer gravitativ induzierten Kornumlagerung in die Simulation mit einbezogen.

Größtmögliche Übereinstimmungen zwischen Modellergebnissen und real beobachteten Plattformgeometrien wurden unter der Annahme erzielt, dass die Geometrien des Plattformwuchses von hochfrequenten Meeresspiegelschwankungen kontrolliert werden, die einen niederfrequenten Meeresspiegelfall überlagern. Für die Modellierung der Plattformen wurde eine an Daten des ODP Site 926 gewonnene Meeresspiegelkurve benutzt. Die Modellergebnisse zeigen für die bearbeitete Region eine maximales Fallen des Meeresspiegels von 70 m an. 50 m entfallen dabei auf ein Absinken des eustatischen Meeresspiegels, 20 m resultieren aus tektonischer Hebung. Die gewonnene Kurve stimmt gut mit einer Kurve des relativen Meeresspiegels überein, die aus den Fluktuationen der Riffdach-Position während der Plattformevolution resultiert. Die beobachteten Meeresspiegelschwankungen wurden durch orbitale Zyklen kontrolliert, dabei stimmen die Perioden der kurzfristigen Schwankungen mit der Präzession überein, wobei während der frühen Plattformevolution eine gewisse Beeinflussung der Präzessionszyklen durch

Obliquität zu erkennen ist. Die Periode des niederfrequenten Meeresspiegelabfalls betrug ungefähr 100 ka, was mit der kurzen Exzentrizitätsperiode übereinstimmt.

Die Gültigkeit der Modellierungsergebnisse wird durch die Anwendung von drei unabhängigen Methoden bestätigt. (1) die äußere Morphologie der realen Karbonatplattformen stimmt mit den Formen und Dimensionen der simulierten Plattformen überein; (2) der Vergleich zwischen mehreren synthetischen geologischen Profilen und modellierten Profilen in gleicher Position zeigt eine gute Übereinstimmung der beiden; (3) die Wachstumsraten der Korallen, die mit der Fisher-Gleichung errechnet wurden, weisen eine ähnliche Rate wie die in heutigen Saumriffen auf, welche bei ca. 2 bis 8 mm/a liegt.

Die Modellierungsergebnisse ermöglichen einen Einblick in die interne Komplexität der Karbonatplattformen sowie die Dynamik der lateralen Veränderungen von Sedimentpaketen und Faziesbereichen. Mit REPRO können verschiedene Sedimentkörper in zeitlich-räumlicher Verbreitung graphisch dargestellt werden, wobei die Muster in der Faziesverteilung innerhalb der Plattformen deutlich werden. Die Modellierungsergebnisse erlauben es weitergehend, den Einfluß von relativen und globalen Meeresspiegelschwankungen auf lokale und regionale Sedimentsequenzen im Messin des westlichen Mittelmeeres zu unterscheiden. Sie machen zudem deutlich, dass die sedimentären Zyklen durch Meeresspiegelschwankungen unterschiedlicher Periodizität beeinflusst wurden. Darüber hinaus zeigen die Ergebnisse, dass sich die Anzahl der sedimentären Zyklen in den neritischen Ablagerungen von der in den pelagischen Ablagerungen unterscheidet, was darauf hindeutet, dass Umweltveränderungen die neritischen und pelagischen Bereiche und deren Sedimente unterschiedlich beeinflussen.

Acknowledgments

During the year 2000, a team of researchers from the University of Frankfurt, formed by Prof. Dr. Christian Betzler, Prof. Dr. Hansmartin Huessner, Dr. Dr. Jochen Roessler, and Dr. Rainer Petschick, decided to carry out a project about the modeling of carbonate platforms with a FORTRAN program. After considerations, they offered me a position to make my Ph´D thesis. My deepest thanks go to all of them for allowing me to join the project. There are thousands of reasons to be deeply grateful to CB for all the time that he spent helping me during the thesis, such as in the nice field trips to Spain, hours and hours revising texts and figures, very interesting conversations about geology, and of course, for make me feel at home in Germany. Very special thanks go also to JR, who introduce me to the complex mathematical world. He offered technical support every time that I had a problem with the main program. I want to thank Mark Peinl, who explained to me the visualization program and was always ready to help me.

My sincere thanks go to J.C. Braga and J.M. Martín, my Spanish professors. They introduced me to the complex geology of the province of Almería and were continuously willing to discuss about the different carbonate platforms with me.

I also want to express my gratitude to Sebastian Lindhorst and Arne Kaiser. They have fixed every single problem with computers and servers that I had during all the time at Hamburg University. I specially appreciate the support offered by my comrades in the Basin Analysis research group: Björn Berning, Merle Benišek, Mustafa Abdullah and Mamat Qrefa, who were always ready for discussions about geology, and to help me with the German language. The bureaucratic stuffs were solved thanks to the inestimable help of Frau Gerhard. Special thanks also go to the rest of the people of the 9th floor. I should also recognize the support of my "Spanish community" in Hamburg, Rubén, Joaquín, Ánder, Pablo, Gonzalo, etc., during the development of the thesis. Thank you guys for all the good moments living together in Germany.

I will be eternally grateful to my parents, José Cuevas Díaz and María del Pilar Castell Serrano. They have make possible all this work with their resolute help and support; Muchísimas gracias por toda vuestra ayuda y por vuestro apoyo. Additional family thanks go to my sisters, Pili and Loli Cuevas Castell, and to Šárka Petivlasová, for her encouragement and for her understanding during the difficult times.

Last but not least, The Deutsche Forschungsgemeinschaft (DFG) is acknowledged for funding this project (Be 1272/9-1, -2) for three years. This financial support has allowed me to actively participate in international meetings, as well as to travel to the study areas several times. I want to express my gratitude to the International Association of

Sedimentologists (IAS), which awarded me for participating in the international meeting organized in Oman 2005.

Chapter 1: Introduction

Integration of outcrop and subsurface data with forward computer modeling and simulation of sedimentary basin fills help to trace and understand the development of stratigraphic sequences in general, but may also be applied to explain and decipher specific stratigraphies (e.g. Bosence et al., 1994, Bowman and Vail, 1999). For carbonate systems, various 2-D modeling programs, which produce solid results, exist (Bosence and Waltham, 1990, Bosence et al., 1994, Whitaker et al., 1997, 1999). PHIL, for instance, is a black box program which provides a set of tools for stratigraphic and basin analysis for predicting the distribution of lithology and facies in a basin, and was developed by Marco Polo Software. SEDPAK, a program developed by the South Carolina University, is a forward sedimentary simulation program which models the sedimentary fill of basins by visualizing stratal geometries as they are produced between sequence boundaries (Kendall et al., 1993). In basins with an irregular substrate, computer programs which produce 3-D results may be used. Even carbonate systems with simple initial slope conditions may develop into complex and laterally incomplete packages of strata (Burgess and Wright, 2003). FUZZIM, a computer program based on mathematical fuzzy logic allows to model the fill of basins using simple geological rules (Nordlund, 1999 a, b). DIONISOS, a 3-D stratigraphic simulator developed by ELF, is currently applied for the exploration of reservoir rock formations (Doligez et al., 1999). CARBONATE 3D is a stratigraphic forward simulator written by the SedTec modeling group at the Royal Holloway University of London. It has been tested for theoretical modeling of atolls (Warrlich et al., 2002). REPRO is a 3-D computer simulation program developed by Hüssner and Roessler (1996) and Roessler and Hüssner (1997) for the modeling of carbonate environments. REPRO, in contrast with the previously described programs, is a FORTRAN program where all the operations and mechanisms for simulating the platform evolution are managed by routines, which can be adapted to the particular characteristics of different platforms. REPRO has been successfully tested in the Miocene Llucmajor Carbonate Platform in Majorca (Hüssner et al., 2001). The corresponding version of REPRO, used for the modeling of the Llucmajor Carbonate Platform, was herein improved with additional routines, which allow a better adjustment between modeling results and real outcrop data.

In this study, stratigraphic 3-D modeling was applied to simulate the evolution of Messinian carbonate platforms in the province of Almería (SE Spain). The modeled carbonate platforms are the Cariatiz and the Níjar carbonate platforms. These platforms show exceptional outcrops displaying platform shape and platform internal geometries and no evidences of major synsedimentary tectonic movements.

Several authors (e.g. Kendall and Schlager, 1981, Bosellini, 1984, Eberli and Ginsburg, 1989, Pomar and Ward 1991, 1994, Pomar et al., 1996, Pomar, 2001) have documented that hierarchical sea-level fluctuations are one of the most important controlling factors of the productivity, the sedimentary geometries, and the sequence stratigraphy of carbonate platforms. During the Late Neogene, hierarchical sea-level fluctuations are paced by the periodicity of Earth's orbital fluctuations. Sea level cycles following the long and short eccentricity (e.g. Williams et al., 2002) and obliquity (Keigwin, 1987, Hodell et al., 1994, Shackleton and Crowhurst, 1997, Sierro et al., 1999, Vidal et al., 2002) were described in numerous papers. Eccentricity and obliquity influence the distribution of solar radiation throughout the year and over periods of 400, 100 and 41 ka. The maximum obliquity-related effects occur in the Earth's poles with insolation changes producing variations in ice volume, which, in turn, results in global sea-level fluctuations. Changes in precession (23 and 19 ka) are thought to have minor effects on global climate than the longer term insolation changes, and as such were not taken into account as trigger of short-term sea-level fluctuations (Sierro et al., 1999, Krijgsman, et al., 1999). This view of a purely precessional control on climate has been recently challenged in studies, which analyze the sedimentary record of sea-level changes (Braga and Martín, 1996). In the meantime, however, also paleoceanographic studies provided evidence of a glacial component in late Miocene precession-driven oxygen isotope changes (Van der Laan et al., 2005).

Numerous studies propose that short-term sea-level fluctuations were the main controlling factor of the western Mediterranean Messinian carbonate platforms, for example, Pomar (1991, 2001), Goldstein and Franseen (1995), Braga and Martín (1996), Esteban (1996), and Warrlich et al. (2005). Other authors (Conesa et al., 1999, Cornée et al., 2004) have, however, proposed that the Messinian platforms grew under stable sea-level conditions.

The best fit of measured outcrop geometries and simulation results is herein obtained by using a curve of sea-level fluctuations, which contains three distinct periods known from the eustatic record. The sea-level record of the carbonate platforms modeled is complex, with an apparent modulation of the oldest precessional cycles by obliquity. The validity of these assumptions is corroborated by the values of reef coral growth rates provided by the models, which are similar to Recent coral growth rates.

The models also show that lateral changes in facies and thickness, which cannot be traced in the 2-D outcrops, were mainly controlled by the initial topography of the basins, erosion, and the parameters related to the spreading of reef debris. The combination of the 3-D spatial distribution of the different facies, together with the facies accumulation volumes, is used to understand the response of the reef system to the relative sea-level fluctuations. The modeling results can thus be used as a powerful tool for the simulation

of reservoir rock formations, which can be of potential interest to exploration of oil and underground water reservoirs.

Chapter 2: Geological setting

The depositional sequences of the Neogene basins in the province of Almería (SE Spain, Fig. 2.1) were thoroughly analyzed during the last decades (Ruegg, 1964, Völk and Rondeel, 1964, Völk, 1967, Iaccarino et al. 1975, Dabrio and Martín, 1978, Serrano, 1979, Esteban and Giner, 1980, Dabrio et al., 1981, Mankiewicz, 1987, Riding et al., 1991, Braga and Martín, 1992, 1996, Martín and Braga, 1990, 1994, and others). These studies provide data about the characteristics and correlations of the different stratigraphic units and the paleoecologic and paleogeographic features of the basins during the late Miocene.

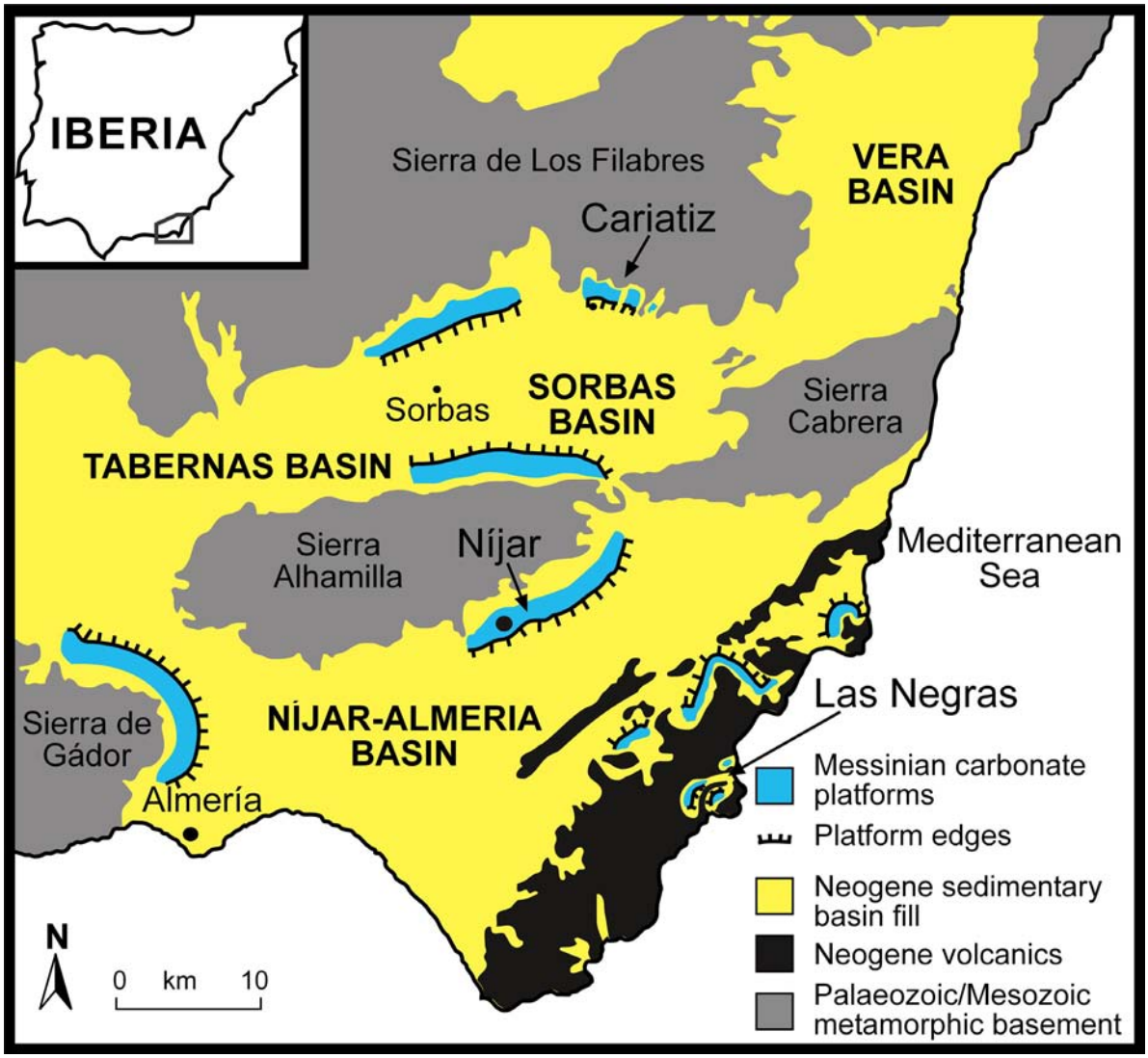

Fig. 2.1. Location and simplified geological map of the study area with the position of the carbonate platforms studied (arrows). These platforms form fringing complexes along basement highs. Modified after Dabrio et al. (1985).

The Messinian sedimentary record of the Neogene Sorbas and Almería-Níjar basins, which is exceptionally preserved, is considered as representing the Messinian pre-evaporitic deposits in the western Mediterranean area. The early Messinian deposits consist of carbonate platforms, which represent stages of reef development predating the Messinian Salinity Crisis (Hsü et al., 1977). Abundant data of three of the Messinian platforms, Cariatiz, Níjar, and Las Negras are available (Dabrio and Martín, 1978, Esteban and Giner, 1980, Dabrio et al. 1981, Dabrio et al., 1985, Mankiewicz, 1987, Franseen et al., 1988, Ott d´Estevou and Montenat 1990, Franseen and Mankiewicz, 1991, Riding et al., 1991, Martín and Braga, 1990, 1993, 1994, Braga and Martín, 1992, 1996, Braga et al. 1993, Goldstein and Franseen, 1995).

Messinian carbonate platforms are mainly formed by fringing reef complexes with minor lagoonal deposits, well-defined reef crests and slopes dipping up to 30°. Shallow water deposits consist of Lagoon Facies (preserved only in Cariatiz), Reef Framework Facies, Breccia and Block Facies, and the Middle Slope Calcarenites Facies. Locally, other facies, such as siliciclastic conglomerates (Cariatiz Carbonate Platform) or volcanoclastic and carbonate sands (Las Negras Carbonate Platform), crop out. These facies were related to episodic inputs of siliciclastic sediments in the platforms. The shallow-water deposits interfinger with basinal sediments formed mainly of marls, diatomites and sapropelic layers. These basinal deposits are arranged in cycles which are interpreted to be controlled by precession (Krijgsmann et al., 1999, 2001, Sierro et al., 1999, 2001).

2.1 The Cariatiz Carbonate Platform

2.1.1. Geological setting of the Sorbas Basin

The Sorbas basin is a narrow, intramontane, Neogene basin in the Betic Cordillera with an approximate W-E orientation (Fig. 2.1). The basin is bordered by the Sierra de los Filabres in the North and the Sierra Alhamilla in the South. The basement of the basin consists of metamorphic rocks from the Internal Betic Zone. The Internal Betic Zone is composed of metamorphic napes (Egeler and Simon, 1969) of Palaeozoic to Triassic age, which represent the deep structure of a Cretaceous subduction complex (Bakker et al. 1989). The Neogene basin fill consists of several sedimentary units separated by unconformities (Martín and Braga, 1990) (Fig. 2.2).

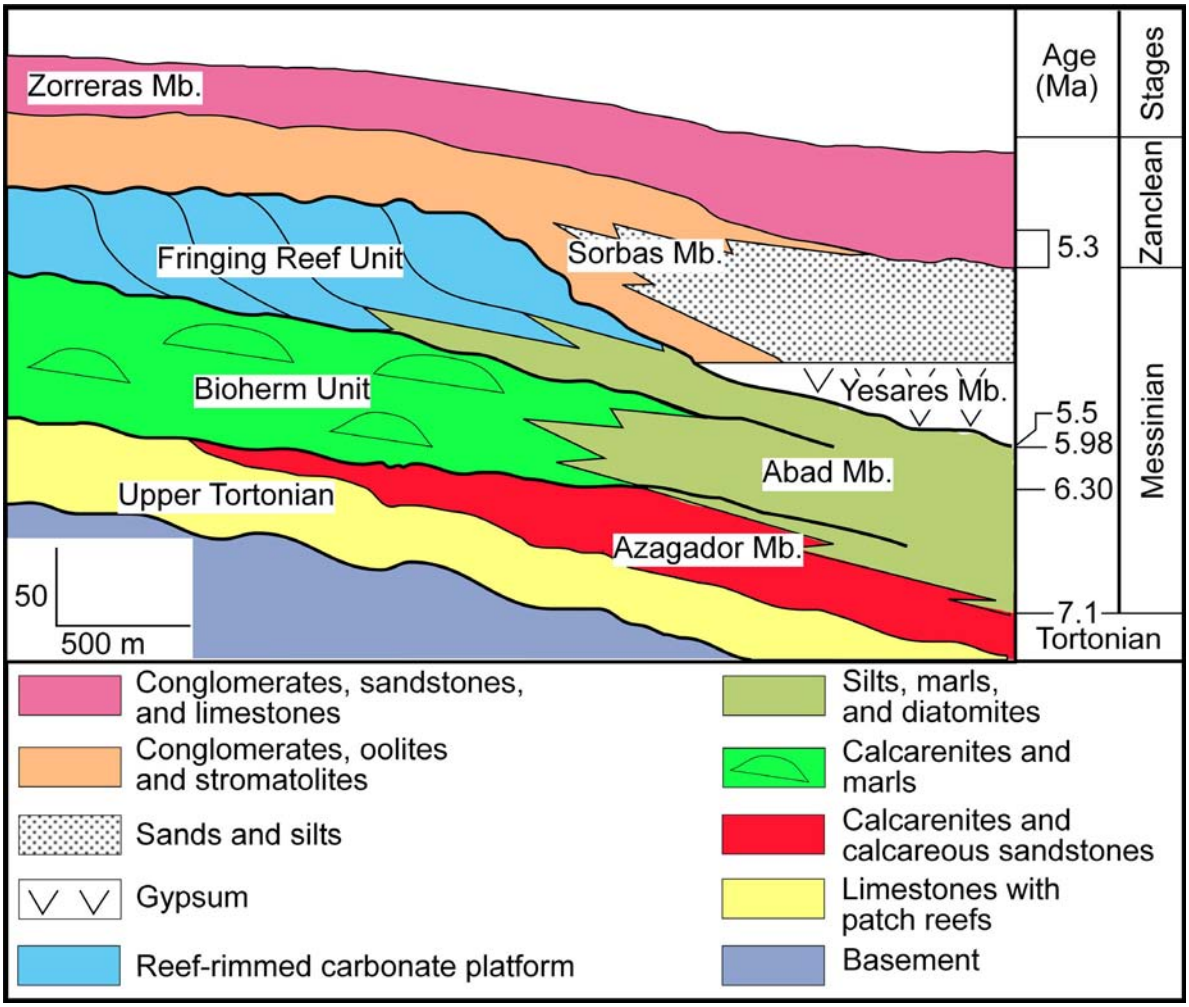

Fig. 2.2. Lithostratigraphy of the Sorbas basin. The basin fill is subdivided into a series of sequences separated by unconformities. The carbonate platform, which was modeled herein, corresponds to the Fringing Reef Unit. Modified after Martín and Braga (1994).

Marine Neogene sedimentation in the Sorbas Basin probably began during the Serravallian and continued throughout the Tortonian and Messinian. The Serravallian unit is mainly composed of conglomerates related to fan delta deposits. The Upper Tortonian Unit consists of temperate water carbonates forming ramps with coral patch reefs. Calcarenites and bioclastic sandstones of the Azagador Mb. (Ruegg, 1964) with abundant remains of bryozoans, coralline algae, mollusks, and echinoids overlie the previous unit. The Azagador Member is late Tortonian to early Messinian in age, according to the planktonic foraminiferal assemblages described by Sierro et al. (1993). The deposits grade upwards and laterally into fine calcarenites and marls of the cyclically layered and bedded lower Abad Member.

A tropical reef unit (Bioherm Unit) overlies the temperate carbonates. At the margins of the Sorbas Basin, this unit consists of platform carbonates mixed locally with siliciclastic sediments. The carbonate deposits are composed of calcarenites, calcisiltites and bioherms formed by serpulids, *Halimeda*, and *Porites* coral reefs (Martín and Braga, 1990, Braga and Martín, 1992, 1996, Braga et al., 1993, 1996, Martín et al., 1997). Basinwards, these facies interlace with marls and diatomites of the Abad Member with some reef blocks and breccia shed from the bioherms on the platform margin. The occurrence of PF-Event 4 (Sierro et al., 1993) in these marls allows dating the uppermost part of the Bioherm Unit at 6.3 Ma.

The Bioherm Unit is overlain by the Fringing Reef Unit (FRU). The FRU is a tropical unit that consists of reef systems developed close to the margins of the Sorbas Basin. The build-up organisms of the reef systems are mainly *Porites*, and stromatolitic crusts (Riding et al., 1991, Martín and Braga, 1994). Several sedimentary cycles have been recognized related to sea-level fluctuations, which managed the development of the carbonate platforms (Braga and Martín, 1996). Distally, the inner-platform deposits of the FRU interfinger with marls and diatomites of the Upper Abad Mb.

An erosional surface caused by subaerial exposure, during the Messinian desiccation of the Mediterranean Sea, marks the top of the carbonate platforms (Dabrio et al., 1981, Martín et al., 1997). In the inner Sorbas Basin, the unconformity is overlain by selenitic gypsum.

Sands and silts of the Sorbas Mb. (Riding et al., 1991 , Martín et al., 1993) overlie the evaporites. The Terminal Carbonate Complex (TCC) that represents the last Miocene marine event in the Sorbas basin is also included in the Sorbas Mb. Towards the margins of the basin, the sediments change to siliciclastic conglomerates, oolitic bars, stromatolites and thrombolites that lie directly on the erosional surface on top of the carbonate platform.

The Zorreras Member (Ruegg, 1964) overlies the TCC sediments. It consists of fluvial conglomerates, sandstones and lacustrine limestones. Lacustrine levels are white or grayish and contain some fresh-water gastropods and ostracods (Roep and Van Harten, 1979, Ott d´Estevou, 1980). Deposits are likely to be Pliocene in age. A thin Pliocene marine unit (Civis et al., 1977) is the youngest unit of the Neogene basin succession.

2.1.2. Location and geological map of the Cariatiz Carbonate Platform

The Cariatiz Carbonate Platform is located along the northern margin of the Sorbas basin, at the foothills of the Sierra de los Filabres (Fig. 2.1). The area of the Cariatiz Carbonate Platform is covered by the sheets 1-1 and 2-1 of the topographic map of Spain (sheet 1031, Sorbas, 1:10000). The geographical coordinates are 30SWG57762-58405 411405-41115. The platform covers a total area of about 18 km^2. The geological mapping (Fig. 2.3) completes a previous geological map of the area described by Braga and Martín (1996).

Upper Tortonian Unit

Overlying the metamorphic basement, the northernmost outcrops of sediments, near the village of the La Mela and the Cerro de Los Lobos are from the Upper Tortonian Unit. It forms hillocks with subhorizontal stratums. Towards the head of the hillocks, the presence of small coral patch reefs with *Porites* at the base and *Tarbellastraea* at the top are common (Martín et al., 1989). Abundant mollusks (*Pecten sp*. and *Chlamys*), brachiopods (terebratulids), echinoids (*Clypeaster*?), and foraminifera are also common. The fossil remains are usually fragmented due to reworking by wave action. Some discontinuous layers, which contain an erosional base and a chaotic aggregate of reworked remains of different benthonic organisms, have been interpreted as tempestites.

Azagador Member

The thickness of the Azagador Mb. in the mapping area is only a few meters. West of the La Mela village, in the northern area of the La Mora ravine, there is a good outcrop which characterizes this member well. It contains condensed bioclastic levels with bivalves (pectinids), brachiopods (terebratulids), echinoids, red algae, barnacles and gastropods. Most of the fossils are fragmented, which is likely due to wave action. Another outcrop of the Azagador Mb. occurs along the southern part of the Cerro de los Lobos, where the facies are more distal and the sediments are composed of calcisiltites and marly calcarenites. The boundary between Azagador Mb. and the Uppermost Tortonian has been marked by the transition from ochre calcarenites, deposited under tropical to subtropical

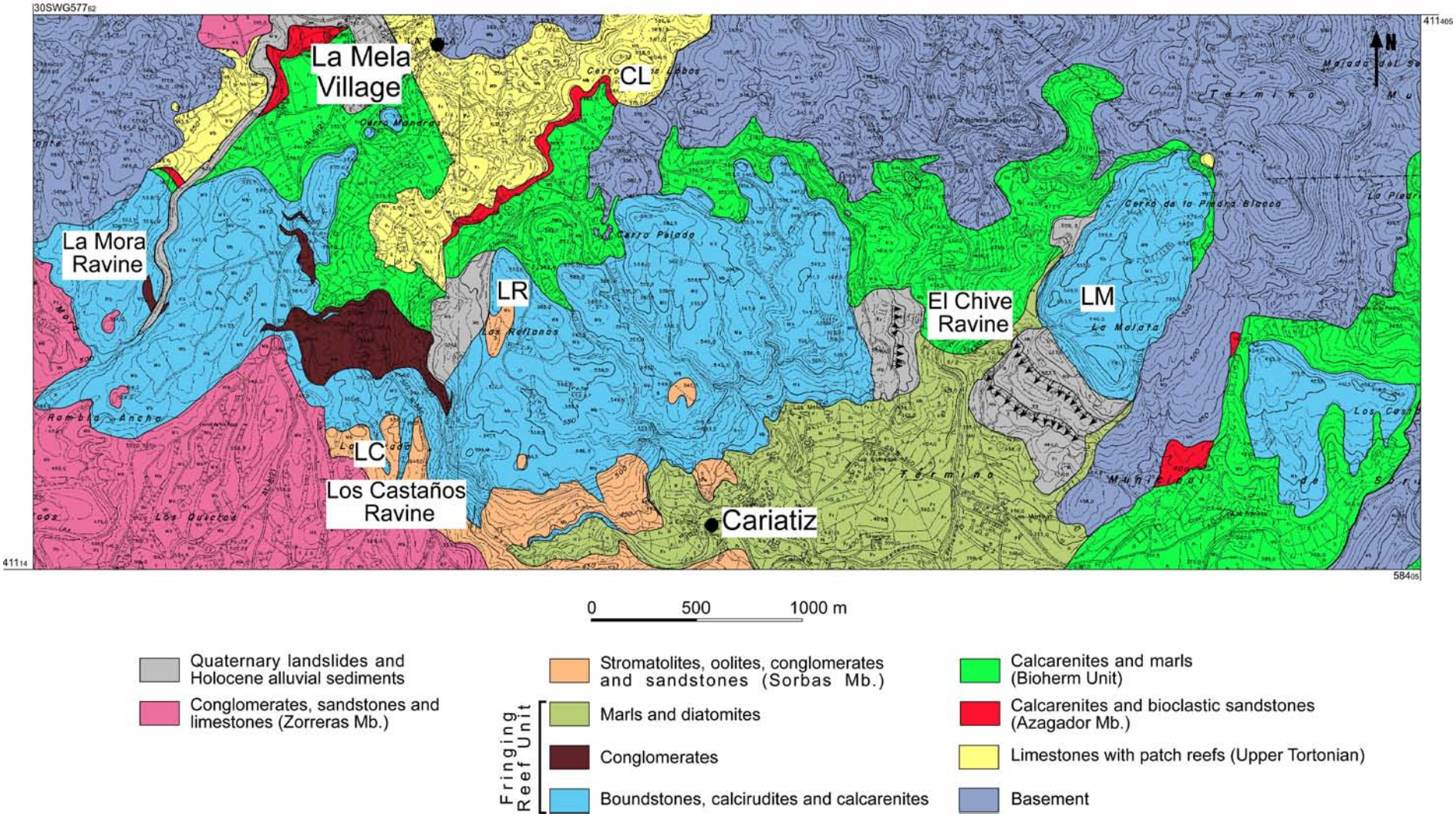

Fig. 2.3. Geological map of the Cariatiz Carbonate Platform with the position of the main ravines which cross-cut the system. Some localities mentioned in the text are also shown here. CL: Cerro de Los Lobos; LC: La Cerrada; LR: Las Rellanas; LM: La Molata.

climate conditions, to yellowish marly calcarenites with a temperate water faunal association.

The Bioherm Unit

The outcrops of the Bioherm Unit consist mainly of well-compacted marls with fish remains and bivalves, and turbiditic layers. The Bioherm Unit overlies the Tortonian deposits in the western area, where the yellowish bioclastic calcarenites from the Azagador Mb. are separated by an erosional unconformity from the white compacted marls of the Bioherm Unit. In the eastern part of the study area, this unit directly overlies the metamorphic basement. Bioherms have been not described in the Cariatiz area before.

The Fringing Reef Unit

The platform of the Fringing Reef Unit progrades from the northern margin of the Sorbas Basin (Sierra de Los Filabres) to the South. In the geological map, the FRU has been subdivided into two mapping units. One contains the platform-interior deposits of this unit, whereas the other contains the distal slope marls and diatomites. The platform-interior deposits have been subdivided into different facies related to the depositional environment. A Lagoon Facies (LF) is formed by calcarenites to calcirudites with abundant remains of gastropods, mollusks, coralline algae, and occasionally small coral patches of *Porites*. Siliciclastic grains are locally mixed with the carbonate sediments. According to Riding et al (1991), a reef framework facies (RFF) is subdivided into three subfacies (Fig. 2.4): A) the deepest subfacies is the lower Pinnacle Zone (approx. 10 to 15 m below reef crest), where the coral grew as vertical poles connected by laminar growth, forming pinnacle morphologies; B) a Thicket Zone (about 4 to 10 m below reef crest) composed of vertical poles and more laterally continuous coral growth; C) a Reef Crest

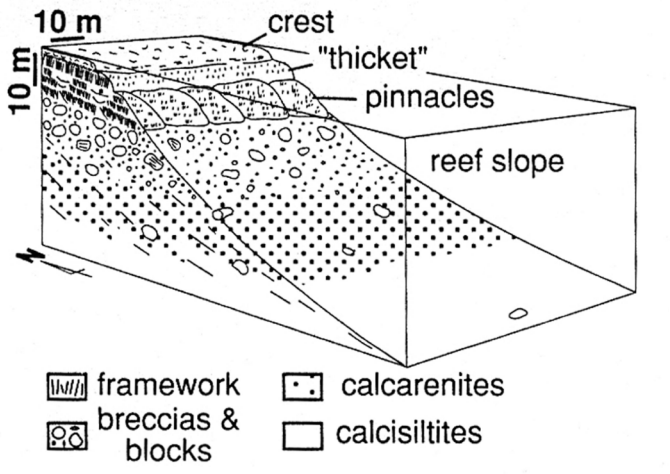

Fig 2.4. Reconstruction of the coral-stromatolite reef at Cariatiz with the distribution of the RFF subfacies (after Riding et al., 1991).

Zone (4-0 m water depth), composed of laminar to contorted *Porites* colonies with stromatolitic crusts. Cavities are mainly filled by a rudstone with regular echinoids and mollusks. This facies array implies a maximal carbonate production in a water depth of less than 15 m.

A Breccia and Block Facies (BBF) deposited at the uppermost slope consists of reef framework blocks and coral breccia with mollusks, serpulids and *Halimeda*. Laminar *Porites* colonies encrusting bioclasts are frequent as well. The Middle Slope Calcarenites Facies (MSCF) consists of well-bedded calcarenites with abundant *Halimeda*. Calcarenites are composed of bioclasts, mainly serpulids, coralline algae and mollusks.

The distal slope and basin deposits of the carbonate platform consist of calcarenites and sandy marls interlaced with marls and diatomite layers, which correspond to the Upper Abad Mb. Layers with fish remains and shell concentrations of *Neopycnodonte navicularis* are common in the marls.

Episodic inputs of fan delta sediments occurred in the western part of the Cariatiz Carbonate Platform. Fan delta deposits consist of conglomerates alternating with sandstones that interfinger with the carbonate platform. Clasts, which are supported by a microconglomeratic or sandy matrix, are mainly derived from the metamorphic basement. Small coral patches grew on the conglomerates during fan delta inactivity.

The Sorbas Member (TCC)

In the study area, the Sorbas Mb. consists mainly of oolitic bars. Stromatolites are also found on the top of the carbonate platform in the area called La Cerrada, where they occur together with calichified carbonate conglomerates. Small outcrops of the Sorbas Mb. were also recognized at the top of the carbonate platform, which were likely deposited during relative sea-level highstands that resulted in flooding of the platform.

The Zorreras Member

Alluvial conglomerates and lacustrine carbonates of the Zorreras Mb. overlie the youngest part of the Cariatiz Carbonate Platform to the west of the study area. A small outcrop of Zorreras Mb. also occurs NW of the La Mela village, overlying Upper Tortonian deposits and the metamorphic paleorelief.

Geological cross-sections of the Cariatiz Carbonate Platform

Several geological cross-sections (Fig. 2.5) have been made in order to decipher the geometrical relationships between the different units and reconstruct the tectonic tilt that affected the region after the carbonate platform evolution. The data of Braga and Martín (1996) and the results of the geological mapping show that the lagoonal beds of the Cariatiz carbonate platform dip three degrees towards the south (basinward). Therefore, it is necessary to rotate the platform deposits back in order to reconstruct a sea-level curve.

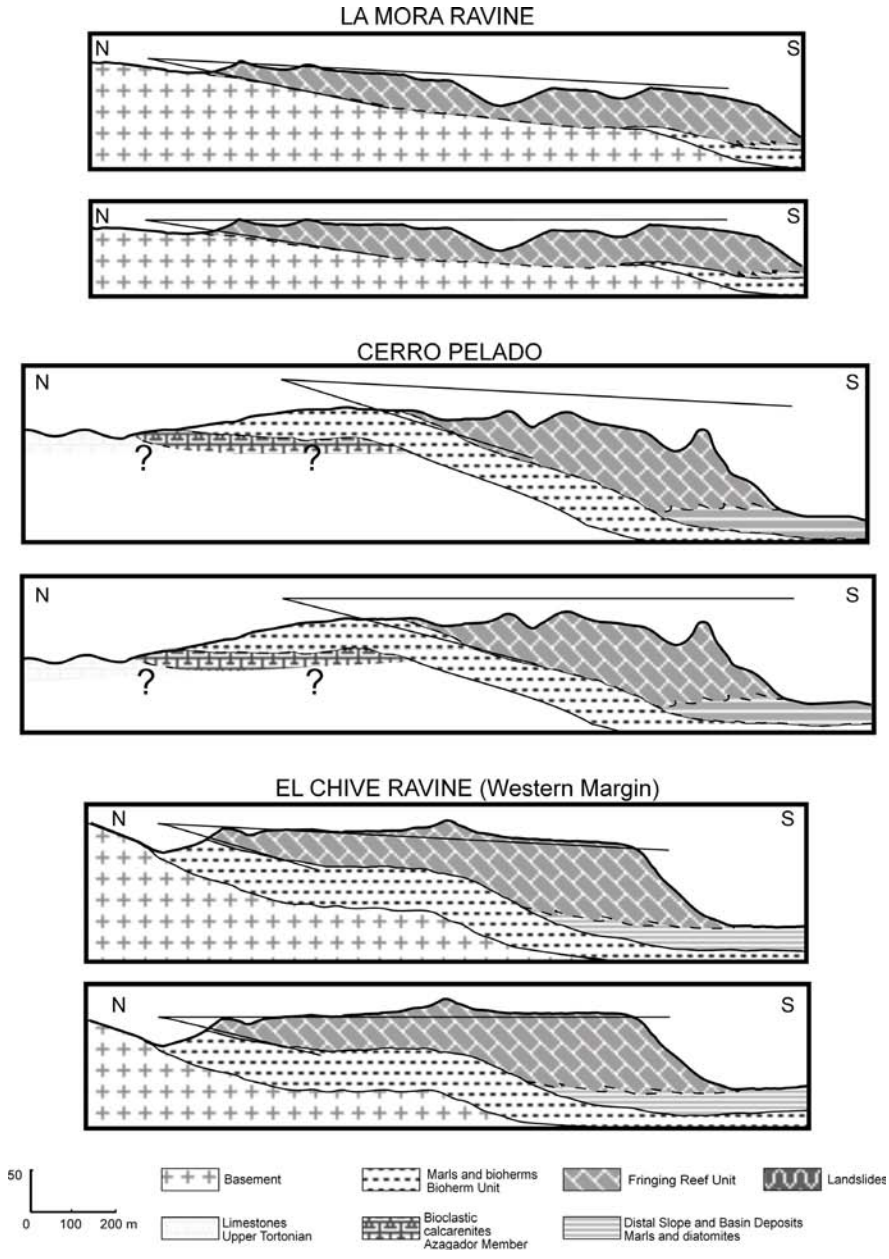

Fig. 2.5. Restored cross section of the Cariatiz carbonate platform. Geological cross-sections were rotated back by 3º in order to reconstruct the tectonic tilt that affected the region. See also next page.

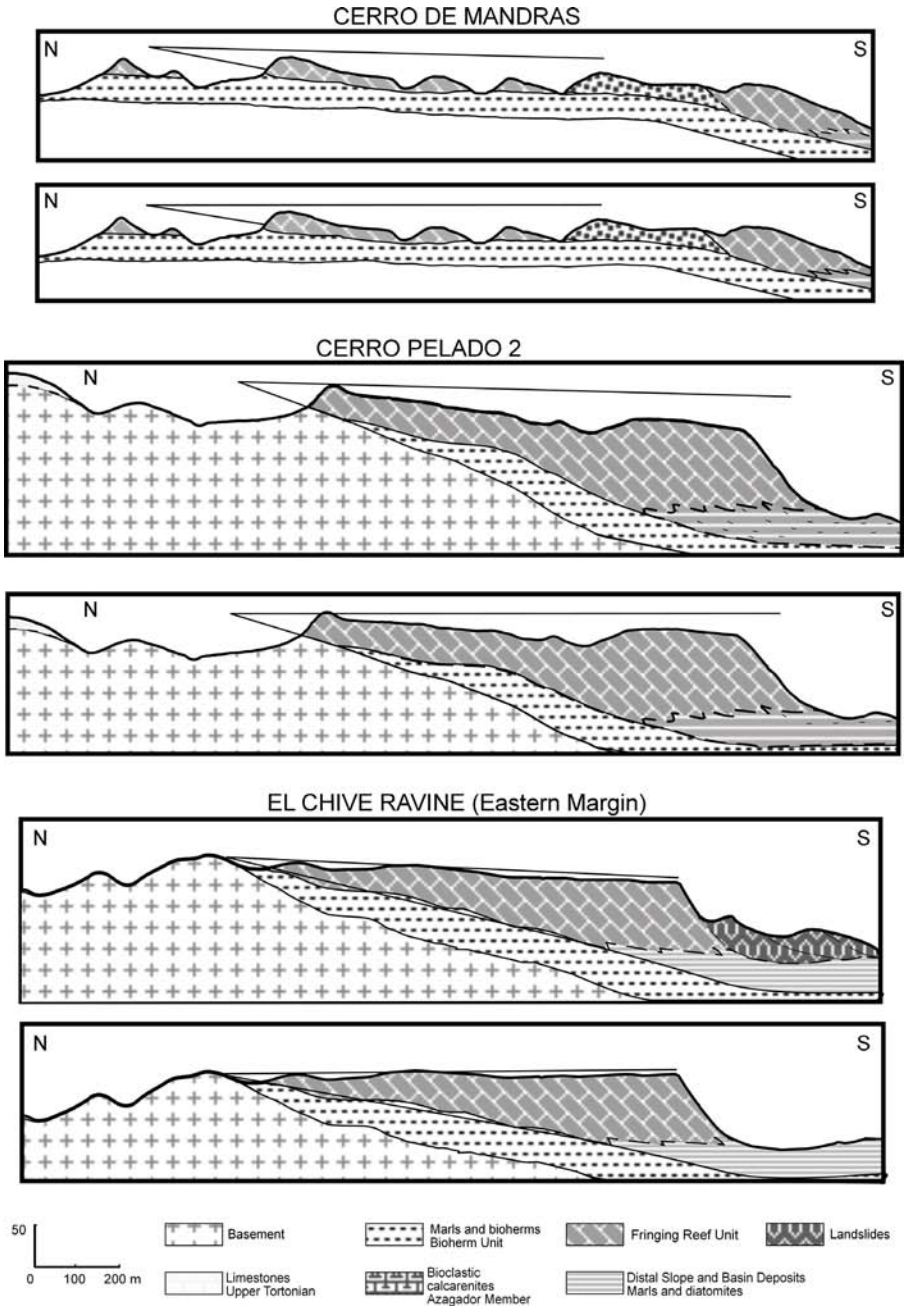

Fig. 2.5. Continued

2.1.3 Initial topography of the Cariatiz Carbonate Platform

For the computer simulation, a reconstruction of the initial topography of the Cariatiz carbonate platform was necessary. The reconstruction was carried out taking in account the geological map and the geological cross-sections, the photo-transects as well as dip data of the basal unconformity of the FRU. A rectangular grid of 100 x 100 m mesh size, which covered the entire study area, was developed by assignment of height positions to the individual grid points. Thus, a rectangular matrix with 45 rows (N-S direction) and 60 columns (W-E direction) was generated with each element representing the height value previous to platform growth.

The shape of the initial topography is shown in Fig. 2.6. This surface is formed by the basal unconformity of the FRU. The model domain has an extension of 6 X 4.5 km. It is a southward-dipping slope, with a western and eastern segment a dipping at 2-5°, separated by a steeper dipping promontory (10°). The initial water level depicted in Fig. 2.6 is positioned according to the position of the wedging out of the lowest onlap of the Fringing Reef Unit. The initial depositional range extends down to a water depth of approximately 160 m over a distance of 4.5 km. This water depth estimate relies on geometric reconstructions of the slope profile and paleobathymetric data on the Abad Marls by Troelstra et al. (1980) and Goubert et al. (2001).

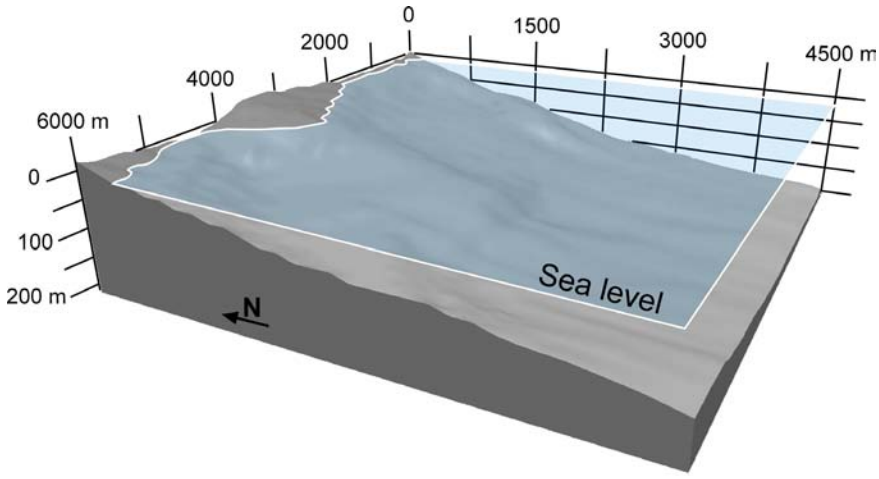

Fig. 2.6. Initial topography used to simulate the Cariatiz carbonate platform. This surface was reconstructed based on the geological map of the study area and geological cross-sections through the platform. The position of the sea-level corresponds to the position for the first time-step.

2.1.4 Depositional geometries and relative sea-level changes

The reef growth geometries of the Cariatiz carbonate platform are well-exposed in several ravines which cross-cut the carbonate platform (Braga and Martin, 1996; Fig. 2.3). Tracing the altitude change of the reef crest and the contact between BBF and MSCF through time, Braga and Martín (1996) developed a curve of relative sea-level changes, which controlled platform growth. This curve was herein improved, using the photo-transects described below (Figs. 2.7, 2.8, 2.9, 2.10, 2.11, 2.12, 2.13, 2.14), especially with regard to higher frequency fluctuations. In order to restore the 3° tilt basinwards of the platform, which is reflected by the dip of the lagoon beds described by Braga and Martín (1996), the carbonate platform is rotated back to the original position for the reconstruction of the sea-level curve.

The paleobathymetric assignment of the different platform facies relies on geometrical relationships shown by Martín and Braga (1994) and Braga and Martín (1996). The LF is assumed to represent water depths between 0 and 5 m. The RFF was formed between 0

and 20 m. In parts of the transect with minimal or no RFF, the downslope occurrence of the BBF was used to give an approximation of water depths. Calibration of the BBF distribution was performed in areas of the carbonate platform where this facies occurs together with RFF. As a result, the lower BBF limit was found to lie 15-30 m below sea-level in the older parts of the platform, whereas it is situated at 50-70 m below sea-level in later stages. Here, higher slope angles may have favored slope instabilities, with the consequence of an increased downslope spreading of the breccia deposits. As such, the water depth assignments of these later stages of the platform evolution are possibly somewhat less precise as in the older stage of the carbonate platform. This implies that the reconstructed sea-level curve may only represent an approximation of the changing sea-level positions in the late stage of platform growth.

Braga and Martín (1996) subdivided the Cariatiz carbonate platform into sedimentary cycles. Each cycle, or reef growth package (RGP), is defined as the stack of sediments deposited between two consecutive lowstand wedges. These lowstand wedges were described as inverted wedges by Braga and Martín (1996). They consist of calcarenites (packstones to rudstones) which contain abundant fragments of mollusks, bryozoans, red algae, and scarce coral fragments. Some of these sedimentary bodies have erosive bases and bar morphologies. The lowstand wedges thin out towards the reef crest. Occasionally, the lowstand wedges are intercalated into middle slope calcarenites. According to Braga and Martín (1996), the lowstand wedges were deposited during sea-level lowstands and related episodes of temperate climate. During these phases, reef growth was very subdued or non-existent. In total, there are eight lowstand wedges in the Cariatiz Carbonate Platform, which delimit 9 RGPs. Each RGP, during sea-level rises, combines aggradation with progradation. For each cycle, during sea-level highstands, the reef facies prograde and aggrade. In the stage of sea-level fall, an offlapping geometry develops. During the lowstand of sea-level, erosion and karstification occurred in the exposed platform, and a lowstand wedge was formed overlying the previous RGP.

2.1.4.1 The La Mora Ravine

Northern part of the La Mora Ravine

Figure 2.7 shows the northern part of the La Mora Ravine, a locality close to the limit between the metamorphic basement and the Neogene infill. This view covers a 450 m broad outcrop. The base of the Fringing Reef Unit at this location unconformably overlies the Bioherm Unit. Three lowstand wedges (LW 1 – 3), indicating three major sea-level drops, subdivide the reef progradation into four RGP.

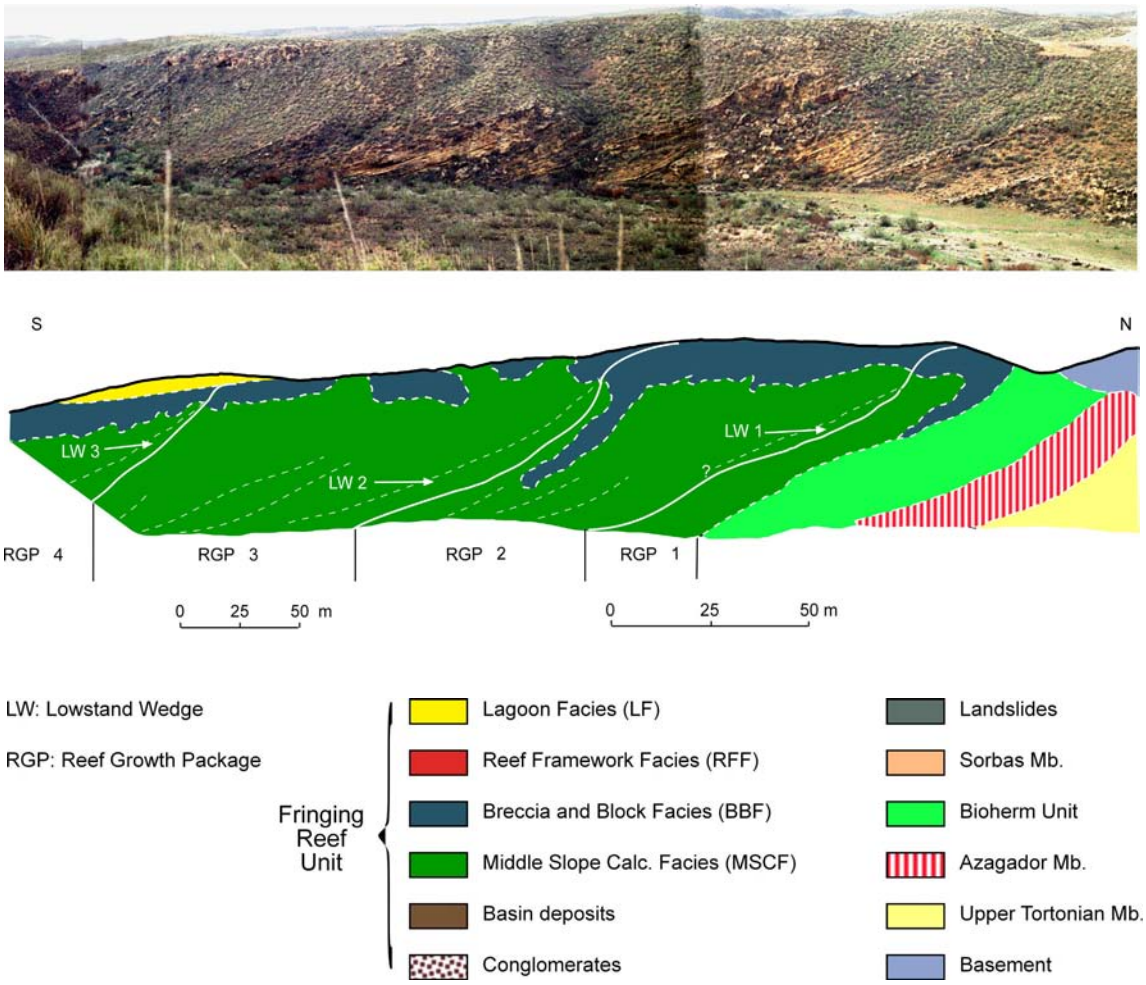

Fig. 2.7. Photo-transect of the northern area of La Mora Ravine. The view shows the oldest Reef Growth Packages (RGP) of the Cariatiz Carbonate Platform. The legend shows the FRU facies, as well as the stratigraphic units that outcrop in the photo-transects of the Cariatiz Carbonate Platform (Figs. 2.7, 2.8, 2.9, 2.10, 2.11, 2.12, 2.13, and 2.14). The distortion of the photo-transect was considered using two different scales.

There is no preserved RFF in this transect. The contact between the BBF and the overlying lagoonal beds is unconformable, and it is assumed that RFF was eroded during subaerial stages occurring during the platform evolution.

Sedimentary geometries in the RGP 1 show that this cycle began with a retrogradation of the reef margin deposits before the system started to prograde. RGP 2 and 3 are dominated by reef progradation with the exception of one episode of a downstepping of Breccias and Blocks Facies in RGP 2. This episode is interpreted reflecting an incipient sea-level fall before the lowstand, which triggered the formation of LW 2. The LW 2 is cross-bedded and has an erosive lower surface. According to Braga and Martín (1996) cross bedding presumably reflects the migration of shoreface coastal bars.

Southern part of the La Mora Ravine

Photo-transect 2.8 covers 275 m of platform progradation with three RGPs separated by the third and fourth lowstand wedges of the platform evolution. Following LW 3, the platform rim progrades approximately 15 m, before there is an input of conglomerates through a small fan delta (Fig. 5A). Conglomerates (up to 3 m thin) form a lenticular body, with a downslope extension of approximately 20 m. The conglomerates are overlain by Middle Slope Calcarenites. The remaining part of RGP 4 is subdivided by prominent clinoforms. RGP 4 was terminated by a major sea-level fall, as it is indicated by the pronounced final downstepping of this facies. The LW 4 has a maximum thickness of 10 m. It consists of two thinning and finning upward cycles. The overlying RGP 5 is characterized by a continuous downstepping of the BBF, which reflects a forced regression triggered by a relative sea-level fall.

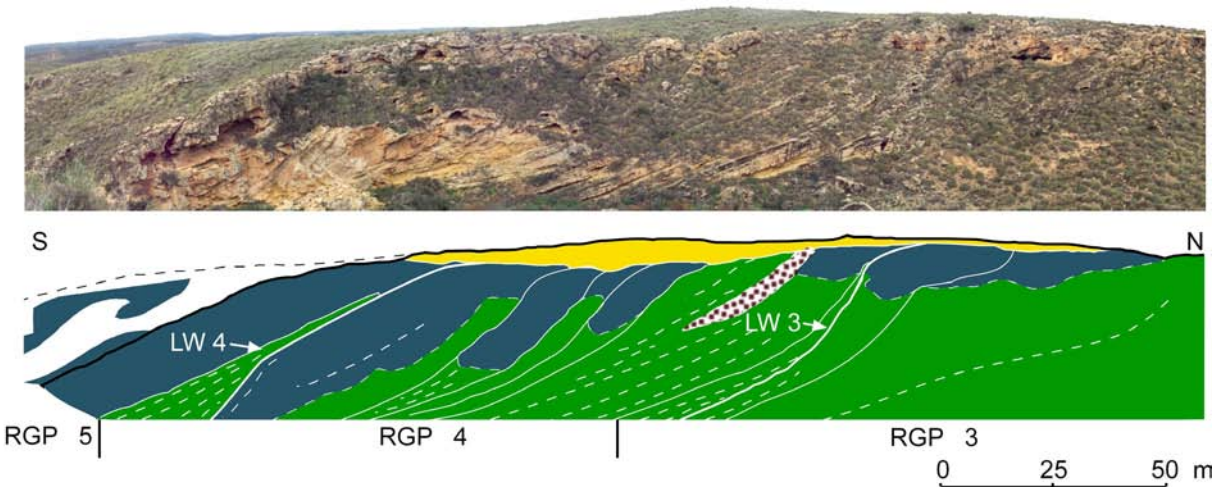

Fig. 2.8. Photo-transect showing the southern part of La Mora Ravine. The RGPs display a progradational to downstepping geometry, and are separated by lowstand wedges (LW). Lowstand wedges are sediment wedges which thin out and disappear toward the platform crest and consist of bryomol calcarenites.

2.1.4.2 The Los Castaños Ravine

The Los Castaños Ravine dissects the Cariatiz Carbonate Platform approximately 2 km to the east of the La Mora Ravine. The reef growth geometries can be widely observed in both sides of the ravine.

Western flank of the Los Castaños Ravine

Figure 2.9 shows a 600 m broad N-S view of the RGP 2 to RGP 6 evolution of the Cariatiz carbonate platform. Deposits in this transect are the BBF, the Middle Slope Calcarenites, as well as sandstones and conglomerates. In contrast to the previously described transects, no LW were recognized in this section. Sea-level falls are traced by downstepping intervals of BBF, which could be also interpreted as response to the lowstand stages.

Middle Slope Calcarenites dip with about 20 degrees to the South, and the angle increases upslope, marking the sigmoidal geometry of the carbonate platform slope. This geometry is especially well developed in RGP 3 and 4. The bottomsets of individual clinoforms show downlapping geometries onto the underlying Bioherm Unit.

Conglomerates and sandstones occur in RGP 5 and 6. The contact between the siliciclastics and the underlying carbonates is conformable. According to Braga and Martín (1996) these deposits are related to the input of a fan delta into the basin. Interbedded into the conglomerates of RGP 6, there are minor BBF patches, up to 5 m thick and 20 m broad.

Eastern flank of The Los Castaños Ravine

The photomosaic covers about 1.2 km of progradation in the eastern margin of The Los Castaños Ravine (Fig. 2.10). In the northernmost part of the photo-transect, the Fringing Reef Unit (RGP 4) overlies the Bioherm Unit. LW 4 is intercalated into the MSCF. As there is a major landslide that covers the lower part of the flank of the ravine, it is not possible to reconstruct the overall geometry of this body.

Most of RGP 5 is covered. In the outcropping parts, only a minor patch of the BBF of this episode is preserved. At the top section of the ravine, are oolitic calcarenites of the Sorbas Member. LW 5 crops out at the top of the hillock of Las Rellanas and is projected in the photomosaic because it is not visible in this view.

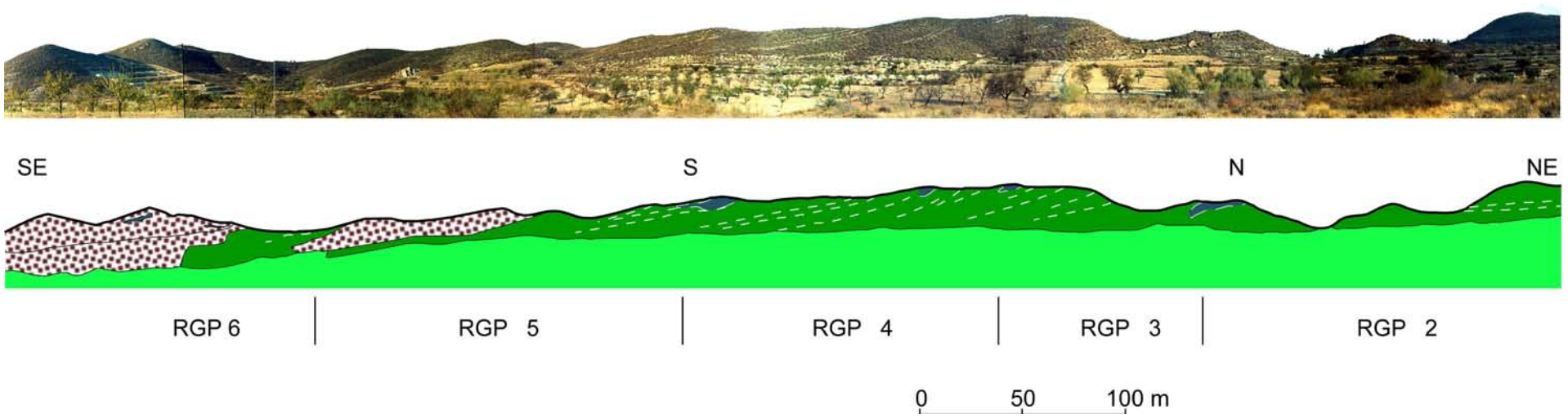

Fig. 2.9. Photo-transect along the western flank of Los Castaños Ravine. Note the outcrop of siliciclastic conglomerates in the southeastern part of the transect.

RGP 6 is dominated by the progradation of the BBF, and the downstepping of these deposits before the lowstand, which is marked by LW 6. At the top of RGP 6, the Lagoon Facies unconformably overlies the BBF.

RGP 7 is an approximately 200 m progradational package. It starts with a backstepping of the BBF during the early transgressive stage of the package. Two episodes of coarse siliciclastics occur in RGP 7, and between both episodes there is a downstepping of the BBF. After the second episode of coarse siliciclastics, there is a major progradation of the platform rim. The calcarenitic layers dip 15° S, the layers of the BBF about 25° S. In the youngest part of the RGP 7, there is a small outcrop of RFF at the top of the section. A downstepping occurs in the BBF and in the RFF in the latest stage of RGP 7 development.

The position of LW 7 marks the lowest sea-level position during the development of the Cariatiz Carbonate Platform. RGP 8 is not entirely seen in the photomosaic. In this transect, only the most proximal parts of the platform deposits with RFF and BBF are exposed.

Southernmost part of The Los Castaños Ravine

This photo-transect covers RGP 8 and 9, which are the last growth packages of the Cariatiz carbonate platform (Fig.2.11). RGP 8 consists mainly of BBF prograding towards the South. Within RGP 8, an episode of downstepping occurs, before there is a minor input of coarse siliciclastics. The most prominent stage of BBF downstepping in RGP 8 overlies the coarse siliciclastics. At the top of the section there are some patches of the RFF.

LW 8 is overlying the BBF and the Middle Slope Calcarenites of RGP 8. The position of LW 8 is slightly higher than the position of the previous lowstand wedge (LW 7) which marks a maximum sea level lowstand during growth of the Cariatiz carbonate platform. After the LW 8 lowstand, there is an episode of BBF backstepping in RGP 9, before the platform flank progrades to the south again.

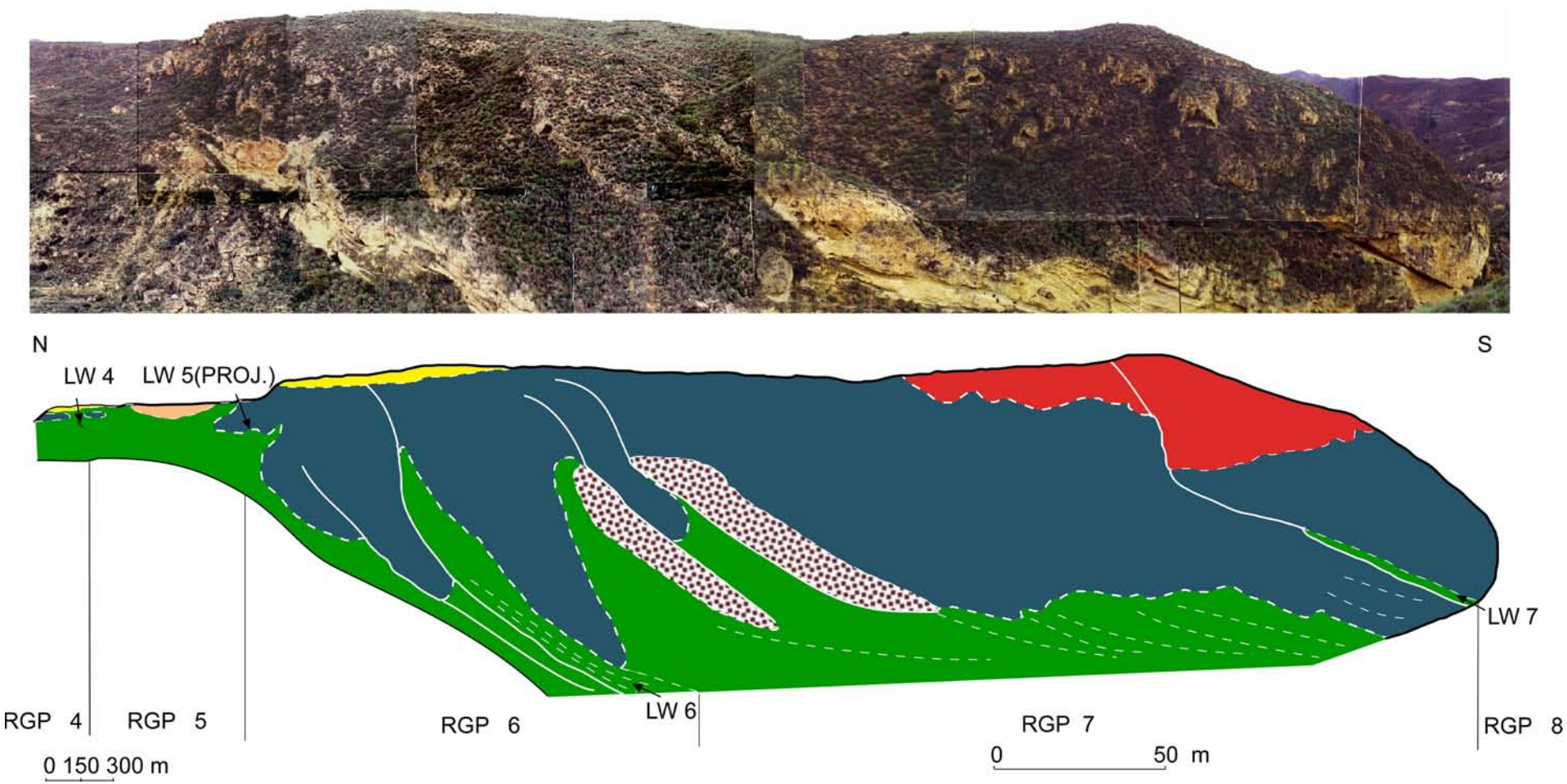

Fig. 2.10. Photo-transect along the eastern flank of the Los Castaños Ravine.

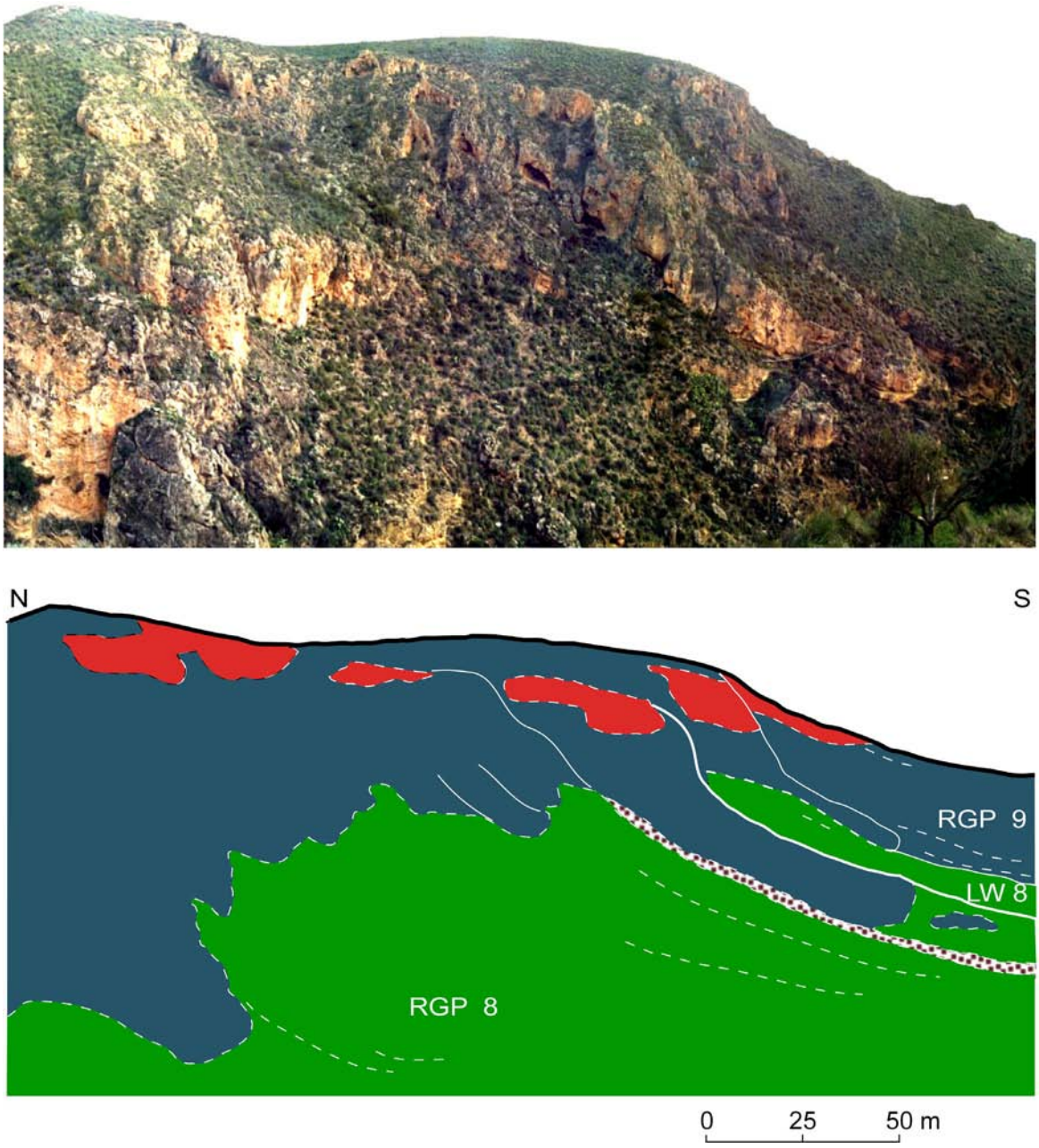

Fig. 2.11. Photo-transect and facies interpretation of the southernmost part of the Los Castaños Ravine. This view shows the youngest growth packages of the Cariatiz Carbonate Platform.

2.1.4.3 The Barranco de Cariatiz

Figure 2.12 shows a detailed view of the last progradational episodes in the Barranco de Cariatiz. It displays two incomplete RGP separated by the LW 8. The geometry of the lowstand wedge can not be traced downslope, because it is covered by reef debris.

The BBF of RGP 9 overlies LW 8. At the top of RGP 9 there is RFF which consists of a 10 to 20 meters thick package of *Porites* and stromatolitic crusts. The RFF passes

downslope to the BBF, which is approximately 70 meters thick. Further downslope, the BBF passes to layers of MSCF. The MSCF interfinger with silty marls, and diatomite layers of the Distal Slope Facies.

The Sorbas Member unconformably overlies the carbonate platform. It consists of oolitic cross-stratified calcarenites forming bars.

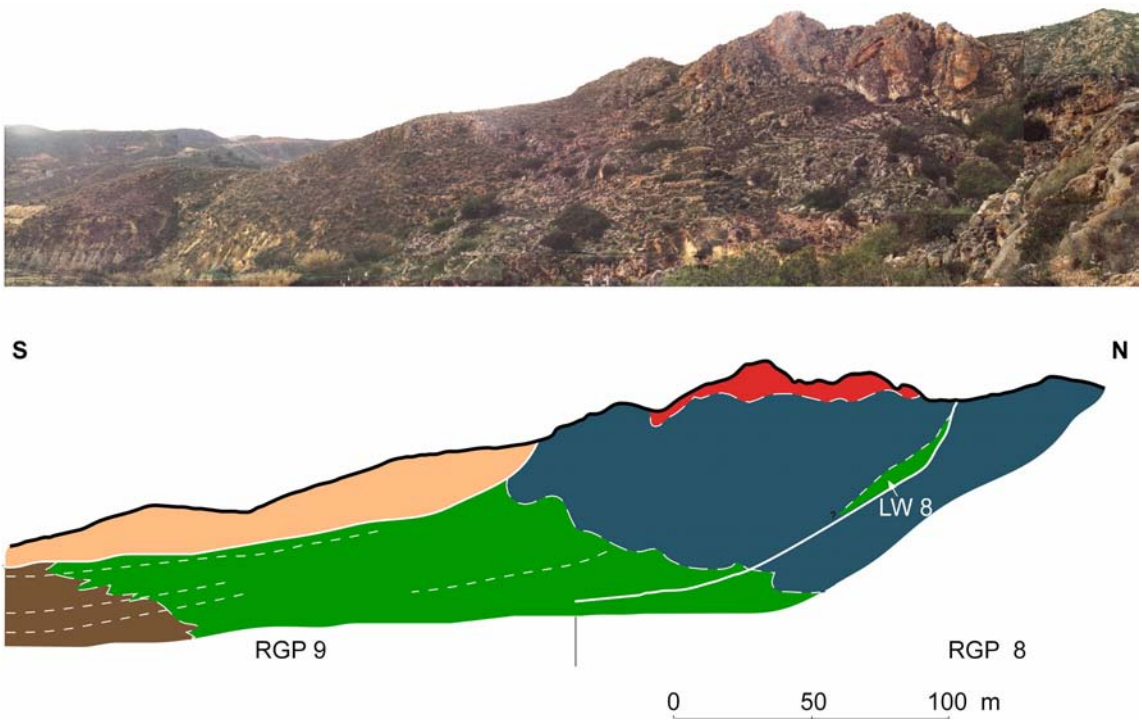

Fig. 2.12. Photo-transect in the Barranco de Cariatiz. The Sorbas Mb. deposits unconformably overlay the FRU deposits.

2.1.4.4 The El Chive Ravine

Western flank of the El Chive Ravine

The most prominent feature of this photo-transect is the downstepping of the BBF, which is interpreted to represent the late part of RGP 6 (Fig. 2.13). Clinoform morphologies occur in this part of the transect, and a patch of RFF marks the maximal sea-level drop of this package.

A landslide occurred in this area, partially covering the MSCF and the contact between the deposits of the Bioherm Unit and the marls and diatomites of the Distal Slope Facies. The

frontal part of the Cariatiz carbonate platform is composed of the BBF interfingering with the MSCF.

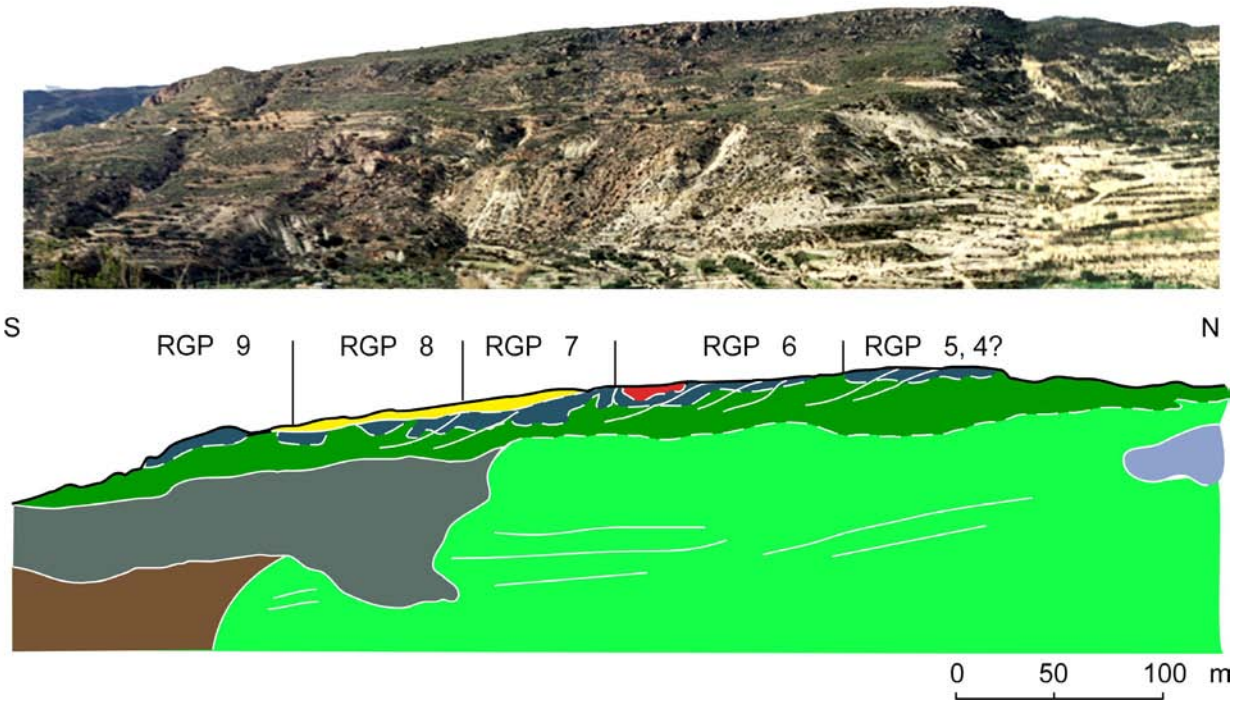

Fig. 2.13. View of the western flank of the El Chive Ravine. The view shows the progradation of platform since RGP 4.

Eastern flank of the El Chive Ravine

Fig. 2.14 covers 200 m of outcrop along the eastern flank of the El Chive Ravine. Deposits are attributed to RGP 6, LW 6, and the older part of RGP 7. RGP 6 sediments are composed of the BBF and MSCF. MSCF overlie the marls of the Bioherm Unit.

Growth of the Cariatiz platform is well-displayed in this section through a number of sigmoidal bodies. In the early stage of RGP 6 the growth of the platform is strictly progradational. Progradation changes to a short-term aggradation in the third sigmoid. The fourth and fifth sigmoids also contain prograding BBF deposits. A major aggradation episode of the platform is displayed in the later stage. A relative sea-level drop in the youngest part of RGP 6 is indicated by the downstepping of the BBF before the formation of the LW 6. Only the oldest part of RGP 7 with BBF deposits and MSCF can be seen in this view.

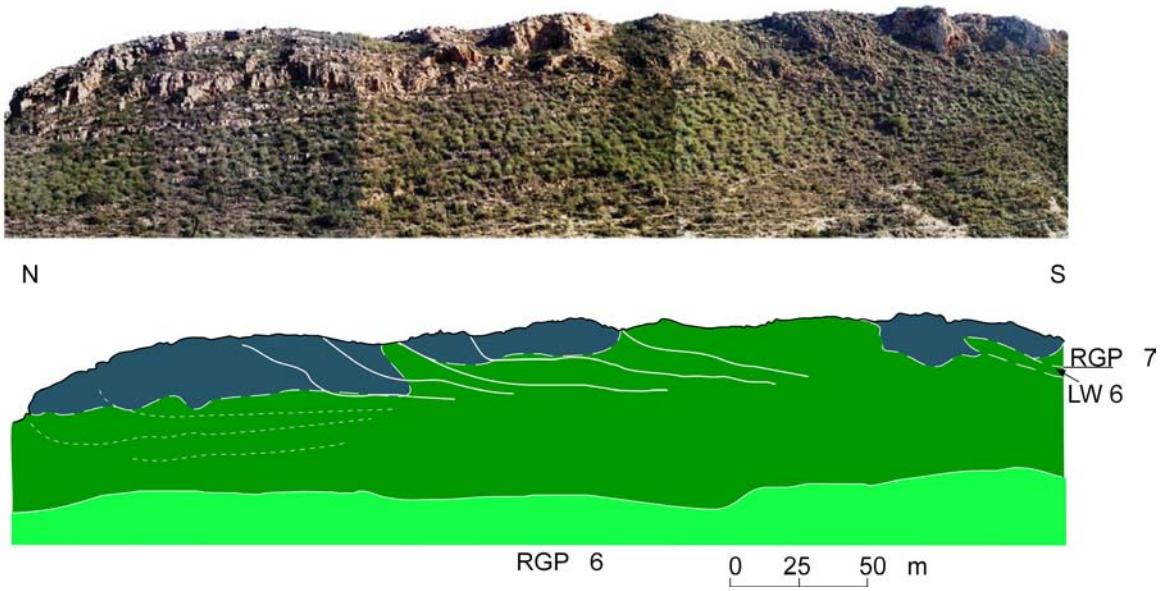

Fig. 2.14. Photo-transect along the eastern flank of the El Chive Ravine.

2.1.5 Curve of relative sea-level fluctuations

A relative sea-level curve, resulting from the superposition of the individual curves reconstructed in each ravine, is shown in Fig. 2.15. The value 0 m reflects the sea-level position at the beginning of the platform evolution. Note that the horizontal axis of the curve is not a time vector, but it represents the count of nine sedimentary cycles or RGPs in which the platform is subdivided. The curve displays a first stage of relative constant sea-level position during the RGPs 1 and 2. A highstand stage occurred during the RGP 3 and 4, where high frequency fluctuations are recognized. A general pattern of sea-level decrease shows up from RGP 5 to RGP 8. This pattern is temporally interrupted by high frequency fluctuations with slight rises in the sea-level position. The limit between RGP 7 and 8, which is the LW 7, marks the maximum lowstand position during the carbonate platform growth. RGP 9, which is not completely recorded, signals the initiation of a new phase of sea-level rise. This is deduced from the retrogradation of the RFF and the deposition of LF over the previously eroded RGPs.

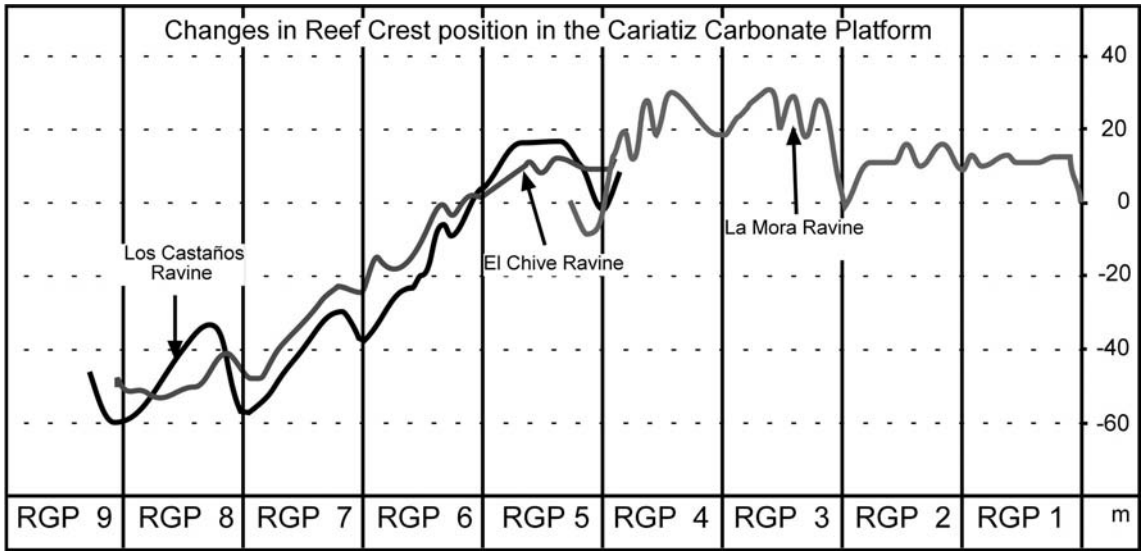

Fig. 2.15. Variations in the Reef Crest position deduced from the analysis of the reef growth geometries observed in the ravines of the Cariatiz Carbonate Platform. Examples of the geometries in these ravines are provided in the photo-transects.

2.1.6 Frequencies of sea-level changes

An age estimate of the Cariatiz carbonate platform relies on biostratigraphic and magnetostratigraphic data of the marls of the Bioherm Unit and of the overlying Yesares Member. As such, the time interval given is a maximum value. Although there is an unconformity between the Bioherm Unit and the Fringing Reef Unit (Martín and Braga, 1994) in the proximal part of the Cariatiz carbonate platform (Fig. 2.3), the limit is conformable in the center of the basin at the interface between the marls of the Bioherm Unit and the Distal Slope Marls Facies of the Cariatiz carbonate platform.

According to Braga and Martín (1996), the base of the Cariatiz carbonate platform is younger than the PF-event 4 of Sierro et al. (1993), which is 6.30 Ma old according to the magnetostratigraphic scale of Hilgen et al. (1995). For the top of the platform, two different ages have been published. An age assignment of 5.96 Ma relies on the astrochronological interpretation of the Yesares Member deposits in the Sorbas basin (Krijgsman et al., 1999), whereas Gautier at al. (1994) proposed an age of 5.90 Ma based on a paleomagnetic chronology record of the same deposits.

Braga and Martín (1992, 1996) distinguished two orders of sea-level cycles with different amplitudes and periods, which controlled the development of the Cariatiz carbonate platform. The cyclicity with a longer period has been assigned to short eccentricity changes (100 ka), whereas the short-term cycles would correspond to precessional changes (21 ka).

The amplitude of the longer term fall, because of uncertainties in depth assignment based on BBF distribution mentioned above, has a maximal value of approximately 80 m, whereas it is several tens of meters (max. 25 m) for the shorter term changes. The longer term period is reflected by the general pattern of the sea-level curve recording a transgressive, a highstand and a lowstand systems tract. The shorter term fluctuations triggered the formation of the RGPs.

During the Neogene, eustatic sea-level fluctuations were triggered by ice-volume changes. Thus, eustatism can be traced using the proxy of $\delta^{18}O$ fluctuations in deep-sea benthic foraminifers (e.g. Shackleton and Kennett, 1975, Miller et al., 1987, Prentice and Matthews, 1988). Based on this approach, Abreu and Anderson (1998) published a eustatic curve with the longer term Cenozoic variations in sea level (1 – 10 Ma). However, the shorter term sea-level fluctuations, which were the main controlling factor of the growth of the Cariatiz carbonate platform are not documented in this sea-level curve.

For the Messinian, there are a number of studies dealing with higher frequency changes of $\delta^{18}O$ (Shackleton and Hall, 1997, Vidal et al., 2002, Spezzaferri et al., 2002, Billups, 2002). Applying the concept developed by Fairbanks and Matthews (1978), which relates a fluctuation of 1 ‰ in the $\delta^{18}O$ concentration to 10 m of sea-level changes, a eustatic sea-level curve can be extracted from such data.

A comparison between the relative curve based on the reef crest positions (Fig. 2.15) and the curves based on the $\delta^{18}O$ isotope record (Fig. 16 A) was done. The curve based on Shackleton and Hall's (1997) data shows a good fit in trends and patterns with the relative curve based on the reef crest positions (Fig. 2.16 B). However, differences in amplitude of about 20 m can especially be observed in the younger part of the curves. These amplitude differences between the global and the relative sea-level curves is explained as a consequence of the regional uplift of the Sorbas basin during the Messinian which has been established at approximately 110 m/Ma by Braga et al. (2003).

A wavelet power spectrum (Fig. 2.17), using a Morlet wavelet, was applied to the isotope curve with the analysis program of Torrence and Compo (1998). This analysis demonstrates that the precessional band, the obliquity band and the short eccentricity band are well marked in the isotope data.

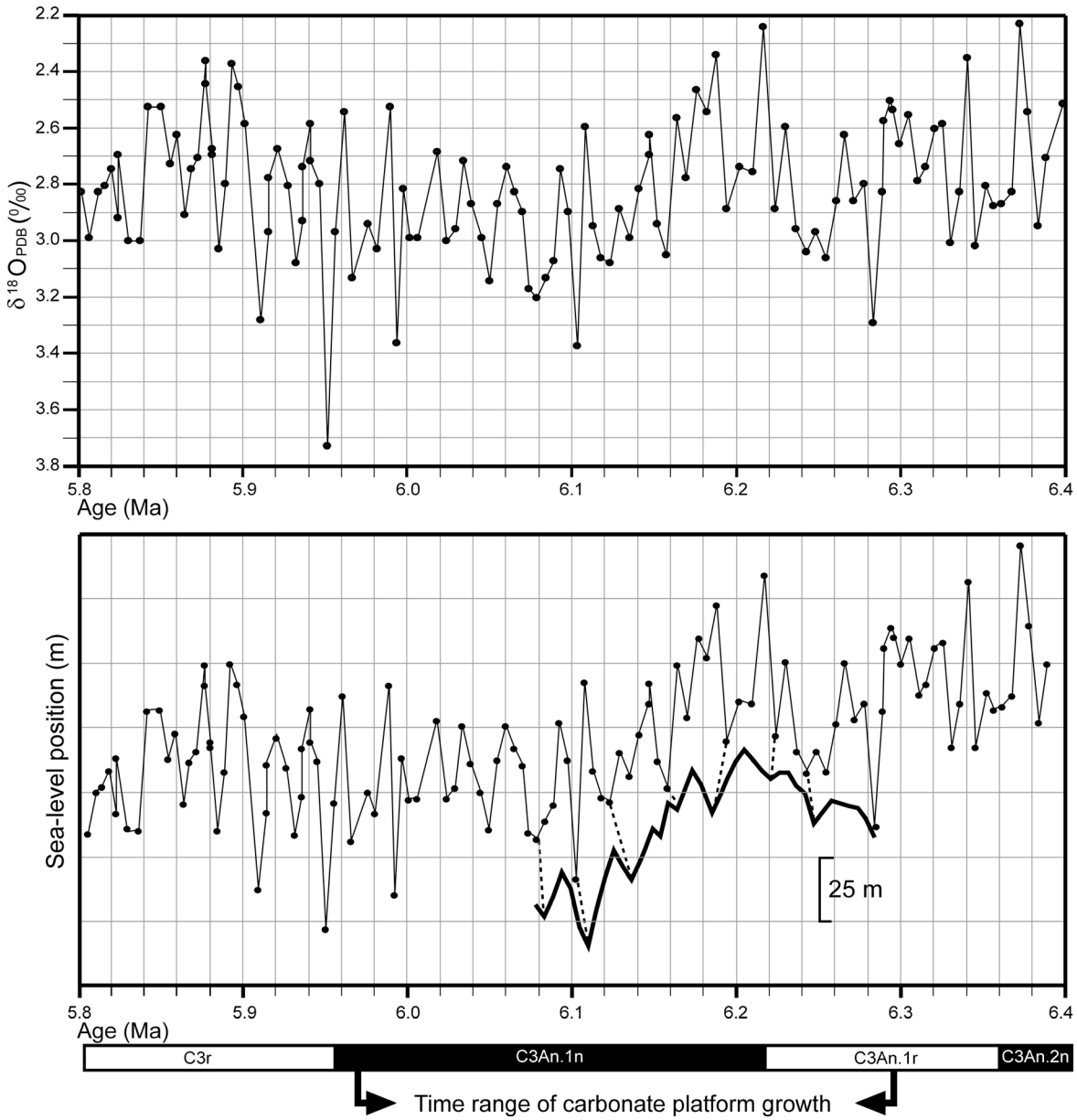

Fig. 2.16 A. Oxygen isotope record of benthic foraminifera at ODP Site 926 (Shackleton and Hall, 1997). **B.** Comparison between the sea-level curve derived from the isotope record in A. and the relative sea-level curve of the Sorbas basin derived from changes in the position of the reef crest and the BBF. Note that the trends of both curves compare well. The magnetostratigraphic scale is after Hilgen et al. (1995). Also indicated is the time interval of the carbonate platform growth.

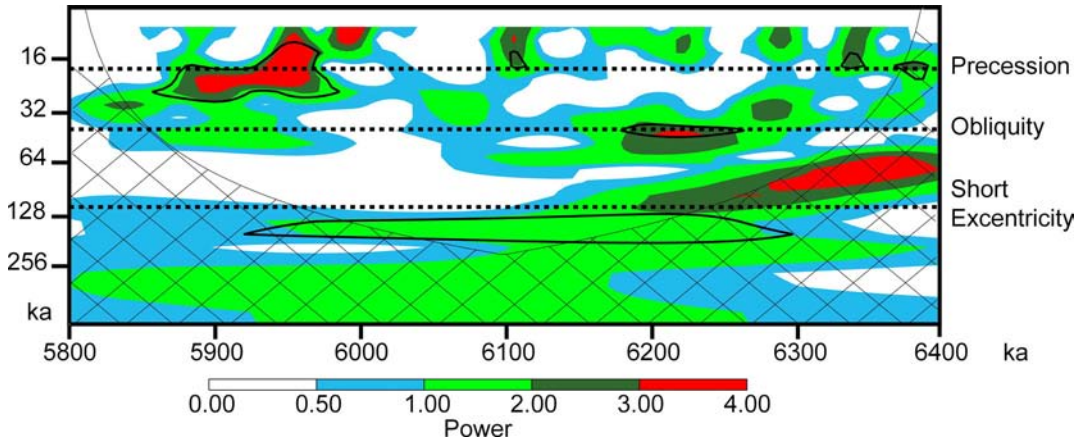

Fig. 2.17. Wavelet power spectrum of the $\delta^{18}O$ isotope record (ODP Site 926; Shackleton and Hall, 1997) between 6.4 and 5.8 Ma. The wavelet analysis was performed with MATLAB using the tool published by Torrence and Compo (1998). The hatched area represents the influence cone. Note that the obliquity signal had a stronger power up to approximately 6.15 Ma. In the younger interval, precession was dominating the high-frequency isotope signal.

The noise and the higher frequency events of the $\delta^{18}O$ isotope record are eliminated by smoothing (five points average) applied to the isotope-derived sea-level curve. The maximum sea-level fluctuations of the smoothed curve is approximately 65 m, which is slightly less than the maximal fluctuation recorded in the curve derived from the depositional geometries (maximum of 80 m) (Fig. 2.15). The value is, however, corroborated by the study of Abreu and Anderson (1998) where a long-term fall of 65 m is observed between 6.5 and 6 Ma.

2.2 The Níjar Carbonate Platform

2.2.1 Geological setting of the Almería-Níjar Basin

The Almería-Níjar Basin is a Neogene basin located south of the Sorbas Basin (Fig. 2.1). It has an NE-SW orientation and is bordered to the S by the La Serrata strike-slip fault ridge and the Cabo de Gata volcanic complex. To the N, the basin is delimited by the Sierra Alhamilla, and to the E by the Sierra Cabrera. To the SW, the basin opens to the Mediterranean Sea. The metamorphic basement of the Almería-Níjar Basin is part of the Internal Betic Zone and predominantly consists of meta-schists and quartzites from the Paleozoic Nevado-Filábride complex, and Triassic dolomites from the Alpujárride complex (Dabrio et al., 1981). The Cabo de Gata volcanic complex is between 14 and 7.5 Ma old (Fernández-Soler, 1992). Volcanic activity also occurred along the northern margin of the Almería-Níjar Basin, at the locality of the Cerro del Hoyazo. The eruption of these cordierite-garnet bearing dacites occurred approximately between 6.57 to 6.2 Ma (Zeck and Williams, 2002, Duggen et al., 2004).

The Neogene basin fill consists of several marine unconformity-bound units. Fig. 2.18 shows a comparison of five different stratigraphic schemes proposed for these deposits by different authors (Dabrio et al., 1981, Franseen and Mankiewicz, 1991, Martín and Braga, 2001, Warrlich et al., 2005). The age assignment of the different units relies on biostratigraphic data (Addicott et al., 1979, Serrano, 1990), absolute age dating of volcanic rocks (Zeck and Williams, 2002, Duggen et al., 2004), and strontium dating of carbonates (Warrlich et al., 2005). In the present study, the stratigraphic subdivision of Martín and Braga (2001), which uses the same Tortonian and Messinian stratigraphic units previously described for the Sorbas Basin, was applied. This scheme is a refined subdivision of the work of Dabrio et al. (1981).

The oldest Neogene marine sediments in the Almería-Níjar Basin consist of intensely folded marls and diatomite layers probably Serravalian-Langhian in age described as Older Neogene Deposits by Dabrio et al. (1981). Breccias and conglomerates, which also occur in this unit, are related to processes of karstification affecting Triassic dolomites of the basement. The Older Neogene Deposits are unconformably overlain by the Marginal Terrigenous Complex (Dabrio et al., 1981), which was assigned to the Azagador Member by Megías (1985) and Martín and Braga (2001). The deposits of the Azagador Member of the Almería basins were dated by Iaccarino et al. (1975) and Serrano (1979) with planktonic foraminifers as late Tortonian to early Messinian in age. The deposits consist of microconglomerates and calcareous sands with an upward-increasing bioclastic content. Distally, the Azagador deposits grade into yellow siltites and marls (lower Abad Mb.) with

tempestitic layers. An older age, Serravallian to early Tortonian, of the Marginal Terrigenous Complex was suggested by Franseen and Mankiewicz (1991).

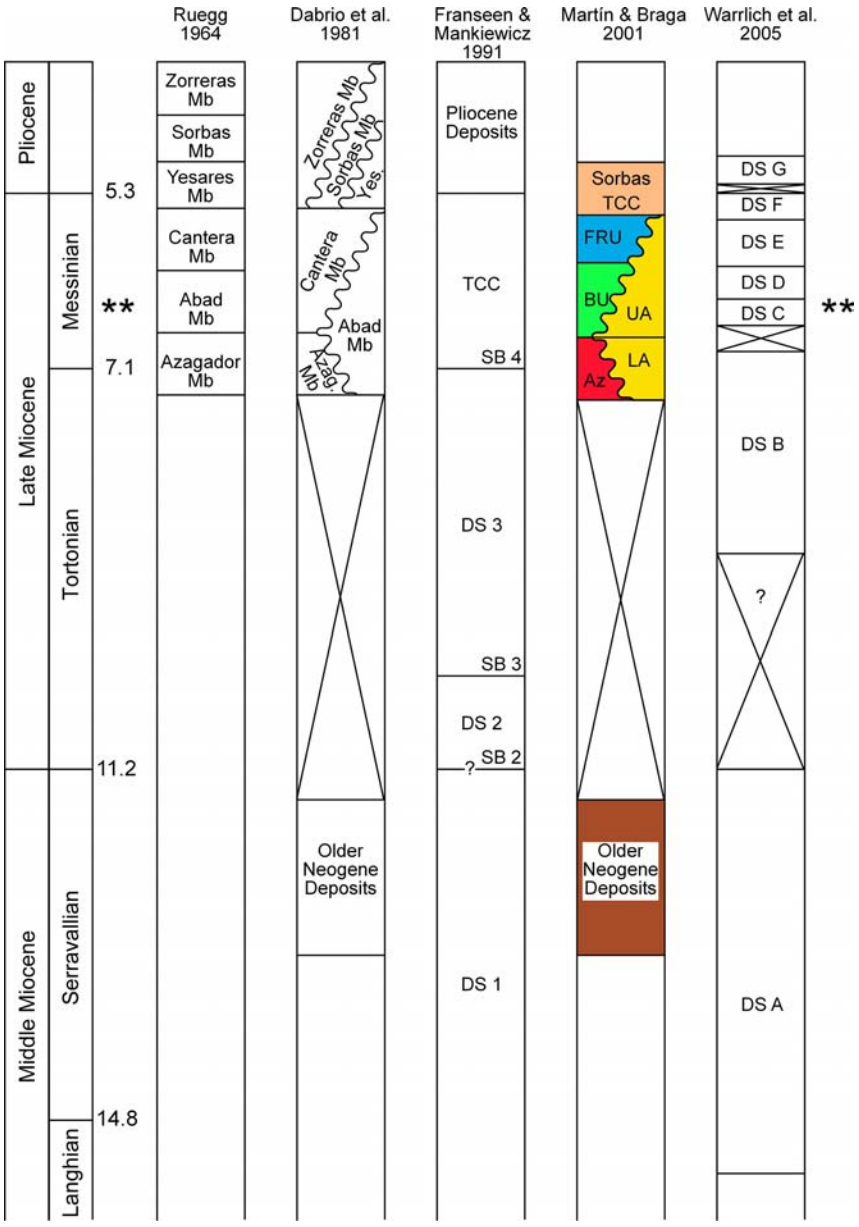

Fig. 2.18. Summary of the different stratigraphic models of the Níjar Carbonate Platform. In this study, the interpretation of Martín and Braga (2001) has been used. Asterisks show the age of the volcanic rocks.

.

Well-stratified siltites and marls overlie the Azagador Member. Locally, bioherms, formed by serpulids and coralline algae, are preserved interfingering with the marls. This unit was correlated by Martín and Braga (1993) to the Bioherm Unit described in the Sorbas Basin.

The siltites and marls of the Bioherm Unit are overlain by the FRU, formed by *Porites* reefs and stromatolitic crusts in the shallow-water part of the platform, grading into

calcarenites and marls of the proximal and distal slope (Riding et al., 1991, Martín and Braga, 1994). The next younger depositional unit (Yesares Mb.), which only occurs in the basin center, consists of evaporites intercalated with marls deposited during the MSC. The basin margins were exposed (Franseen and Mankiewicz, 1991), and an erosional unconformity separates the FRU of the younger units.

The FRU of the Níjar Carbonate Platform is unconformably overlain by the TCC, which consists of large stromatolites and thrombolites, *Porites* reef patches and oolitic bars (Esteban, 1979, Esteban and Gíner, 1980, Riding et al., 1991). Riding et al. (1991) have postulated that the TCC formed after the reflooding of the Mediterranean Sea, whereas Van de Poel (1991) and Fortuin and Krijgsman (2003) suggest that the formation of the TCC was coeval with the deposition of the evaporitic deposits during the MSC. The TCC is partially overlain by the marls of the Feos Formation (Van de Poel, 1991), which was interpreted as the post-evaporitic "Lago-Mare episode" (Hsü et al., 1977, Rouchy et al. 2001). The youngest unit in the Almería-Níjar Basin is the Pliocene Cuevas Fm with fossiliferous calcisiltites and calcarenites (Cuevas Formation, Völk and Rondeel, 1964).

2.2.2 Location and geological map of the Níjar Carbonate Platform

The Níjar carbonate platform is located along the northern margin of the Almería-Níjar basin, at the foothills of the southern flank of Sierra Alhamilla (Fig. 2.1). The area of the Níjar Carbonate Platform is covered by the sheets 4-1 and 4-2 (sheet 1045, 1:10000), and 1-1 and 1-2 (sheet 1046, 1:10000) of the topographic map of Spain. The geographical coordinates are 30SWF571485-576593 408999-409363. The study area covers a total surface of approximately 19 km^2 (Fig. 2.19).

Older Neogene Deposits

This unit crops out in an approximately 300 m wide W-E running strip bordering the road from Níjar to Lucainena. Further, spatially disconnected outcrops of breccia and conglomerates occur N of the Cerro de la Rellana.

Azagador Member

The Azagador Mb unconformably overlies the Older Neogene Deposits, but also covers a large area at and E of the Cerro de la Campana, where it unconformably rests on the metamorphic basement. Several of the facies known from the Azagador Mb. (Martín et al. 1996) also occur in the sedimentary succession of the Níjar Carbonate Platform. The transition between the shoals and the factory zone is located in the area of "El Cortijo del Álamo" near the village of Níjar. The outcrop S and SE of the "Embalse de Isabel II" is

composed of reddish calcarenites with abundant reworked fossils, such as bivalves (pectinids), echinoids, brachiopods and rhodolithes. According to the model of Martín et al. (1996), this facies was probably deposited in the shoal area.

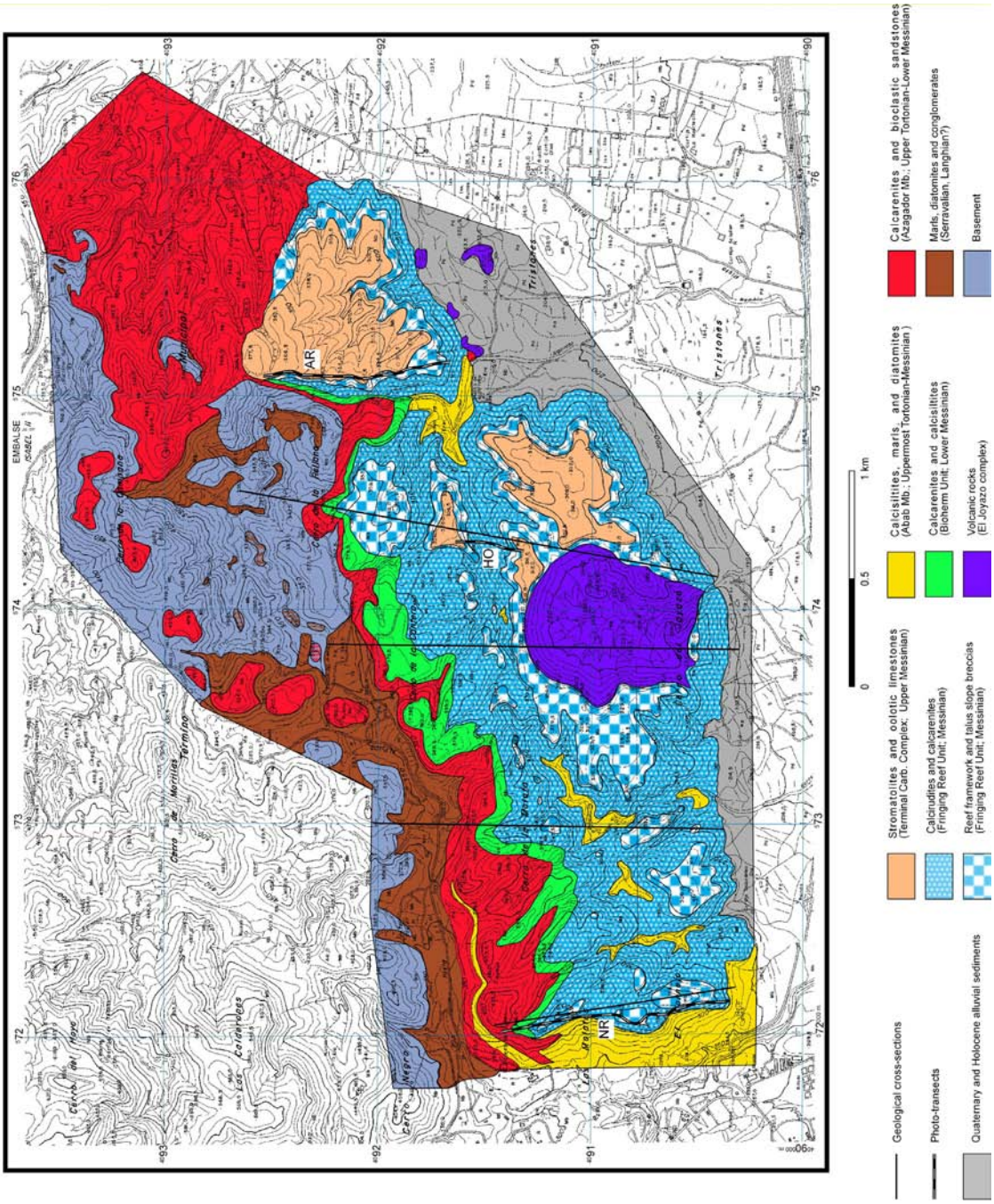

Fig. 2.19. Geological map of the Níjar Carbonate Platform with the positions of the geological sections and the photo-transects.

In the western zone of the Níjar Carbonate Platform, the Azagador Member outcrops in the well-exposed section of the Las Molatas, which is the northern termination of the Níjar Ridge. This area contains more distal facies, which probably belong to the shoal or factory

zone of the cool-water carbonates. These calcarenites and bioclastic sandstones interfinger with calcisiltites of the Abad Mb.

The Abad Member

The Abad Mb. is the distal facies of the Azagador Mb., Bioherm Unit, and FRU. The Abad Mb crops out along the Níjar Ridge, at the bottom of ravines located between the Níjar Ridge and the Cerro del Hoyazo, and at the bottom of the Algarrobo Ravine. On the geological map, the Abad Mb. has not been subdivided into different facies, although Warrlich et al. (2005) subdivided the Abad Mb. into three packages attributed to different depositional sequences (DS C – E).

The volcanic dome of the Cerro del Hoyazo

The volcanic dome of the Cerro del Hoyazo with an approximate diameter of 800 m, is located near the southern margin of the mapping area. More volcanic rocks outcrop between the Algarrobo Ravine and the locality Los Tristanes. The volcanic rocks are high-potassium calc-alkaline dacites (Zeck, 1970, Zeck and Williams, 2002). Partially digested metamorphic rocks and euhedral garnets are very common. At the southern end of the Algarrobo Ravine, an outcrop shows partially assimilated calcarenites of the Azagador member. This shows that the volcanic eruption occurred after the deposition of the Azagador Mb, which is corroborated by an $^{40}A/^{39}A$ age date of 6.57 Ma for the Cerro del Hoyazo rocks (Duggen et al., 2004).

The Bioherm Unit

Deposits of the Bioherm Unit outcrop to the S of the Azagador Mb. in a W-E strip. The predominant facies are siltites and marls. Bioherms are only preserved in the Algarrobo Ravine. These sigmoidal-shaped bioherms show an internal layering, where layers with abundant remains of serpulids, coralline algae and bivalves interfinger with siltites and marls. The Bioherm Unit has a thickness of several meters (20-25 m) and dips 20° to 25° towards the south.

The Fringing Reef Unit

Three different facies of the FRU were mapped in the Níjar area: a reef-core facies formed by reef framework and talus slope breccia, a calcirudites-to-calcarenites facies, and the distal calcisiltites (Abad Mb.). No lagoonal deposits of the carbonate platform are preserved at Níjar. The outcrops of reef-core deposits, RFF and BBF, are located on the top of small hillocks, fringing the paleorelief formed by the volcanic dome of the Cerro

del Hoyazo. The predominant lithologies are breccias composed of blocks and bioclasts with abundant remains of corals (*Porites*), bivalves (*Venus* and pectinids), and regular echinoids. In some outcrops, the corals and stromatolites are preserved *in situ* forming small patches.

The BBF grades to well-stratified MSCF of the fore-reef area. The calcarenites are composed of reworked carbonate sands from the reef system, and remains of bivalves, serpulids and coralline algae. The S-SW dip of the layers varies between 2° and 5°.

The distal slope facies in the Níjar Carbonate Platform consists of calcisiltites and marls, which overlie the Lower Abad Member. The main outcrop of the distal facies is located in the section of "Las Molatas". In this outcrop, marls and well-stratified calcisiltites dip 3°to the SW. Other distal slope marls outcrops are located at the bottom of ravines which dissect the Níjar Carbonate Platform -- for example the Cebollero Ravine or the Algarrobo Ravine. These outcrops are characterized by flat-lying, well-cemented calcisiltites.

The Terminal Carbonate Complex (TCC)

Several outcrops of the TCC with cross-bedded oolites, small reef patches, and stromatolites are preserved in the proximity of the Algarrobo Ravine. Another outcrop of the TCC is located at the eastern flank of the Algarrobo Ravine. In the northern part of the ravine, the oolitic bars are the most common features, and small stromatolites can also be found. To the S well-preserved reef patches with stromatolites overlie the breccias and blocks of the FRU. Reef patches are formed by *Porites* and stromatolitic crusts.

Quaternary and Holocene alluvial sediments

The youngest mapping unit in the Níjar Carbonate Platform is the Quaternary deposits, which consist of alluvial conglomerates, sands and clays. This unit overlies the distal deposits of the FRU.

Cross-sections of the Níjar Carbonate Platform

Fig. 2.20 shows several N-S oriented cross-sections through the Níjar Carbonate Platform. This orientation is roughly parallel to the direction of platform progradation. The paleohigh of the Cerro del Hoyazo was fringed by a small atoll-like platform with a radial progradation, which is also shown in the cross-sections. There is no evidence of a tectonic tilt.

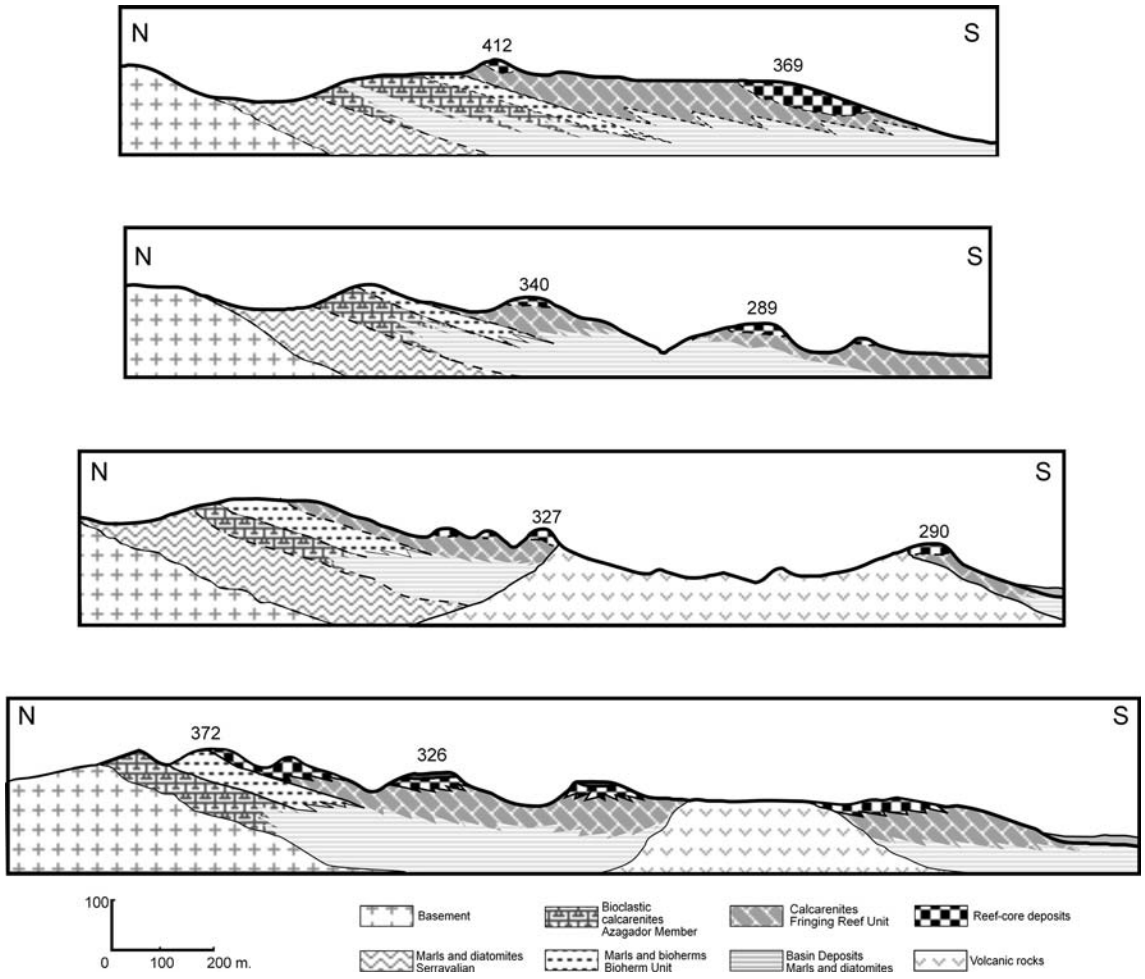

Fig. 2.20. Geological cross-sections of the Níjar Carbonate Platform. The position of the sections is shown in the geological map (Fig. 2.19).

2.2.3 Initial topography of the Níjar Carbonate Platform

Based on the cross sections and on the mapping of the basal surface of the FRU, the initial topography of the carbonate platform was reconstructed. A rectangular grid of approximately 80 x 80 m mesh size, covering the entire study area, was developed by assignment of height positions to the individual grid points. This way, a rectangular matrix with 56 rows (N-S direction) and 62 columns (W-E direction) was generated, with each element representing the height value previous to platform growth.

The shape of the initial topography is shown in Fig. 2.21. The model domain has an extension of approximately 5.0 x 4.7 km. The initial water level used for the modeling is depicted in Fig. 2.21. The initial sea-level position was estimated according to the location and altitude of the oldest FRU deposits. The direction of the shoreline is ENE-WSW. The maximum water depth of the modeled domain is 240 m over a shore to basin distance of

4.7 km. The initial surface has variable slope angles. Three kilometers basinwards of the shoreline, slope angles increase from 5° up to 15°. The volcanic dome of the Cerro del Hoyazo is located at this break of slope angles. The volcano has slopes dipping with approximately 20° - 25°.

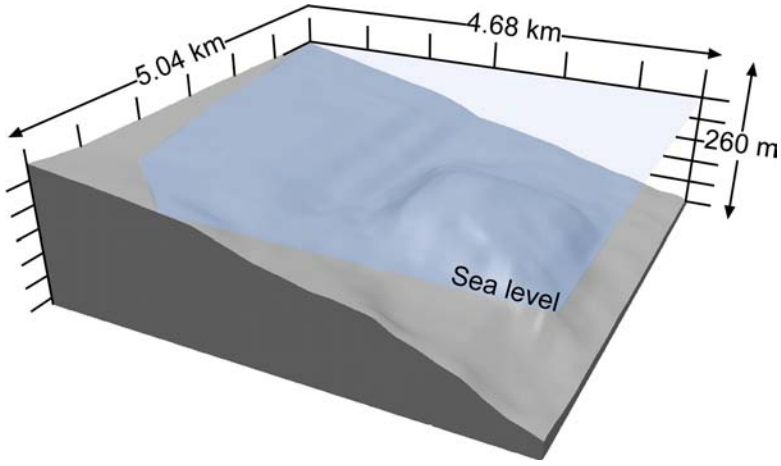

Fig. 2.21. Initial topography of the Níjar Carbonate Platform. Note the paleo-high formed by the volcanic dome in the central area of the initial surface.

2.2.4 Depositional geometries and relative sea-level changes

The internal growth geometries and the facies distribution of the Níjar Carbonate Platform were analyzed in several ravines, which dissect the platform. Two photomosaics, parallel to the direction of progradation, were reconstructed along the flanks of The Níjar Ridge and the Algarrobo Ravine. The third photomosaic was analyzed along a small ravine to the NE of the Cerro del Hoyazo.

The Níjar Carbonate Platform, in contrast to the Cariatiz Carbonate Platform, does not contain lowstand wedges. Therefore, the RGPs were defined as the stack of sediments deposited during two consecutive downstepping BBF packages, which represent Falling Stage Systems Tracts. Five RGPs were recognized in the platform.

2.2.4.1 The Níjar Ridge

The photo-transect of the Níjar Ridge (Fig. 2.22) covers about 1 km of outcrop. This section displays the entire progradation of the Níjar Carbonate Platform (Dabrio et al., 1981, Jiménez and Braga, 1993).

In the Níjar Ridge, the FRU unconformably overlies the Bioherm Unit. The oldest RGP of the platform, RGP 1 and RGP 2, are dominated by subhorizontal MSCF strata. Small BBF outcrops are located at the top of the hillocks. It is assumed that these patches are erosive remnants of more extensive reef-core deposits. RGP 3 contains a 150 m wide outcrop of

reef-core deposits in the younger part of the package. BBF layers dip to the S with approximately 15° and interfinger with and prograde upon subhorizontal layers of MSCF. Reef-core deposits of RGPs 4 and 5 are massive and characterized by downstepping.

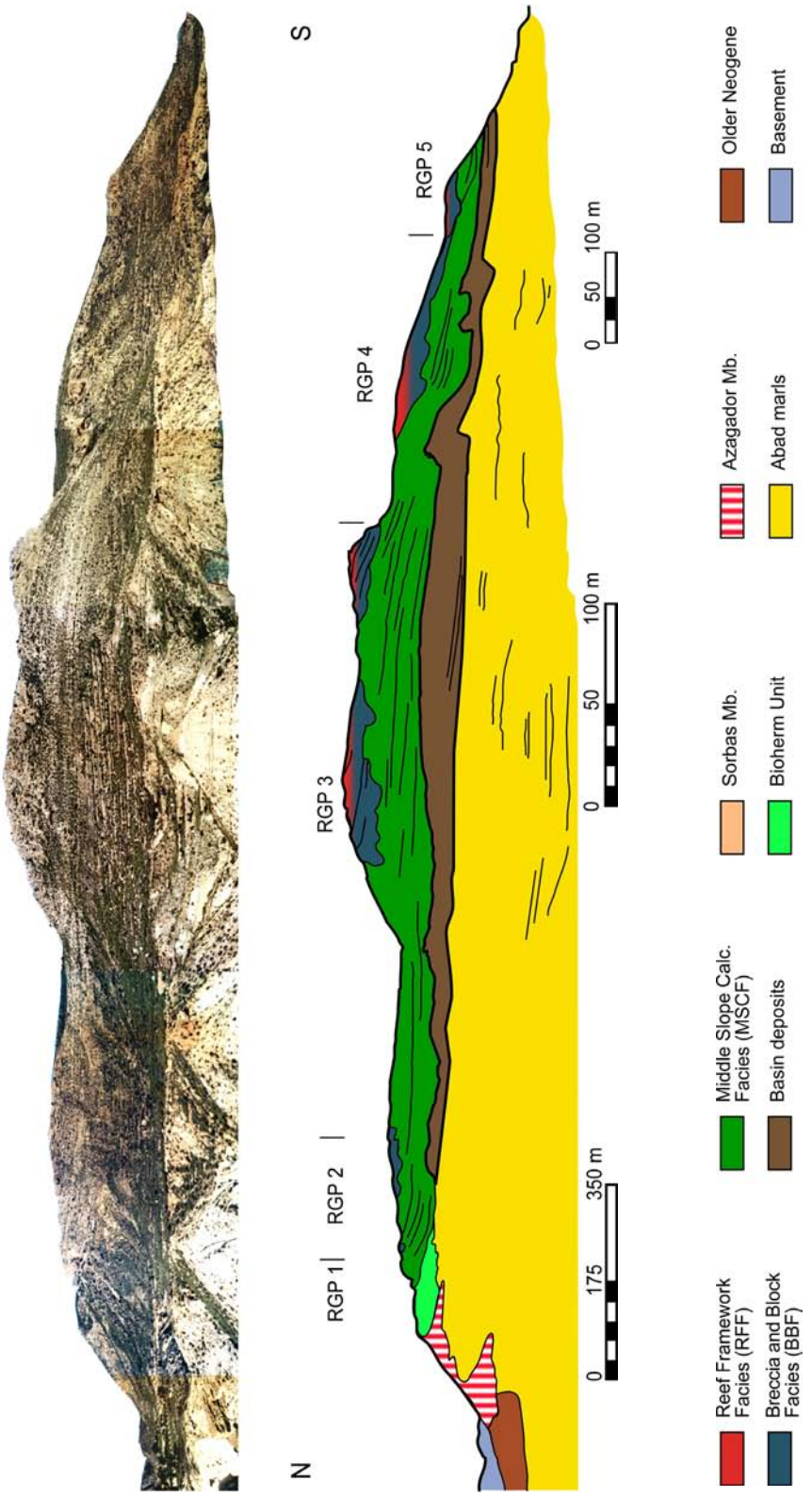

Fig. 2.22. Photo-transect along the Níjar Ridge, the westernmost margin of the Níjar Carbonate Platform. The legend shows the FRU facies, as well as the stratigraphic units that outcrop in the photo-transects of the Níjar Carbonate Platform (Figs. 2.22, 2.23, 2.24). The distortion of the photo-transect was considered using different scales.

2.2.4.2 The Algarrobo Ravine

The photo-transect in the Algarrobo Ravine covers about 700 m of platform rim progradation (Fig. 2.23). The RGP limits are poorly defined in this transect, and boundaries were traced at the limits of offlapping to aggrading or prograding sediment geometries. In this section, the most proximal part of RGP 1 consists of BBF deposits, which overlie the Bioherm Unit. Distally, the BBF sediments grade into MSCF deposits with a dip of about 10°. RGP 2 is characterized by poorly-stratified BBF deposits at the top of the section, which interfinger with subhorizontal layers of MSCF deposits. The upper limit of RGP 2 is placed above an interval characterized by a strong downstepping of BBF deposits. RGP 3 has an offlapping geometry and is dominated by inclined banks of reef-core deposits dipping at about 15°. Downslope, these deposits interfinger with MSCF with a gentler dip. The limit between RGPs 3 and 4 is defined by a backstepping of the BBF deposits. RGP 4 has an offlapping growth pattern.

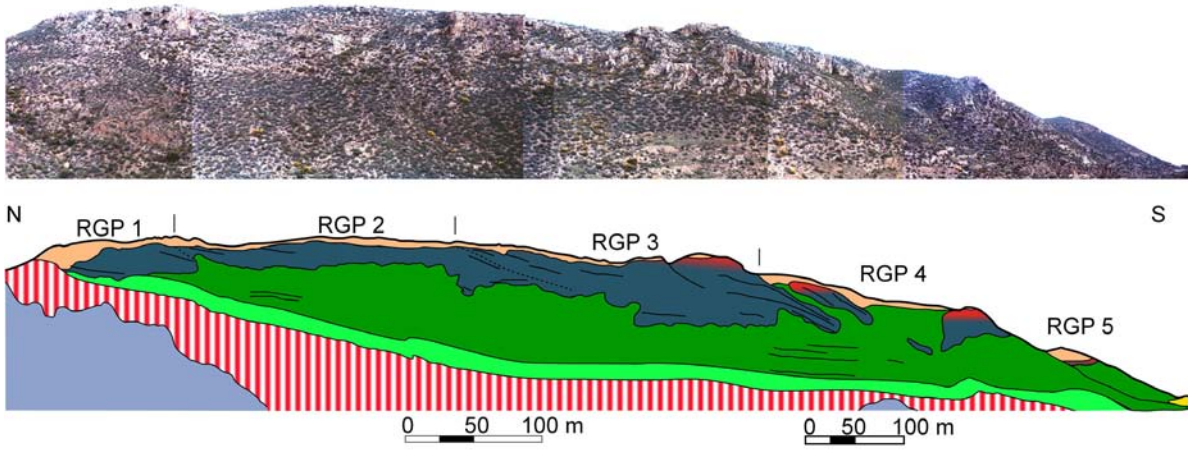

Fig. 2.23. Photo-transects of the eastern flank of the Algarrobo Ravine. Note the downstepping of the reef-core facies towards the south.

2.2.4.3 Proximity of the volcanic dome of the Cerro del Hoyazo

This photo-transect (Fig. 2.24) shows the different direction of platform rim progradation in the area N of the volcanic dome during formation of RGP 4. At this stage of the platform evolution, a shallow-water carbonate factory had established on the volcanic dome and an annular fringing reef system detached from the main carbonate platform formed on the slopes of this paleohigh. On the northern flank of the volcano, this rim prograded towards the N, whereas the rim of the main platform prograded to the S. The low separating both reef rims was interpreted as the main drainage channel of the reef system by Dabrio et al. (1985). The photo-transect shows dips of 20-25° to the North and

dips of 18-20° to the South. BBF deposits occur at the top of both flanks of the ravine. These deposits interfinger with MSCF layers, with the dip of the later decreasing downslope.

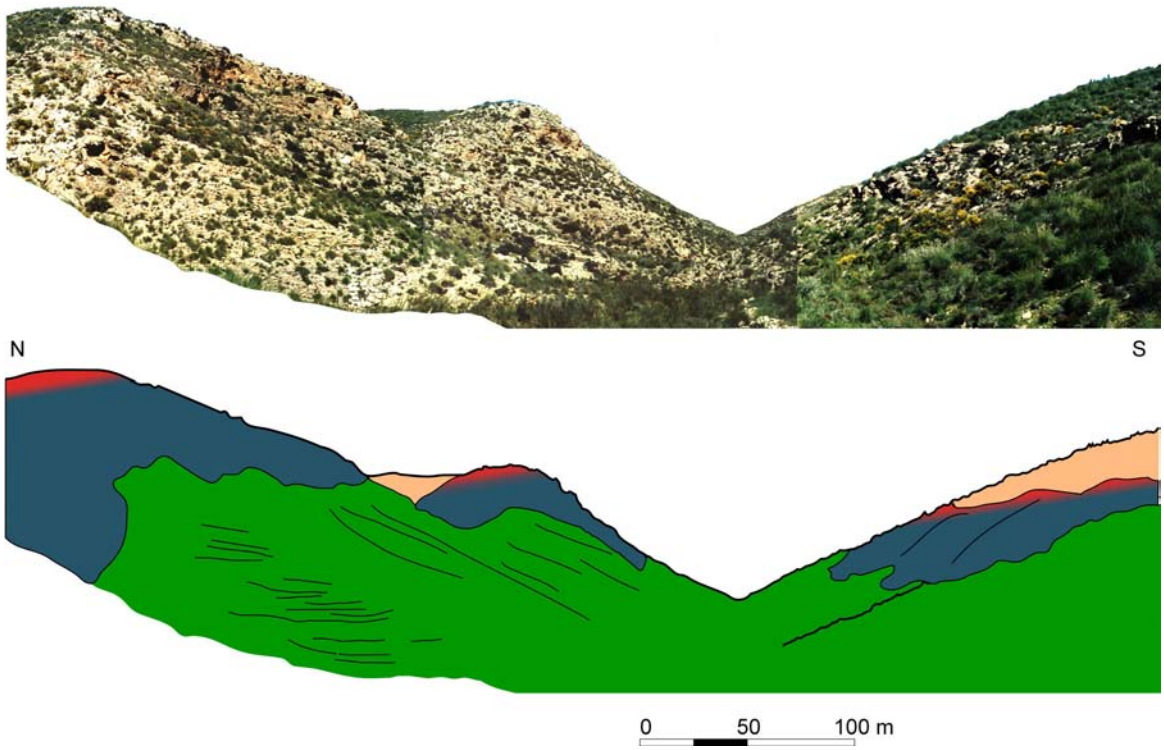

Fig. 2.24. Photo-transect along the main drainage channel of the Níjar Carbonate Platform. The volcanic dome of the "El Hoyazo" is located to the South and this paleohigh triggered the progradation landwards of the platform deposits.

2.2.5 Curve of relative sea-level fluctuations

To reconstruct a curve of relative sea-level changes for the Níjar Carbonate Platform, the sections along the Níjar Ridge and the El Algarrabo Ravine were used. Fig. 2.25 shows the curve for each of the transects.

The boundary or the transition between the BBF and the MSCF was used as indicator of sea-level fluctuations. The boundary has depth assignment uncertainties, which were partially solved by a calibration of the boundary in areas of the carbonate platform where the reef-core deposits occurs together with patches of in situ *Porites* and stromatolites, suggestive of deposition near sea level. It appears that the platform growth occurred during a longer term sea-level fall of around 80 m with a superposition of five higher frequency fluctuations.

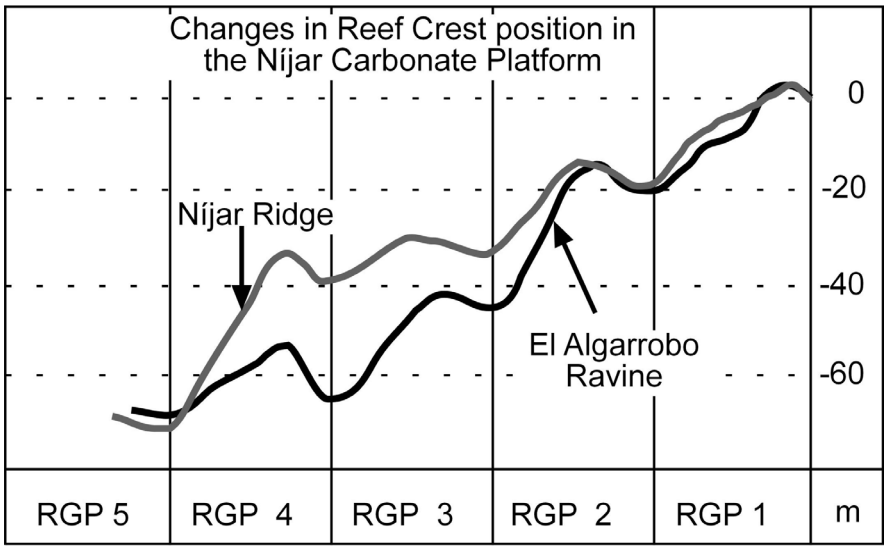

Fig. 2.25. Oscillation in the reef crest position according to the reef growth geometries observed along the ravines which dissect the Níjar Carbonate Platform.

If the sea-level curve of the Níjar Carbonate Platform is compared to the curve of the Cariatiz Carbonate Platform (Fig. 2.26), a good fit is achieved if one correlates the Níjar RGPs 1 –5 with the Cariatiz RGPs 4 – 8. This is corroborated by the newest age models for the Níjar Carbonate Platform (Duggen et al., 2004, Warrlich et al., 2005), which indicate that platform growth occurred between 6.2 and 5.9 Ma. This implies that the entire development of the Níjar Carbonate Platform occurred during 100 ka. Consequently, the platform growth geometries reflect the precessional and the short eccentricity cycles.

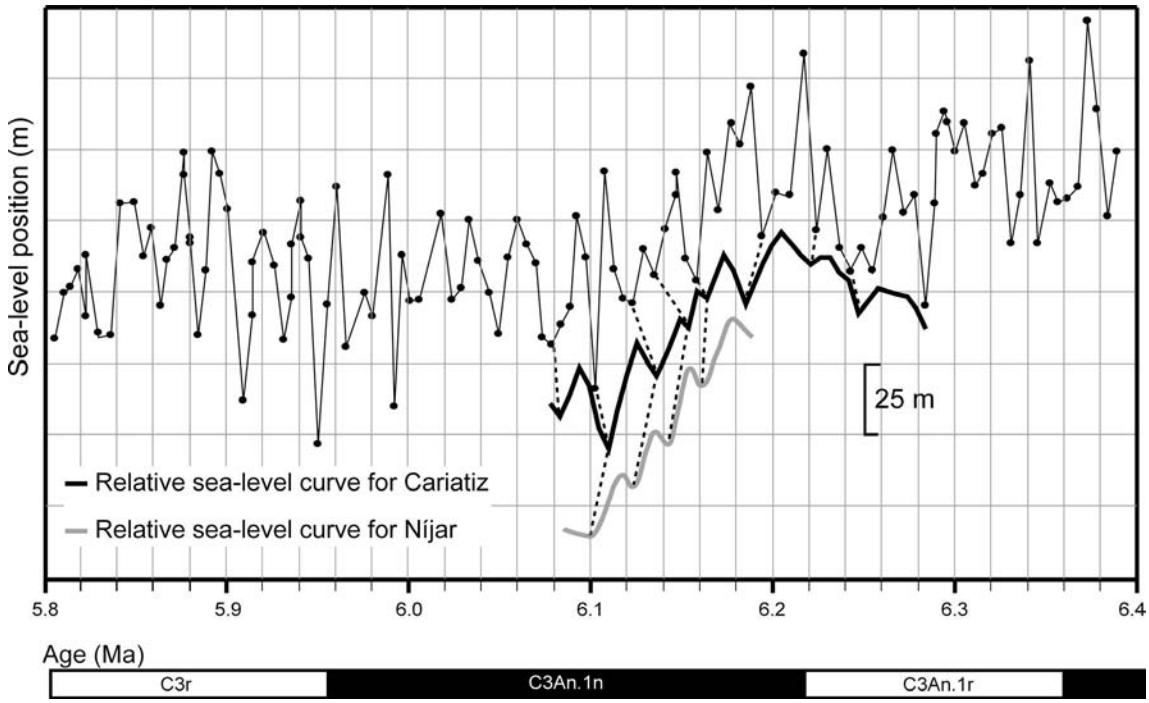

Fig. 2.26. Comparison between the relative sea-level curve of the Níjar platform based on growth geometries with the isotope and the Cariatiz curves.

2.3 The Las Negras Carbonate Platform

The Las Negras Carbonate Platform in the Cabo de Gata volcanic province was visited in order to text the feasibility of a computer modeling of this system. It will be shown, however, that several aspects of the geology of the Las Negras Carbonate Platform impede modeling it with REPRO. The main reason is that the platform was affected by significant synsedimentary tectonic movements and that the actual version of REPRO cannot take into account such processes during platform growth. It is especially not possible to display the morphological change of the initial topography caused by the synsedimentary uplift movements with the visualization program. Moreover, the lack of chronostratigraphic markers in the deposits does not allow a good assessment of the time interval involved in the reef development.

2.3.1 Geological setting of the Las Negras Carbonate Platform

At Las Negras, a Neogene carbonate platform overlies the Cabo de Gata volcanics, which formed from 16 to 6 Ma (López and Rodríguez, 1980; Bellon et al., 1983; Di Battistini et al., 1987). This calc-alkaline volcanism is related to the compression caused by the collision of the African and the Iberian plates. Two different stratigraphic models were proposed for the Las Negras Carbonate Platform (Fig. 2.27). According to Martín and Braga (1993), the Neogene sedimentary units in Las Negras area correlate to the sedimentary units described in the nearby Almería-Níjar Basin and Sorbas Basin. Reef deposits are assigned to the Bioherm Unit and the Fringing Reef Unit. The stratigraphic model presented by Franseen and Mankiewicz (1991, 1993), Franseen and Goldstein (1996), and Montgomery et al. (2001) subdivides the Las Negras succession into five depositional sequences.

Both models differ by their age assignment of the distinct units, but also in their sedimentological interpretation. The major difference in the sequence-stratigraphic models is the interpretation of the DS 2 or Bioherm Unit. Franseen and Mankiewicz (1991) and Montgomery et al. (2001) interpreted the coral blocks of DS 2 as a lowstand megabreccia, whereas Martín and Braga (1993) interpret this interval as the Bioherm Unit with reef mounds and coral blocks. According to Martín and Braga (1993), the blocks were produced by submarine breakage of shallow patch reefs and bioherms, as it is observed at the Hueli area in the Sorbas Basin.

Biostratigraphic, paleomagnetic, and $^{40}Ar/^{39}Ar$ analyses were carried out in the Cabo de Gata volcanics and sediments in order to establish age models of the different stratigraphic units (Esteban, 1979; Addicott et al., 1979; Bellon et al., 1983; Di Battistini et al., 1987; Mankiewicz, 1987; Franseen et al., 1988; Serrano, 1990; Franseen and Mankiewicz, 1991;

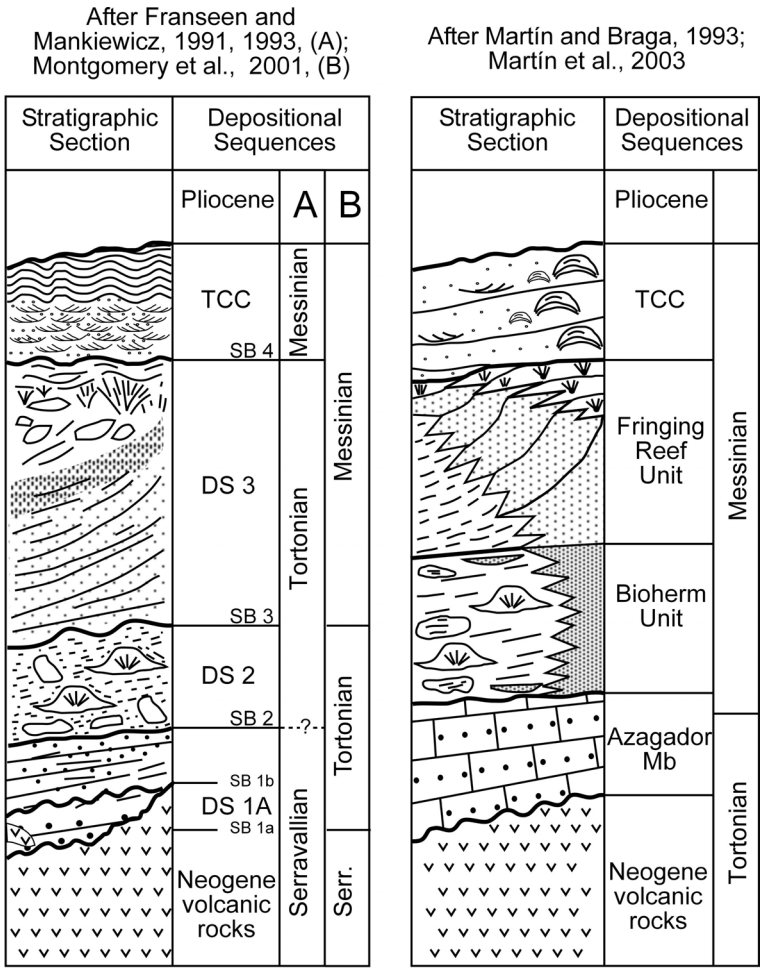

Fig. 2.27. Stratigraphical models for the Las Negras Carbonate Platform

Montgomery et al., 2001; Duggen et al., 2004). Herein, the stratigraphic model and the age model proposed by Martín and Braga (1993) were adopted. It is based on a planktonic foraminiferal age of marls on top of the volcanics (Serrano, 1990), the radiometric data provided by Bellon et al., (1983) and Di Battistini et al., (1987), and the correlation to the well-dated reefs of the Sorbas Basin (Riding et al., 1991).

2.3.2 Location and geological map of the Las Negras Carbonate Platform

The Las Negras Carbonate Platform is located at the SE margin of the Almería-Níjar basin, in a depression of the volcanic chain. The area of the Las Negras Carbonate Platform is covered by sectors of the sheets 2-3, 3-3, 2-4, and 3-4 (sheet 1046, 1:10000) of the topographic map of Spain. The geographical coordinates are 30SWF587060-589200 407988-408191 (Fig. 2.28). The study area covers a surface of approximately 4.25 km^2. The basement of the Las Negras Carbonate Platform consists of andesites and dacites of the Cabo de Gata volcanic region (Duggen et al., 2004), which have been age dated as late Serravallian to early Messinian.

Azagador Member

The Oldest Neogene sediments in Las Negras area pertain to the Azagador Mb. At the base of this unit, volcaniclastic and carbonate conglomerates overlie the volcanic basement. Outcrops of this facies are located in the western area of the La Molata, and in the eastern part of the La Molatilla hillock (Fig. 2.28). In the NNW part of the La Molata, the deposits of the Azagador Mb wedge out due to postdepositional abrasion.

The conglomerates are overlain by calcarenites with abundant red algae, mollusks, and brachiopods. Distally, the calcarenites interfinger with burrowed calcisiltites and marls, which contain abundant remains of mollusks, brachiopods, echinoids, as well as molds of mollusks. *Thalassinoides burrows* are abundant in the area of the Castillo de San Ramón (ESE of La Molata).

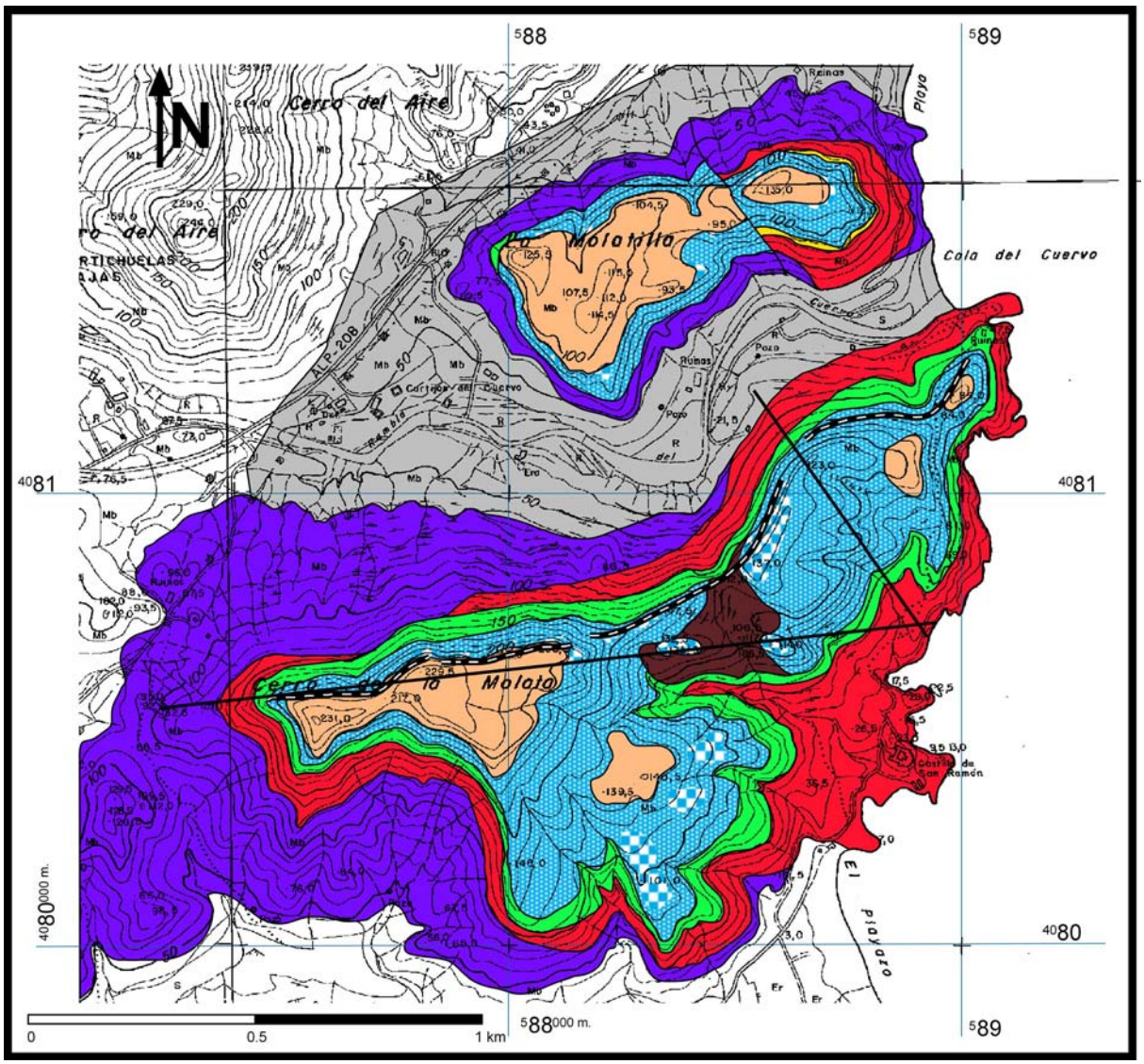

Fig. 2.28. Geological map of the Las Negras Carbonate Platform. Color-code according to the map of the Níjar Carbonate Platform. The brown deposits are the volcaniclastic and carbonate sands.

The Bioherm Unit

The Azagador Mb. is overlain by the early Messinian Bioherm Unit. In the Las Negras area, the Bioherm Unit consists of (1) well-stratified fine-grained silts and calcarenites; (2) bioherms with serpulids, *Halimeda*, red algae and corals, which are mainly *Porites* and *Tarbellastrea*; (3) coral blocks and breccias, shed from the bioherms on the platform margin; and (4) channelized calcarenites. Outcrops of this unit are principally located at La Molata; only a small outcrop with abundant *Tarbellastrea* was mapped in the westernmost part of La Molatilla.

The thickness of the Bioherm Unit varies from 2 m in proximal areas up to 30 m in most distal zones. The maximum thickness of the Bioherm Unit is in the central part of the northern flank of the La Molata hillock, where large bioherms, formed by serpulids, *Porites, Tarbellastraea, Siderastraea,* foraminifera, red-algae, mollusks and gastropods, are well-preserved. The layers of the Bioherm Unit dip between 10 to 20° to the E or SE. The bioherms are embedded into silty marls, which drape around the morphology of the bioherms. The distal areas of the Bioherm Unit are located toward the SE of La Molata. Distal outcrops are composed of white marls with abundant fish remains.

The Fringing Reef Unit

The FRU deposits of the Las Negras Carbonate Platform are subdivided into four facies. The uppermost deposits of the FRU consist of reef-core deposits which are formed by RFF patches with *Porites* and stromatolitic crusts. These sediments crop up together with massive- to poorly-stratified proximal slope BBF deposits. Remains of mollusks, serpulids, regular echinoids, encrusting organisms such as coralline red algae and foraminifers, gastropods and minor amounts of green algae are also found filling the voids of the reef framework. The reef-core deposits interfinger with well-stratified middle slope calcirudites and calcarenites.

Locally, the calcarenites occur interbedded with volcaniclastic and carbonate sands. This sediment package is represented in brown on the geological map. Franseen and Mankiewicz (1991) interpreted these strata as being deposited during a relative fall in sea-level. The trigger of the sea-level drop cannot be resolved with our data. A synsedimentary tectonic uplift, however, may have been implied, as the next younger sediment package overlies these sediments with an angular unconformity.

At the easternmost termination of the La Molata, the youngest stages of the Carbonate Platform evolution of the FRU are represented by medium to thick beds of *Halimeda* float- rudstones, which also contain red algal fragments, mollusks, serpulids, and *Porites*

fragments. The *Halimeda* strata are intercalated with middle slope calcarenites. *Halimeda* plates are preserved as molds only.

The Terminal Carbonate Complex (TCC)

The FRU is unconformably overlain by the TCC. Franseen and Goldstein (1996) described four cycles in the TCC deposits. The outcrops of TCC are located at the top of the mesa-like hillocks of La Molata and La Molatilla. TCC deposits are cross-bedded oolites, stromatolites and small reef patches. The nuclei of the ooids are skeletal or peloidal grains. The stromatolite horizons are laterally continuous and the maximal thickness of the strata is about 1 m. At the top of the La Molatilla hillock, small patch reefs occur together with the stromatolites.

Quaternary and Holocene alluvial sediments

The youngest mapping unit in the Las Negras area consists of alluvial conglomerates and sands in the El Cuervo Ravine. These sediments overlie the volcanics and part of the Neogene deposits.

Cross-sections of Las Negras Carbonate Platform

Two geological cross-sections were constructed in the Las Negras Carbonate Platform (Fig. 2.29). A 1.7 km, W-E oriented section shows the W-E progradation of the oldest stages of platform evolution. The other section, which is oriented NW-SE, displays the progradation of the youngest episodes of the FRU platform.

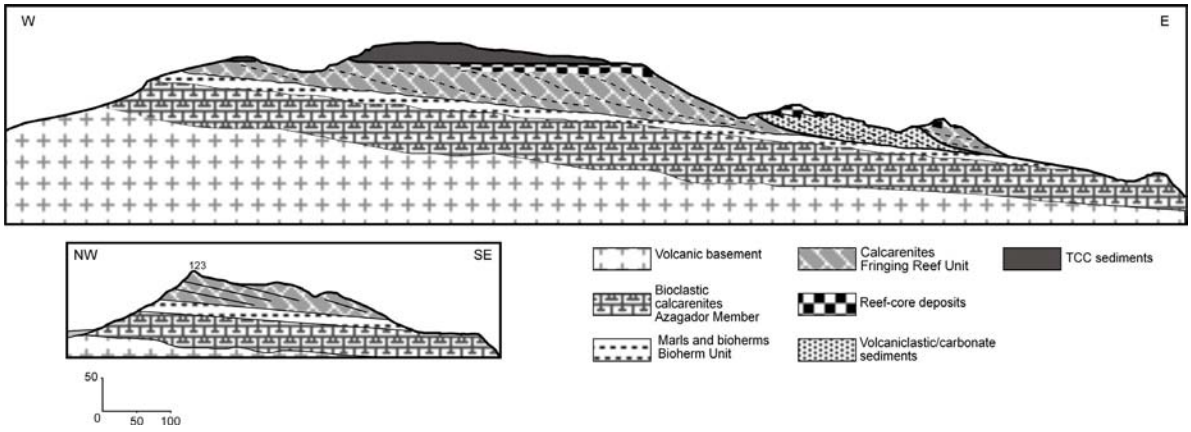

Fig. 2.29. Geological sections of the Las Negras Carbonate Platform oriented according to the main progradational directions

2.3.3 Depositional geometries and relative sea-level changes

The geometries of reef advance in the Las Negras Carbonate Platform were analyzed using four photomosaics, which cover the well-exposed northern flank of the La Molata hillock. The photo-transects were numbered from 1, in the westernmost part of the La Molata hillock, to 4, in the easternmost part. In the western part of the La Molata hillock, the photo-transects 1 and 2 show sections oriented approximately parallel to the direction of progradation of the oldest stages of the FRU. In the photo-transects 3 and 4, the carbonate platform is dissected approximately oblique to perpendicular with respect to the direction of progradation.

2.3.3.1 Photo-transect 1

Figure 2.30 shows an approximately 550 m wide view of the oldest FRU deposits in the westernmost area of the hillock. The oldest deposits consist of well-stratified middle slope calcirudites and calcarenites, which dip approximately 20°to the E. In the middle part of this photo-transect there is a poorly stratified calcarenite body which was interpreted as a slump by Franseen and Goldstein (1992). Two outcrops of reef-core deposits, which are

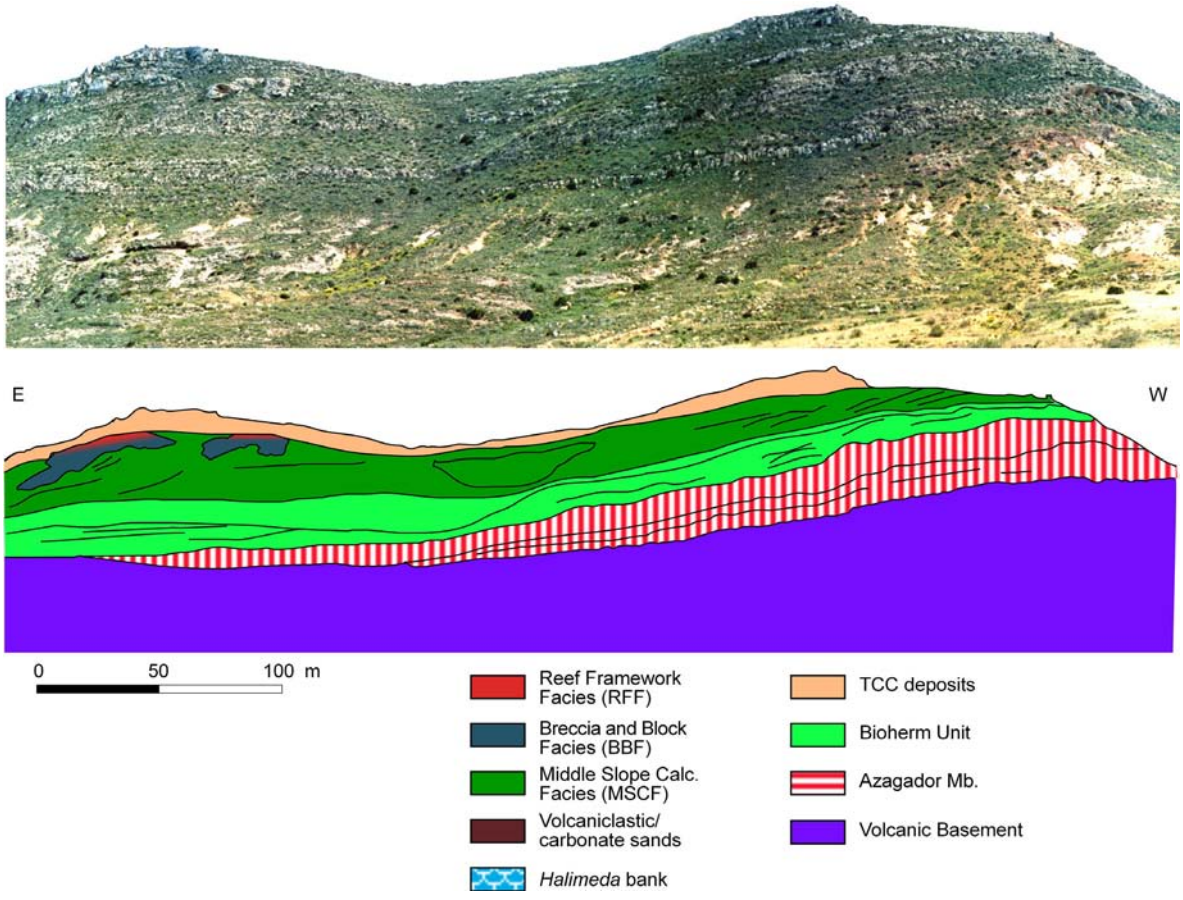

Fig. 2.30. Westernmost area of the La Molata Hillock. Note the slumped deposits outcrop in the middle part. The legend is used for the different photo-transects of the Las Negras Carbonate Platform.

composed of large reworked blocks of *Porites* and in situ colonies of *Porites* with stromatolitic crusts, occur in the easternmost part of the photo-transect. The reef-core deposits grade into layers of middle slope calcirudites and calcarenites with dip angles of about 25°.

2.3.3.2 Photo-transect 2

Figure 2.31 shows the 300 m-wide photo-transect 2, which is located eastward of the photo-transect 1. At the top of the section, several massive patches of reef-core deposits are preserved at the same altitude. This reveals that no major sea-level fluctuations affected the carbonate platform evolution during the deposition of these sediments in a situation of a relative sea-level highstand. Proximal deposits grade into poorly stratified middle slope calcarenites, which dip to the E. In the eastern area of the photo-transect, a downstepping of the reef-core deposits which interfinger with poorly stratified calcirudites occurs. The youngest deposits in this view show an aggradation of around 15 m and a related landward encroachment of the reef-core deposits overlying the previous episodes.

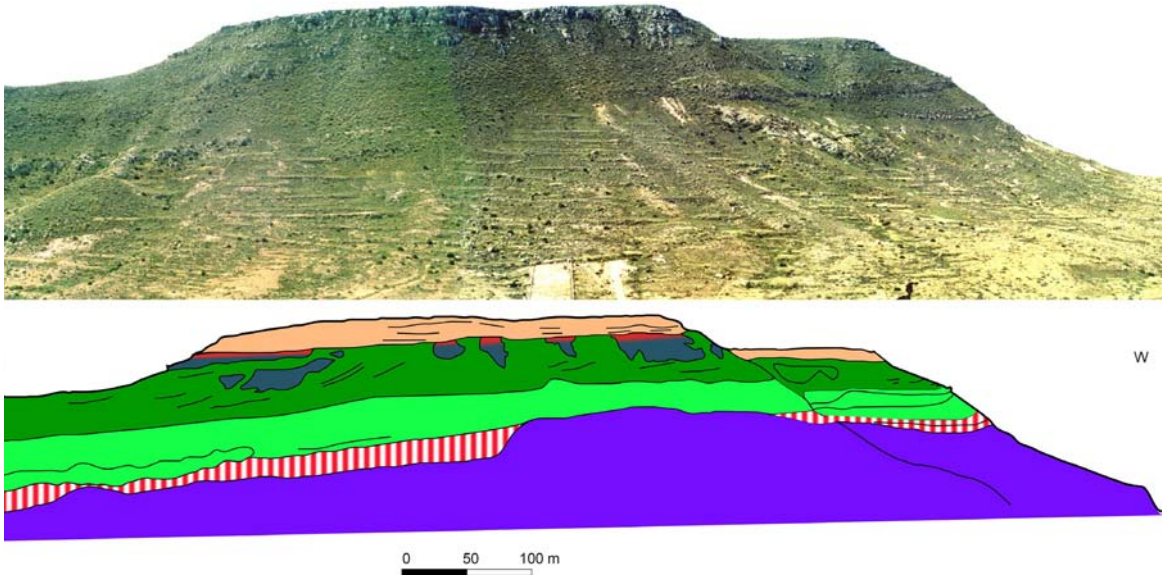

Fig. 2.31. Photo-transect and facies interpretation of the oldest deposits of the FRU at the Las Negras Platform.

2.3.3.3 Photo-transect 3

Photo-transect 3 covers 700 m of platform progradation in the central part of the La Molata hillock (Fig. 2.32). In this part of the carbonate platform, the FRU unconformably overlies a bioherm structure of the Bioherm Unit, which contains serpulids, corals, and red algae.

In the western part of the photo-transect there are poorly stratified middle slope calcirudites and calcarenites, as well as two outcrops of reef-core deposits that prograde towards the E. In the middle part of the transect, a wedge of mixed volcaniclastic/carbonate sediments occurs. The dip of the volcaniclastic/carbonate layers oscillates between 12 to 20° and the dip direction is predominantly to the East (90°). Calcarenites which overlie the volcaniclastic/carbonate sediments, dip towards the SE (135°). Massive reef-core deposits with in-situ reef colonies are preserved at the hilltop.

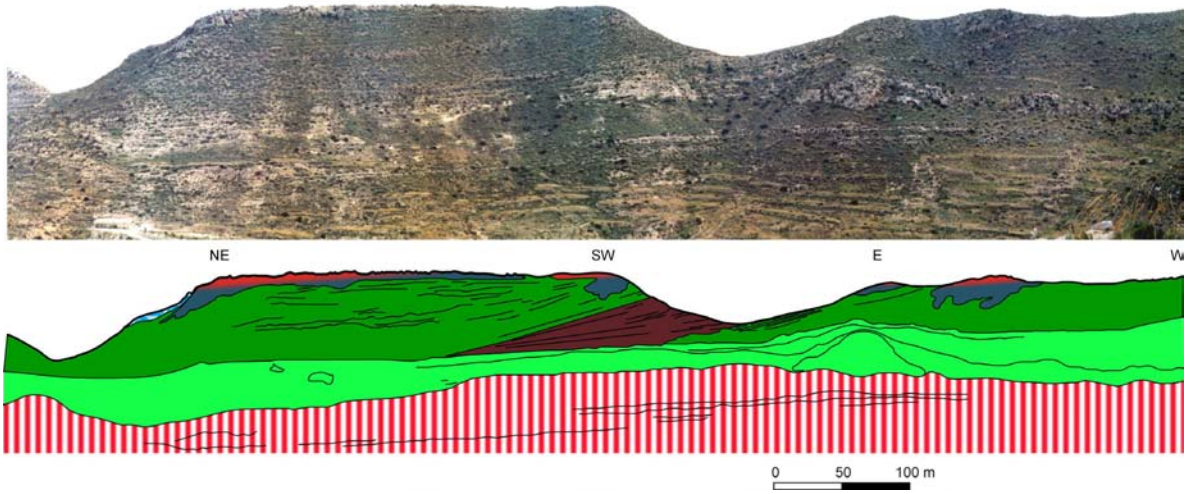

Fig. 2.32. Photo-transect 3 of the La Molata hillock. Note the presence of the Volcaniclastic/carbonate layers in brown.

2.3.3.4 Photo-transect 4

The fourth photo-transect (Fig. 2.33) covers about 500 m of outcrop in the easternmost area of Las Negras Carbonate Platform. The orientation of the photo-transect is approximately WSW-ENE. The reef-core deposits at the hilltop are the same deposits as shown in photo-transect 3 (Fig. 2.32). Reef deposits and middle slope calcarenites are conformably overlain by a package of *Halimeda* floatstones, which were interpreted as a *Halimeda* bank by Franseen and Goldstein (1992). The bank is up to 6 m thick in its western part, and wedges out towards the ESE. The *Halimeda* bank is overlain by middle slope calcarenites deposited during the last stage of platform evolution. The top of the calcarenites, as well as the top of the reef-core deposits were intensively eroded during later subaerial exposure. The Messinian deposits of the TCC overlie the FRU in the eastern part of the photo transect.

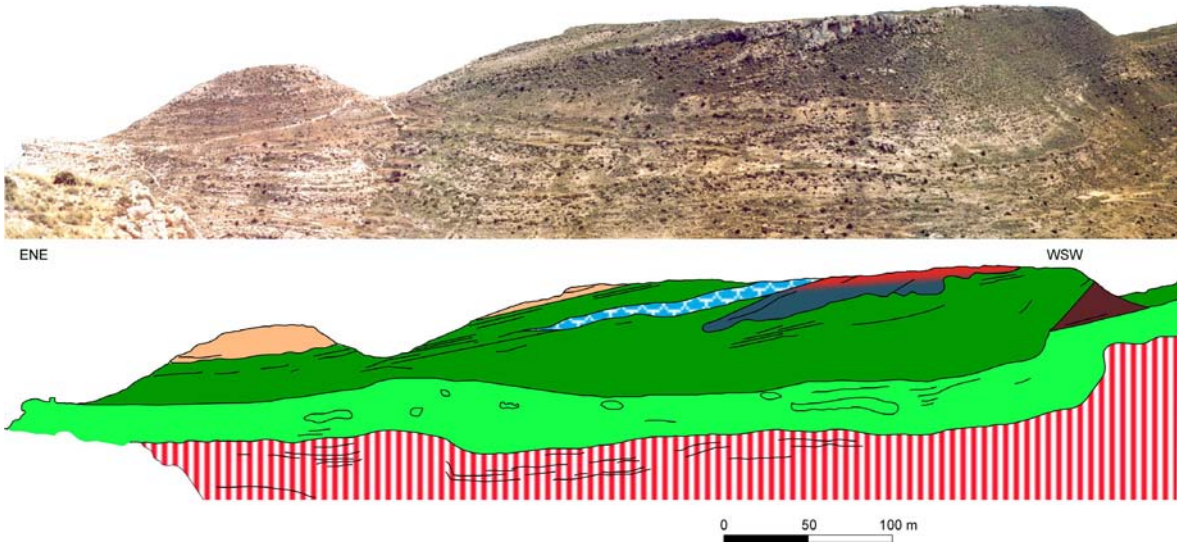

Fig. 2.33. Photo-transect 4. This transect shows the youngest deposits of the FRU where an *Halimeda* bank is preserved.

2.3.4 Curve of relative sea-level fluctuations

A relative sea-level curve for the development of the Las Negras carbonate Platform was already presented by Franseen et al. (1993) and Goldstein and Franseen (1995) using pinning points, which are shallow-water facies or indicators of subaerial exposure. According to this study, onset of FRU reef growth was after a sea-level rise of 130 m. The FRU-part of the Las Negras Carbonate Platform subsequently formed during one cycle of sea-level rise and fall and is framed by pinning points 8 to 14.

Using the same approach of sea-level reconstruction as performed for the Cariatiz and Níjar carbonate platforms, a different reconstruction of sea-level changes is proposed herein (Fig. 2.34). The most important difference between the three carbonate platforms is that no reef growth packages can be determined in the las Negras Carbonate Platform. This is because these outcrops do not provide a continuous record of the reef-core deposits that could be used as sea-level indicators. Fig. 2.34 shows the changes in reef core facies position of the Las Negras Carbonate Platform. The curve of relative sea-level fluctuation which results from these changes shows that, after the relative sea-level highstand of early platform growth, a slight sea-level fall of about 20 m occurred. This lowstand was followed by a sea-level rise of 15 m. This sea-level rise triggered the aggradation and the landward encroachment of reef-core facies described in the photo-transect 2 (Fig. 2.31). Afterwards, a drastic sea-level fall of 70 m affected the platform. During late stage of platform evolution, a sea-level lowering of about 25 m occurred.

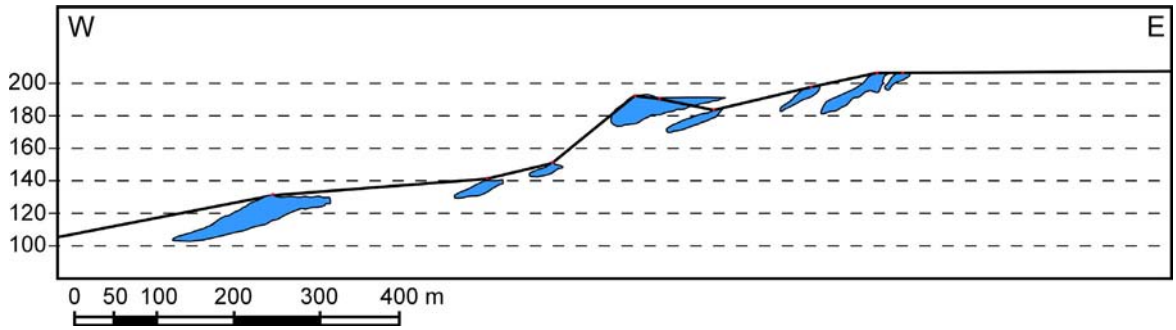

Fig. 2.34. Altitude, position and thickness of the reef core deposits at the La Molata Hillocks.

Whereas, apart from tectonic uplift, major synsedimentary tectonic movements can be ruled out for the Cariatiz and Níjar carbonate platforms, the mapping results at Las Negras and the results of the analyses of the photo transects indicate that the Las Negras Carbonate Platform was affected by significant syndepositional tectonic activity. This is reflected by the change in direction of platform rim progradation after deposition of the wedge of volcaniclastic/carbonate sediments (Figs. 2.32, 2.33). It is proposed that this change reflects a tectonic tilt of the basin, which probably was a consequence of uplift of the northwestern basin margin.

Chapter 3: Methods

3.1 Computer simulation of carbonate platforms

The different Messinian carbonate platforms were modeled using REPRO, a 3-D computer simulation program developed for the modeling of carbonate environments, especially for systems with coral reefs (Huessner and Roessler, 1996; Huessner et al., 2001). REPRO consists of three main parts: A MATLAB script, a FORTRAN program, and a visualization program.

3.1.1 The MATLAB script

The initial topographies of the carbonate platforms are represented by rectangular grids which contain the altitude values. In the MATLAB script, the rectangular grids of the initial input topographies are converted to triangular grids by interpolation. The use of such triangular grids, which are more difficult to implement than rectangular grids in both mathematical and programming aspects, proved necessary, because the use of rectangular grids distorted the geometry of the solutions by inducing spurious rectangular patterns, whereas the triangular grids did not induce triangular patterns (Roessler & Huessner, 1997). The sea-level curve used for the modeling is introduced as a MATLAB file formed by two columns that represent time values and respective sea-level positions. In order to get better adjustments between the modeled and real platforms, additional parameters, which can occasionally be controlling factors of the platform evolution, such as subsidence rates or ecological factors (nutrients, water temperature), could be also included.

3.1.2 The FORTRAN program

The actual simulations of the carbonate platforms are performed by a FORTRAN program. In order to explain the procedure of simulation of the FORTRAN program, two main groups of routines will be separately explained. One group of routines, namely Zoning Routines, involves the geographical distribution of the different depositional environments interrelated to the sea-level position for each time step, which is the time period that defines the interval that each calculation is made in the model. The second group of routines takes into account the reef production, the export mechanism of debris from the reef crest, the pelagic rain, and the dispersion of the sediments deposited in the different zones.

3.1.2.1 The zoning routines

The first subroutine in the time loop, which skips the model back after each time step, is the **ZONE** subroutine. It identifies several reef zones (Fig. 3.1), which together define the reef or carbonate complex with its environment. This subroutine is called up in the time loop several times, i.e., after every simulation of a geological process, which changes the topography of the reef complex. ZONE itself calls up various subroutines as well. A schematic cross section through a carbonate platform shows the main zones (Fig. 3.1):

1. Subaerial area
2. Lagoon area
3. Reef Framework area
4. Fore reef area
5. Distal area

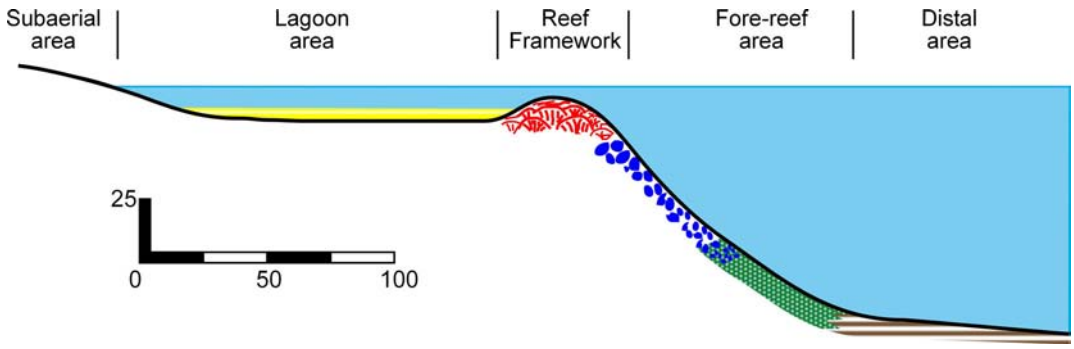

Fig. 3.1. Schematic cross section through a carbonate platform showing the main reef zones.

Before starting the zoning and identification process of the various regions, two matrix arrays are declared. They represent the rectangular grid of the model area and are initialised to zero. During the zoning process the individual zero elements of one of these arrays – here named ID matrix – are replaced by integer numbers or indices, which are assigned to the different zones. Therefore, this ID-matrix maps the individual zones by indices. In the other array – here named WL-matrix – the water line is represented during zoning by ones as entries. In this case each pair of points or elements, respectively, between which the water line passes, the one element whose height lies below the water line is set to “1”, (Fig. 3.2).

The subaerial zone is identified by the subroutine **ZONE11** by a simple comparison of heights between the grid points and the sea level. If the height value of the grid point is

above the sea level, it is declared as subaerial and obtains in the ID-matrix an identification number (in this case 1).

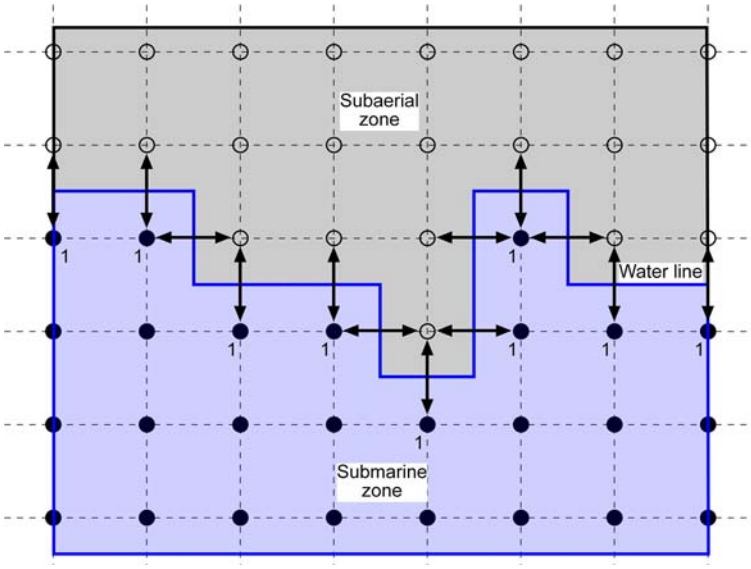

Fig. 3.2. Schematic course of the water line in the rectangular grid. The pairs of points separated by the water line, identified by double-headed arrows and with submarine points below marked by ones, are used in the ensuing zoning and saved in an array. Changes in the direction of the water line can cause some points to be marked two or three times.

Height lines, and thereby the water line as well, are identified by the subroutines **H2O_LINE01**, **H2O_LINE02** and **H2O_LINE03**. **H2O_LINE01** scans the borders of the ID-matrix for water lines, which start and end at the borderlines of the model domain and are therefore open. Once a change between two neighbouring borderline elements from subaerial identification (1) to initialisation (0) or vice versa is detected, the beginning of an open water line is identified and **H2O_LINE03** is called up to follow this water line.

Closed water lines around islands or depressions below the water level are detected by **H_2O_LINE02** by scanning the ID-matrix column by column and detecting a change of identification as described above. **H_2O_LINE03** is called again to follow this water line.

H_2O_LINE03 follows up on the water line by checking the identification of the four elements defining a grid mesh it enters for subaerial (1) and initial identification (0) (see Fig. 3.2). This way, the direction in which the water line exits the grid mesh and enters a neighbouring mesh can be determined. Evidently, only the three directions right, straight ahead and left are possible for exiting; a mesh can be entered from four sides, which leaves 12 ways for the course of a water line. Besides, the two cases must be distinguished, whether upon entry in a mesh the subaerial node is to the left and the submarine node to the right or vice versa. In total, this leaves 24 combinations for entry

and exit of the water line per mesh, addressed individually in **H2O_LINE03**. Row and column numbers of the pairs of points separated by the water line are stored in arrays. In order to make the course of the water line for later operations available, the water line is entered in the WL-matrix by setting the submarine entries of these point pairs to one. Via the WL-matrix, **H2O_LINE01** and **H2O_LINE02** are now able to check if a water line has already been detected and identified.

Identification of the remaining zones is substantially more elaborate and difficult as the identification of subaerial zone and water line, as these zones do not simply depend on height values only, but mainly on changes in topography. Precise separation lines between the different zones (except of course the separation line along the subaerial zone) therefore exist just as rarely as on the actual reef in nature. Logically, further realistic zoning will depend on the reef ridge as separation line between lagoon and fore reef, which must therefore be identified next.

A relatively simple method is to scan the height values along columns and rows of the height matrix, which is done by the subroutines **ZONE11RW** for rows and by **ZONE11CL** for columns. If a height value is detected to be higher than its two neighbour values and if the water depth is shallower than a user-set value, the point belonging to this height value qualifies as a possible candidate for the reef crest. In case several candidates per column or row are detected, this way the one with the maximal height or shallowest water depth, respectively, qualifies as reef crest element. As a rule, this way no continuous reef crest will be identified, because – similar to the growth characteristics of an actual reef – the model can develop openings and gaps in the reef crest and only approximate separation lines between lagoon and fore reef can be defined between the disconnected reef ridge segments. Therefore, the model draws connection lines between the individual reef segments, thus creating a continuous separation line between lagoon and fore reef. **ZONE11RW** and **ZONE11CL** call up the routine **CONNECT110** in order to create this extension to a continuous line. Row and column numbers of this line are saved in arrays by the routine **ZONE101** in order to enable the program to follow this line in later operations. Once this line is identified, several test operations are performed to determine the final zoning.

The first test is done by the routine **ZONE33**. It follows the water line and scans along rows and columns of the ID-matrix in seaward direction. In case the separation line between lagoon and fore reef is encountered, the grid points between water line and separation line obtain lagoon identification and the points beyond the separation line are identified as fore reef. In case no separation line is encountered, no reef crest has developed yet and a fore reef identification takes place.

The next test is done by routine **ZONE55** and follows the separation line between reef and lagoon. It scans rows and columns on both sides of this line. In case the water line is encountered on one of the two sides, the scanned points obtain lagoon identification. If points with fore reef identification are detected, the remaining scanned row or column is identified as fore reef.

The routine **ZONE66** follows the separation line as well and scans rows and columns of the ID-matrix on both sides of the line. If on one side lagoon or fore reef identifications, respectively, are encountered, the scanned points obtain lagoon or fore reef identifications appropriately whereas the remaining points on the row or column on the opposite side of the separation line obtain opposite identification.

The last test is performed by the routine **ZONE77**, which scans rows and columns of the ID-matrix as well in order to track down points still unidentified. In case such a point with identification zero is detected, it obtains the identification of neighbouring points with lagoon or fore reef identification, respectively. This test is repeated until no more unidentified points are encountered.

3.1.2.2 Reef production, export mechanism, pelagic rain, and dispersion routines

The central device of the reef production is a Fisher equation (Fisher, 1936), which simulates the coral reef growth (Roessler & Huessner, 1997). This Fisher equation is a logistic growth equation with a 2-dimensional diffusion term added in order to account for lateral spreading and growth of the coral colonies. It is adapted to the marine environment by use of a carbonate production profile developed by Bosscher & Schlager (1992). The resulting equation used for modeling reef growth has been largely explained by Huessner et al. (2001). It has the form:

$$dh/dt = p*c*h*(sl-h-b) + D*\Delta h \qquad (1)$$

Where, h = reef height; dh/dt = time derivative or growth rate of reef height; c = growth coefficient; p = Bosscher-Schlager production profile (see Fig. 3.3 and next paragraph for detailed explanation); sl = the sea level position, changing temporally; b = height of initial or bottom topography; D = diffusion coefficient; Δh = Laplace operator or second spatial derivative of h accounting for diffusion or lateral spreading of the reef.

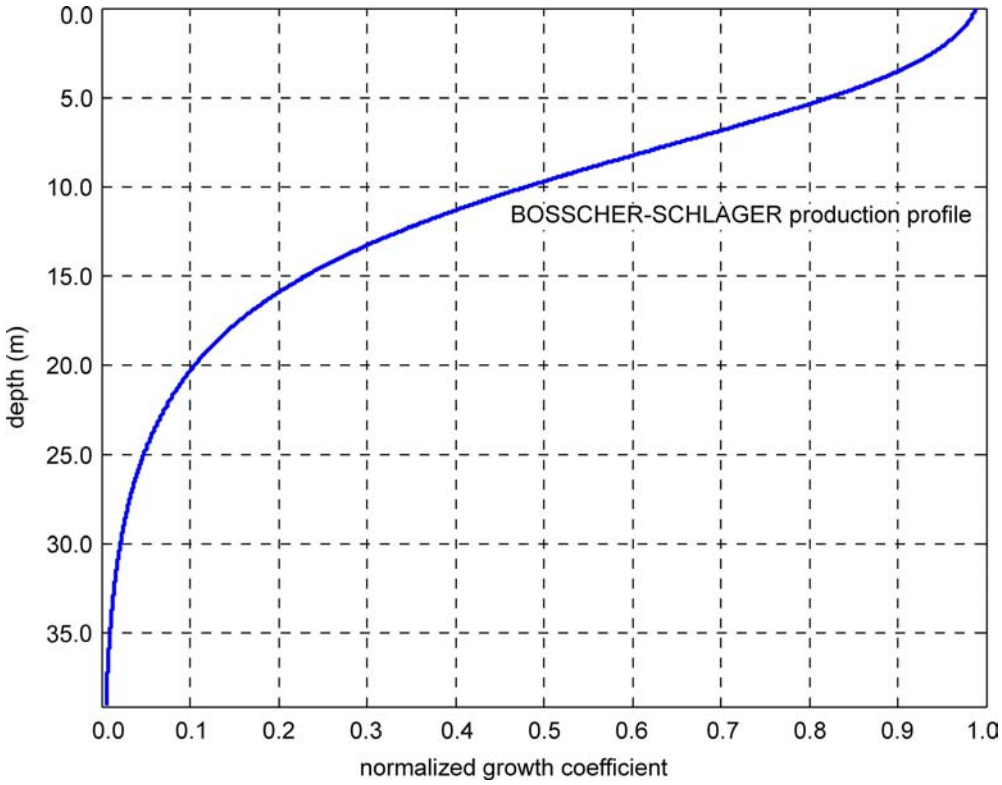

Fig. 3.3. Depth-dependent production profile used in the simulation of the Cariatiz Carbonate Platform. Equation for p is represented by the formula (4) according to Bosscher & Schlager (1992).

The production profile after Bosscher and Schlager (1992) is a function of light intensity (I), which itself is a function of water depth according to the Beer-Lambert law of exponential light extinction (2) (Fig. 3.3). The actual production profile used for the modeling of the carbonate platforms takes into account the depth distribution of the different reef subfacies.

$$I = I(z) = I_0 * exp(-kz) \qquad (2)$$

I_0 = surface light intensity; k = light extinction coefficient; z = water depth. Using the dependence of growth rate G on light intensity I according to a hyperbolic tangent (*tanh)* after Chalker et al. (1988), it results that

$$G = G_0 * tanh(I/I_k), \qquad (3)$$

G_0 = surface growth rate; I_k = saturation light intensity
(see Chalker et al., 1988, or Bosscher & Schlager, 1992, for details)

Bosscher & Schlager (1992) derive a depth-dependent production profile like

$p = p_0 * tanh[I_0/I_k exp(-k(sl-b-h))]$ (4)

p_0 = surface production rate; *sl* = sea level position which is changing temporally; *b* = height of initial or bottom topography; *h* = reef height. In the present models, p is not employed as production rate, but as depth dependent weight factor of the growth coefficient (Fig. 3.3).

In the growth equation (1) the entire growth substance represented by the height *h* contributes to the growth rate *dh/dt*, which is correct for most ecological growth processes modeled by the Fisher equation. In the case of coral or carbonate growth, however, only the top layer is alive and therefore can contribute to further growth, whereas the underlying carbonate structure has died off and is calcified. In the present models, *h* is therefore continuously reduced to the thickness of the living top layer and the amount of reduction is added to the initial bottom topography *b*.

This partial differential equation (1) is solved by finite element methods on the above-mentioned triangular grid, which carries the nodes on the center points of the sides of its equilateral triangles. The solution of the growth equation is the only simulation performed on this triangular grid. All other processes simulated are performed due to reasons of ease of programming and acceptable geometries on a rectangular grid, extracted from the triangular grid by omission of certain nodes which can be reinstalled by interpolation, in order to recover the triangular grid.

The simulation of the lagoon is carried out by a function of water depth-dependent carbonate production. The carbonate growth process is accompanied by processes of subaerial erosion, material export, redistribution and sedimentation. Subaerial erosion is performed by a simple reduction of height values. Material transport and re-sedimentation which composes the simulation of the BBF as well as the MSCF is simulated by passing material volume elements (represented by changing height values) downslope along gradients. Dispersion, partial redeposition and inter-particle friction characteristics of the individual volume elements can be simulated by retaining a certain fraction of the material element on each node the element passes on its way downslope. This fraction is represented as a function of the gradient and the so-called ‘slip factor’ – the higher this factor is set, the lower the friction and thereby the retained fraction will be. Dispersion of fine-grained material suspended in water follows the slope gradient only approximately. This effect is simulated by a random walk process, i.e., a neighbor node of the node currently occupied by the material element is randomly selected. The random selection can be weighted so as to increase the probability of selection the closer the neighbor node is to the gradient.

The mechanism for modeling the distal slope and basin deposits is a “pelagic rain” function, which considers the depth and the dispersion of the particles by currents. This mechanism takes into account the simulation of pelagic sediments, mainly marls, that composes the basinal deposits.

The technical and physical control parameters for the development of the carbonate platforms are contained in a parameter file read by the main program. This is a file where values such as coefficient of reef growth, coefficient of light extinction, production of breccia and calcarenites, etc. are assigned to the main control factors of the system. Each facies is controlled by several parameters which have been taken into account in the different subroutines of the FORTRAN program. For instance, the breccia production and flow rate are managed by a set of parameters. One parameter controls the number of debris particles produced on the reef crest which form the BBF. The next parameter sets the initial size of the individual debris particles generated in the reef crest. In the modeling, the initial size of the particles forming the BBF is approximately 40 cm in height. Downslope, the size of the particles decreases because of the partial retention of particle fractions on the successive “downslope” nodes. A final parameter controls the deposition of particles downslope. The spreading of the debris depends on the slope gradient, which is the inverse tangent of the slope angle, and a weight factor function of the grain size. According to the values given to the slip factor, the deposition will occur at high slope angles, when the values are low or, on the other hand, the spreading is higher when the slip factor values are high.

Using REPRO, the temporal supply of siliciclastic conglomerates can be controlled in time and in space. This is managed by a subroutine for temporal supply of siliciclastic sediments. For instance, in the case of the Cariatiz Carbonate Platform, this subroutine models the eventual influx of fan delta conglomerates.

3.1.2.3 The flux Diagram of REPRO

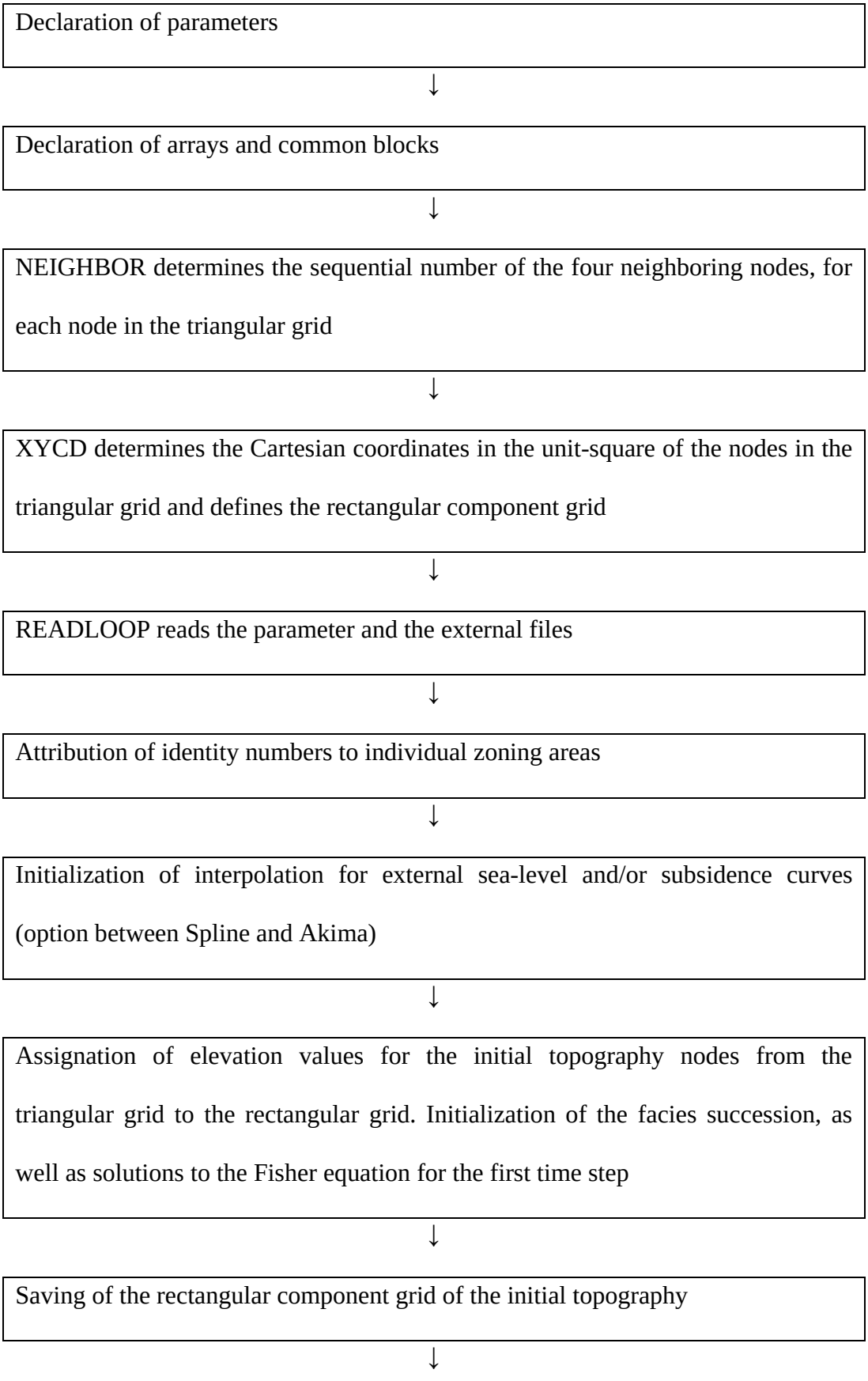

Initialization of the time-dependent variables fro the time loop

Start of the Time Loop

ZONE identifies the different zoning areas

↓

Since the 2nd time step, the subaerial regions are reduced in height by EROSION

The rectangular component grid is saved

ZONE identifies the different zoning areas

↓

INTERPOL expands the elevation values, growth parameters and identifies numbers of the zonation of the rectangular component grid to the triangular grid

↓

In case of absence of a lagoon zone, ICSET sets initial conditions for reef growth on nodes of the triangular grid beneath sea-level

↓

The integrator RKF45 initiates the subprogram FISYST, which simulates the reef growth

Values of maximum and mean average growth rates are saved

The elevation values of the rectangular component grid are extracted from the triangular grid and are saved

ZONE identifies the different zoning areas

↓

LAGOON simulates Lagoon Facies growth

The rectangular component grid is saved

ZONE identifies the different zoning areas

The following sequence of the request of REEF_SED, including saving and zoning, is repeated with different parameter adjustments to the number of simulated facies layers:

REEF_SED requests DOWN_HILL and generates the facies distribution of the reef rubble and lagoonal sediments in the fore reef or lagoonal areas

The triangular component grid is saved

ZONE identifies the different zoning areas

If siliciclastic input exists, these will be modeled by the following sequence of subprograms:

RIVER_TRACE determinates the course of the river from its streams or its entry point to the model area.

RIVER_SED generates the distribution of fluviatile sediments starting from the river mouth as point source

The triangular components grid is saved

End of Time Loop and program REPRO

3.1.3 The visualization program

Results of the FORTRAN simulation program are graphically displayed by a visualization program, which was written in C level. It uses OpenGL, which is a 3-D graphics language developed by Silicon Graphics. The program allows the visualization in a rectangular grid of views and cross-sections of the carbonate platforms. “Time slices” can be displayed in order to unravel the internal geometries and facies structures during the platform development. Dynamic growth animations are also available showing the platform evolution together with the sea-level fluctuations. The actual version of the visualization program allows the volume of the reef-related facies in the carbonate platforms to be displayed individually.

Chapter 4: Computer Simulation Results

4.1 Coral growth rates of the modeled Cariatiz and Níjar carbonate platforms

Coral growth rates for the Cariatiz and Níjar carbonate platforms are provided by the computer program REPRO in a separate numerical output file (Figs. 4.1, 4.2). The coral growth rates are simply the time derivative of reef height or the term *dh/dt,* respectively, in the modified Fisher equation introduced in Chapter 3 as equation 1. The numerical values represent the average value (mm/year) for each individual time step. The coral growth rates are used as a test to verify the consistency of the program, because the obtained growth rates in the different models compare well with recent growth rates of tropical corals.

Maximum coral growth rates of 18 mm/a are obtained during periods of optimal growth conditions in the Cariatiz Carbonate Platform (Fig. 4.1), and the average values for the coral growth rates oscillate between 2 and 8 mm/a. In the Níjar Carbonate Platform, the obtained maximum growth rates do not exceed 10 mm/a during optimal conditions (Fig 4.2). The average values fluctuate around 4 mm/a. The periods of optimal conditions for coral growth occurred during relative sea-level highstands, where extensive areas of the platforms were flooded. These values do not exceed the recent maximum rates growth of *Porites*, which average 10-12 mm/yr (Lough & Barnes, 2000; Siciliano et al., 2003).

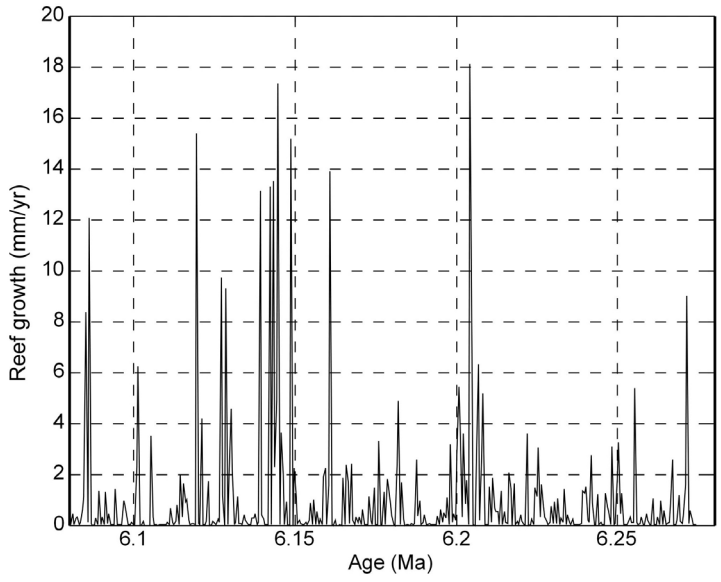

Fig. 4.1. Curve showing the fluctuations of coral growth rates during the development of the Cariatiz Carbonate Platform.

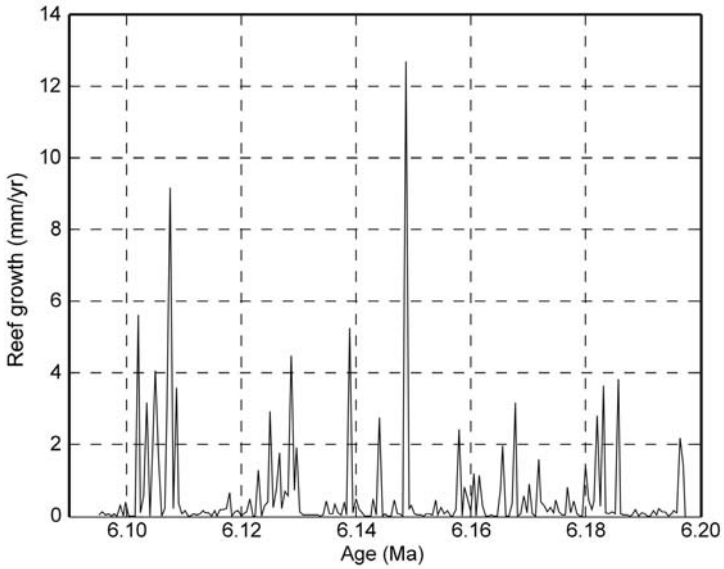

Fig. 4.2. Fluctuations of coral growth rates during the development of the Níjar Carbonate Platform. Note that maximum growth rates occur around 6.15 Ma in both platforms.

4.2 The simulated Cariatiz Carbonate Platform

4.2.1 Shape and internal geometries

Figs. 4.3 A and B display the 3-D outer morphology of the simulated Cariatiz Carbonate Platform, after 200 ka of development, as well as several fence diagrams of the platform, which provide views of the reef advance geometries. In the figures, the LF is shown in yellow, the RFF in red, the BBF in blue, the MSCF in green, and the pelagic facies in brown. Note that the interfingering of the different facies is marked by transitional colors.

The spatial dimensions and the morphology of the simulated platform match well with the real morphology and dimensions of the Cariatiz Carbonate Platform (shown in the geologic map, Fig. 2.3). Later processes of erosion, mainly ravinement, produced differences in the morphologies between the simulated and the real platform, especially in the northern area of the platform, where small ravines and valleys dissect the platform.

Fig. 4.4 shows a view from a slice of the latest growth stage of the Cariatiz Platform, produced through uncovering the uppermost meter of the platform. This view thus allows the facies belts produced during the distinct RGP to be documented. The figure shows a pattern of facies belt distribution which characterizes each RGP. A thin belt is dominated by BBF, a second belt is dominated by the MSCF, and another belt is dominated by the BBF. This distribution is related to the high-frequency sea-level fluctuations which affected the evolution of the Cariatiz Carbonate Platform. The first BBF belt corresponds to the sea-level rise phase after a previous relative lowstand; the MSCF belt was deposited

during the relative sea-level highstand; the BBF belt is connected to the phase of sea-level lowering for each cycle.

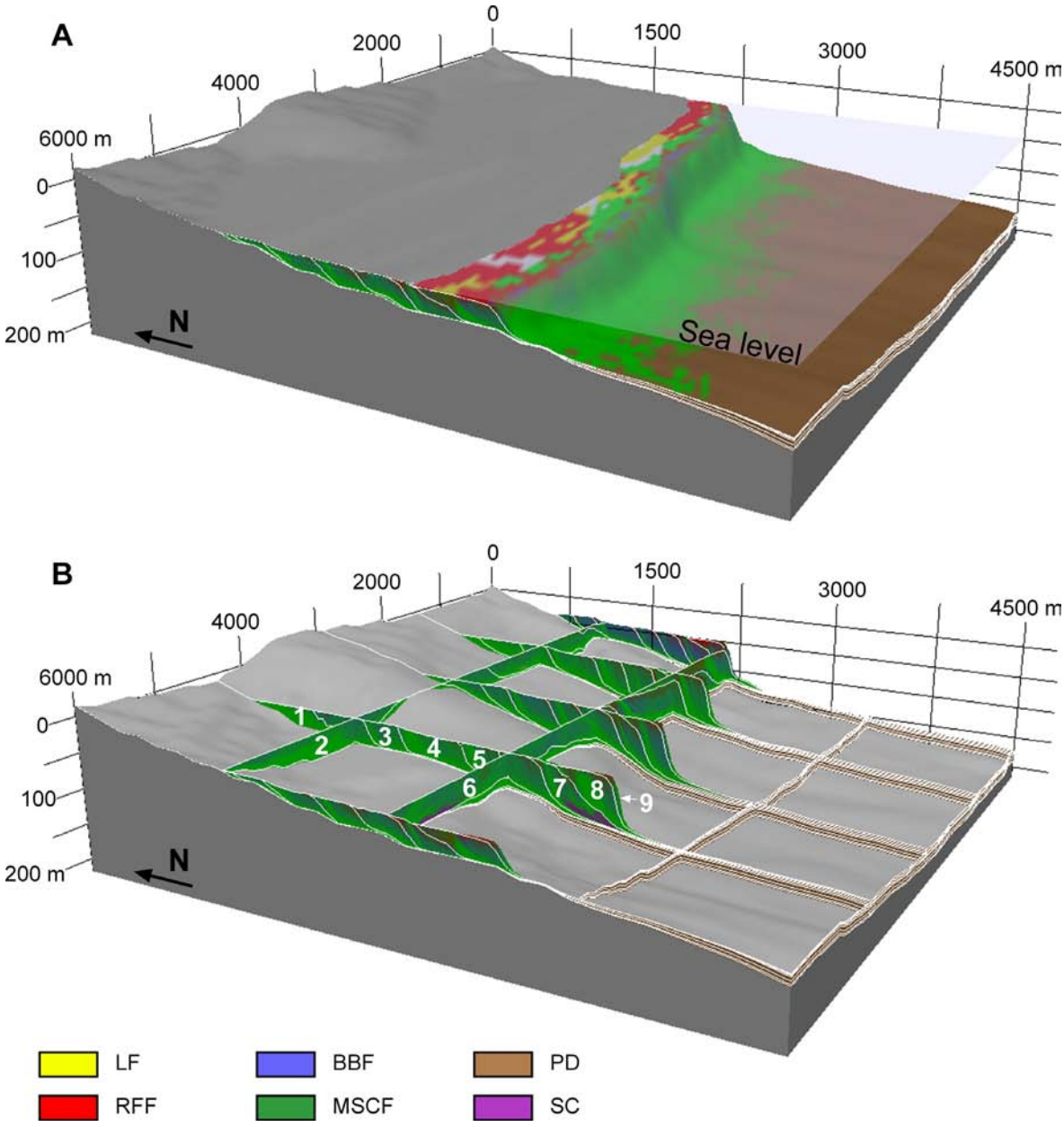

Fig. 4.3. A. Final result of the computer simulation of the Cariatiz Carbonate Platform. **B.** Fence diagrams of the simulated Cariatiz Carbonate Platform. Numbers indicate reef growth packages. Note the internal complexity of the platform, e.g. the lateral wedging out of RGP 6. Legend: LF: Lagoon Facies; RFF: Reef Framework Facies; BBF: Breccia and Block Facies; MSCF: Middle Slope Calcarenites Facies; PD: Pelagic Deposits; SC: Siliciclastic Conglomerates.

Note that the facies belts of RGP 1 to 3 are poorly developed, and that the deposits of these packages consist mainly of MSCF. This is a consequence of the erosion of the shallow and proximal deposits of the early RGPs during the major phase of subaerial exposure, which occurred in later stages of platform evolution, during the deposition of the RGP 4 to 8.

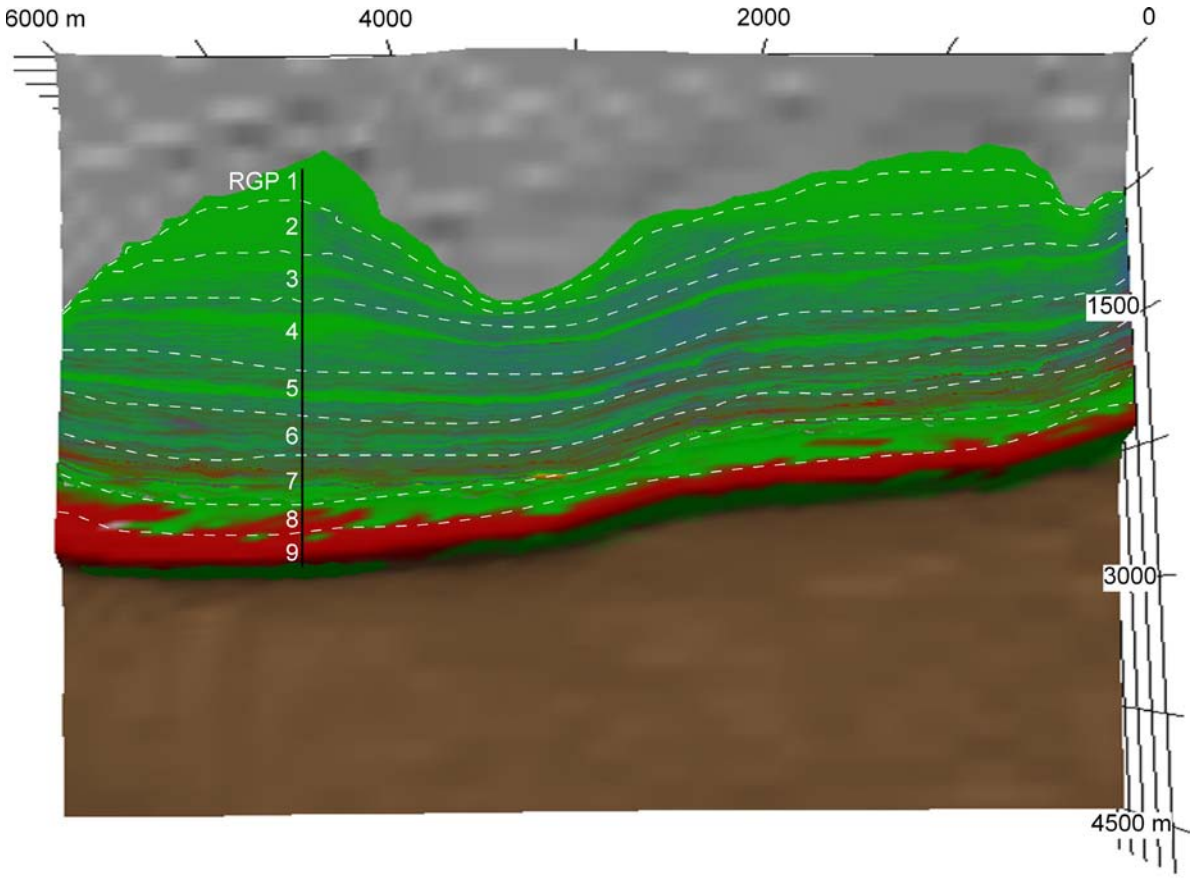

Fig. 4.4. Aerial view of the simulated Cariatiz Carbonate Platform showing the RGPs and the facies distribution at the top of the platform.

4.2.2 Comparison of geological and simulated cross-sections of the Cariatiz Carbonate Platform

In the Cariatiz Carbonate Platform, the reef growth packages are sigmoidal bodies which prograde onto the pelagic sediments, with the exception of the older packages (RGP 1-4), where downlap geometries are produced especially in the proximity of the La Mela village. The potential of reproducibility of the 3-D simulation results with REPRO is shown by Fig. 4.5. Three synthetic sections measured along the ravines, which dissect the Cariatiz carbonate platform, were compared with sections of the model located in the same position in the simulated platform. Good fits in the distribution of facies, as well as in the sedimentary geometries of the reef growth packages are observed in the compared sections. For instance, the comparison between the section at La Mora Ravine and the modeled section (Fig. 4.5 A) shows the same pattern from RGP 1 to RGP 4. RGPs 1 and 2 are mainly composed of MSCF with small outcrops of BBF at the top. In RGP 3, a domain of MSCF is observed in the first half of the package. A downstepping of the BBF occurs just before LW 3. A similar pattern occurs during the deposit of RGP 4, however, with a more pronounced downstepping. At Los Castaños Ravine (Fig. 4.5 B), the comparison

was carried out from RGP 5 to RGP 8. In this part, the BBF outcrops are laterally continuous. The downstepping geometries, responding to the major phase of sea-level drop, are well-documented in the model section.

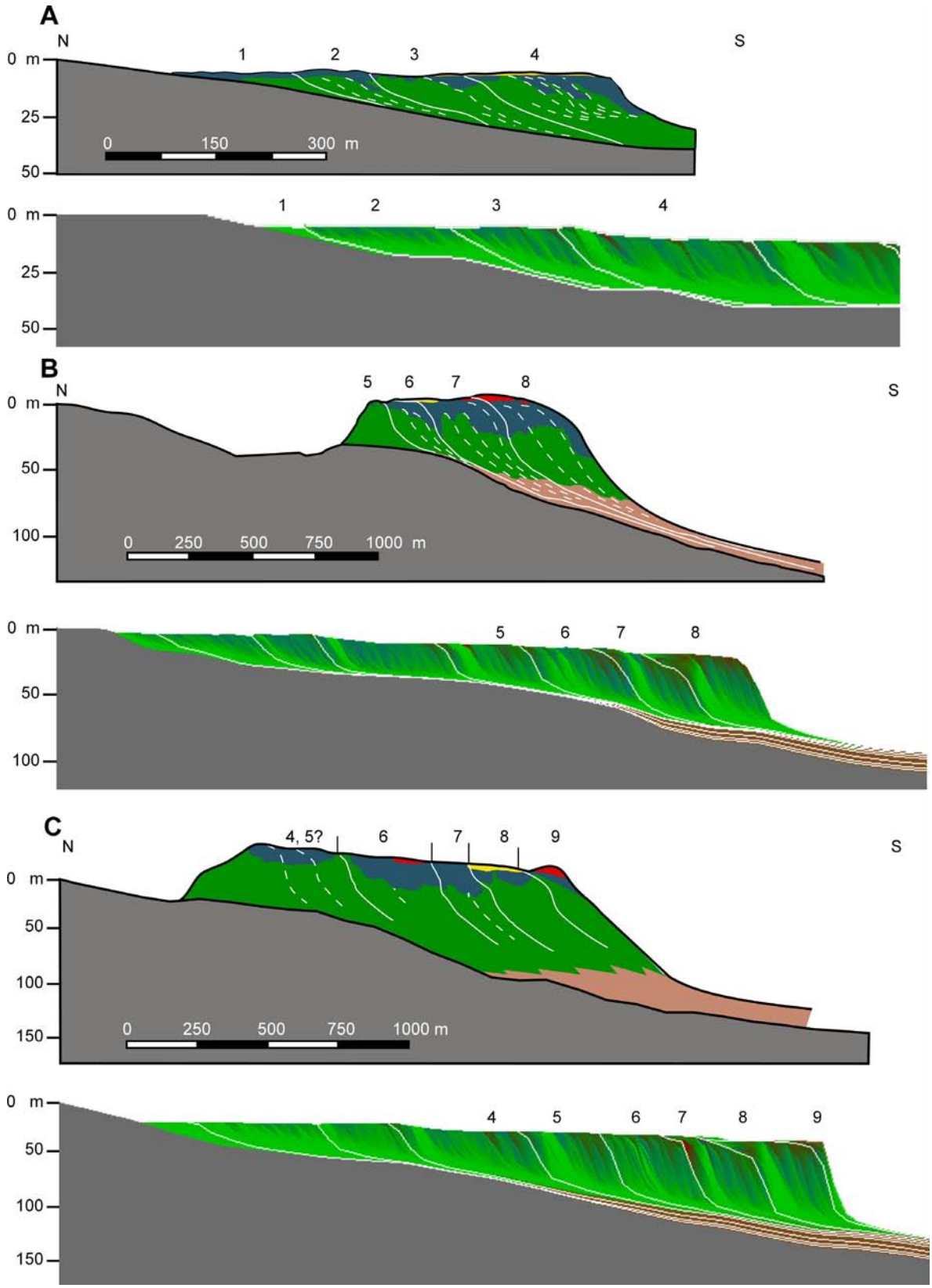

Fig. 4.5. A. Comparison between the geological cross section at La Mora Ravine (upper part) and a section in a corresponding position of the simulated platform. **B.** Comparison between the cross section at Los Castaños Ravine and the section of the simulated platform. **C.** Same for El Chive Ravine.

The position of the third section coincides with the location of the El Chive Ravine (Figs. 4.5 C). In this section, which cross-cuts the platform with an angle of around 20° with respect to the main direction of progradation, there is a reasonable fit in the lateral extension and in the sedimentary geometries of RGPs 4 to 9. The main difference between this and the previously described section is the lower amount of BBF deposited in this part of the Cariatiz carbonate platform. This lateral facies heterogeneity, however, cannot be modeled by the simulation program, which simplifies the export of the BBF to homogeneous conditions in the entire platform, producing a minor mismatch between the section and the simulation.

4.2.3 Facies distribution and facies bodies in the Cariatiz Carbonate Platform

The facies distribution and the growth geometries observed in the two carbonate platforms are not only a result of the build-up processes, such as creation of accommodation space and morphology of the initial topography, but also of the destructive process of erosion, which occurred during relative sea-level lowstands, and triggered the subaerial exposure of the platforms. REPRO incorporates a method which consists of a reduction of the height values of the exposed deposits, to simulate the subaerial erosion produced during the development of the carbonate platforms.

The effects of the erosion process on the Cariatiz Carbonate Platform are illustrated by Fig. 4.6. Fig. 4.6 A shows a section through the Cariatiz Carbonate Platform after 90 ka of the inception of platform growth. At the platform edge, a body of RFF is evident in RGP 3. Deposits of this package and the overlying RGP 4 encroach the entire area of the platform, thus also overlying RGP 1 and 2. Note that the model predicts minor reef patches and lagoonal deposits in this area. Fig. 4.6 B shows the platform advanced to RGP 7 after approximately 170.3 ka of development. Note the erosion-reduced top of the platform is in such a way that the reef patches and back-reef deposits of RGP 3 and 4(Fig. 4.6 A) have disappeared except for minor remnants.

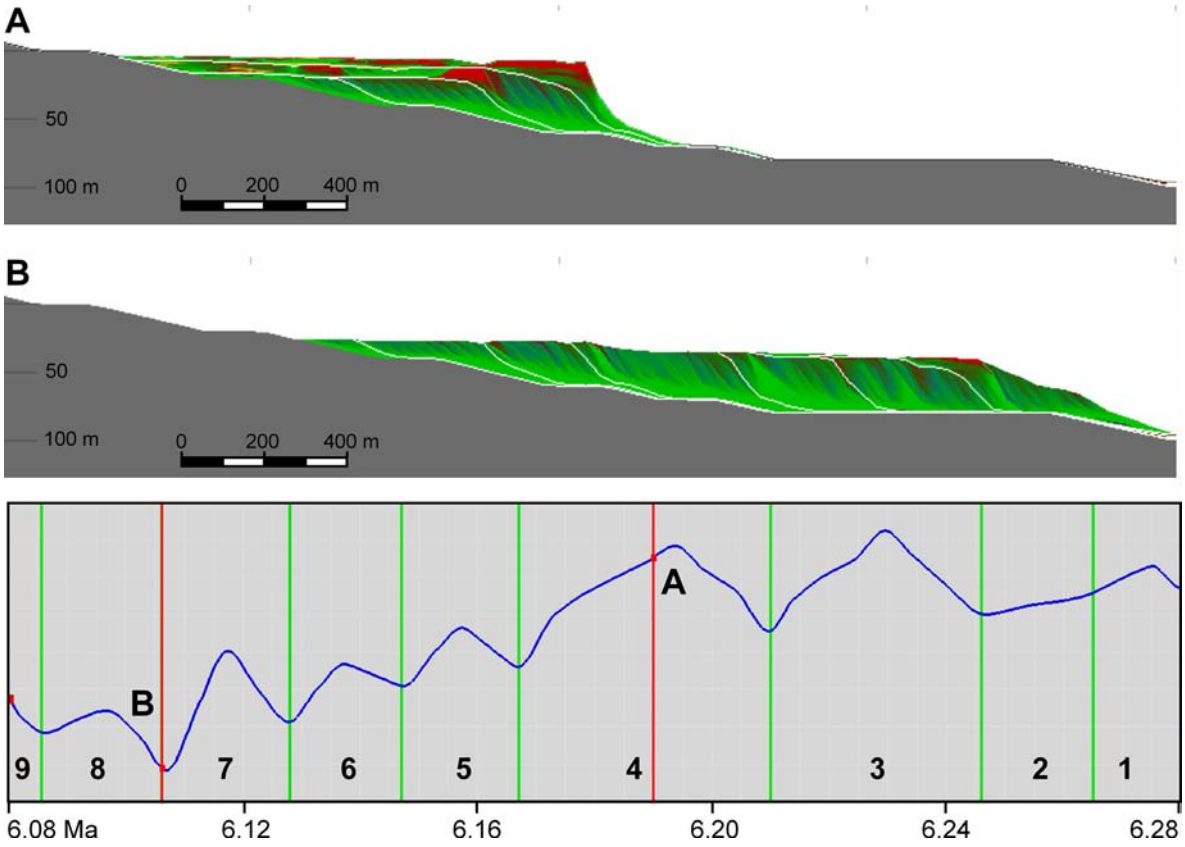

Fig 4.6. A. Section through the Cariatiz Carbonate Platform after 90 Ka of platform growth in a position corresponding to La Mora Ravine. **B.** Same section after 170.3 Ka of platform growth. Note that at this stage of the platform evolution, large parts of the older platform were eroded and that only remnants of these earlier RGPs are preserved. In the lower part of the figure, the sea-level curve used for simulation of platform growth is shown. A and B designate position of time steps shown in 4.6. A and 4.6. B.

As a result of the erosion, the final remnants of RFF are two laterally discontinuous belts shown in Fig. 4.7 A. The two belts were deposited during the latest stages of platform evolution after the major episode of sea-level lowering. As expected, there is more substance of the BBF left (Fig. 4.7 B), as it is positioned in deeper layers which are beyond reach of major subaerial erosion. The deposition of the MSCF, shown in Fig 4.7 C, was almost unaffected by the subaerial erosion, and only part of the MSCF deposits from the oldest stages of platform evolution was abraded. The RFF, the BBF, and the MSCF distributions are color coded in compliance with the sea-level curve shown in Fig. 4.7 D. Note that mainly highstand BBF and MSCF deposits were eroded during the subaerial exposure of the platform.

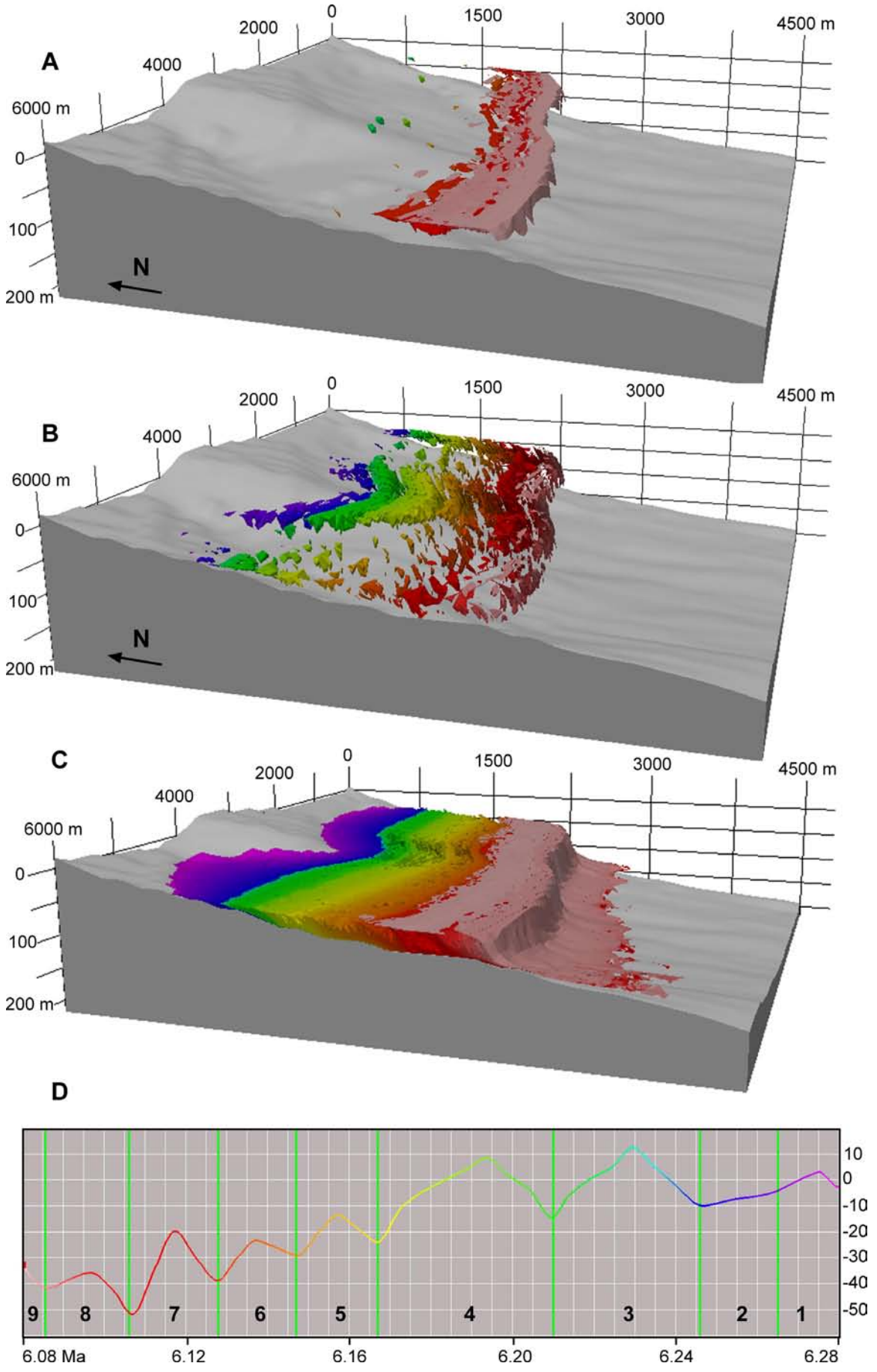

Fig. 4.7. A. RFF distribution in the Cariatiz Carbonate Platform. Note that only the reef bodies from the youngest phases of reef growth are preserved in two laterally discontinuous belts. Color-to-age relationship is shown in the sea-level curve in D. **B.** Distribution of bodies of BBF in the Cariatiz Carbonate Platform. **C.** Situation of MSCF deposits in the Cariatiz Carbonate Platform. **D.** Sea-level curve used for simulation of the platform. The color coding of the sea-level curve indicates the age of the corresponding interval.

4.3 The simulated Níjar Carbonate Platform

4.3.1 Shape and internal geometries

The 3-D outer morphology of the Níjar Carbonate platform is shown in Fig. 4.8 A. The shape of the simulated platform matches well with the morphology of the Níjar Carbonate Platform recorded in the geological map. The WSW-ENE-oriented platform edge forms a promontory where reefs grew on the Hoyazo volcano. The amount of general reef advance is approximately 1 km, and 1.5 km in the area of the El Hoyazo Volcano. These are the same values which occur in the real Níjar Carbonate Platform (Fig. 2.19).

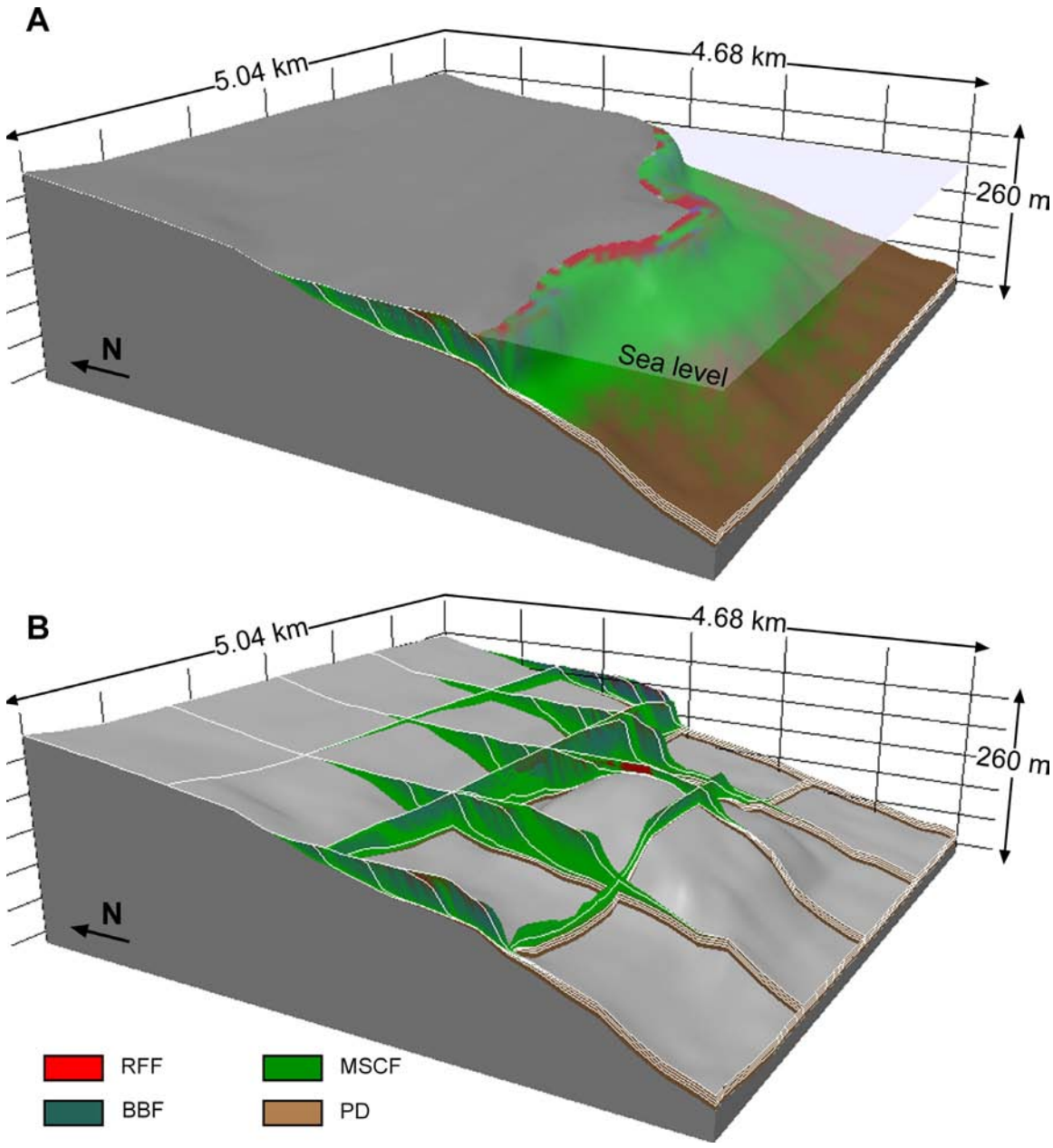

Fig. 4.8. A. Final view of the simulation of the Níjar Carbonate Platform after the entire development of platform. **B.** Fence diagram of the simulated Níjar Carbonate Platform. Note the different progradational directions.

Fig. 4.8 B displays the simulated platform-interior geometries of RGPs 1 – 5. The sections show the internal complexity of the Níjar Carbonate Platform controlled by the El Hoyazo paleohigh. Thickness of platform deposits overlying this structure is around 10 m, and deposits are assigned to RGPs 4 and 5.

The view from a slice of the latest episodes of platform evolution, produced through uncovering the uppermost meter of the Níjar Carbonate Platform (Fig. 4.9), shows that RGP 1–3 have an internal facies pattern similar to the one described for the Cariatiz Carbonate Platform. From the first RGP, mainly the MSCF belt is preserved. Shallower and more proximal facies were eroded during the major subsequent sea-level lowering, which produced a subaerial exposure of the shallowest areas of the platform. From later packages, the entire range of facies belts is preserved. Note that the slice shown in Fig. 4.9 does not contain the RGP 5 deposits, because the crest of this last RGP lies below the slice horizon.

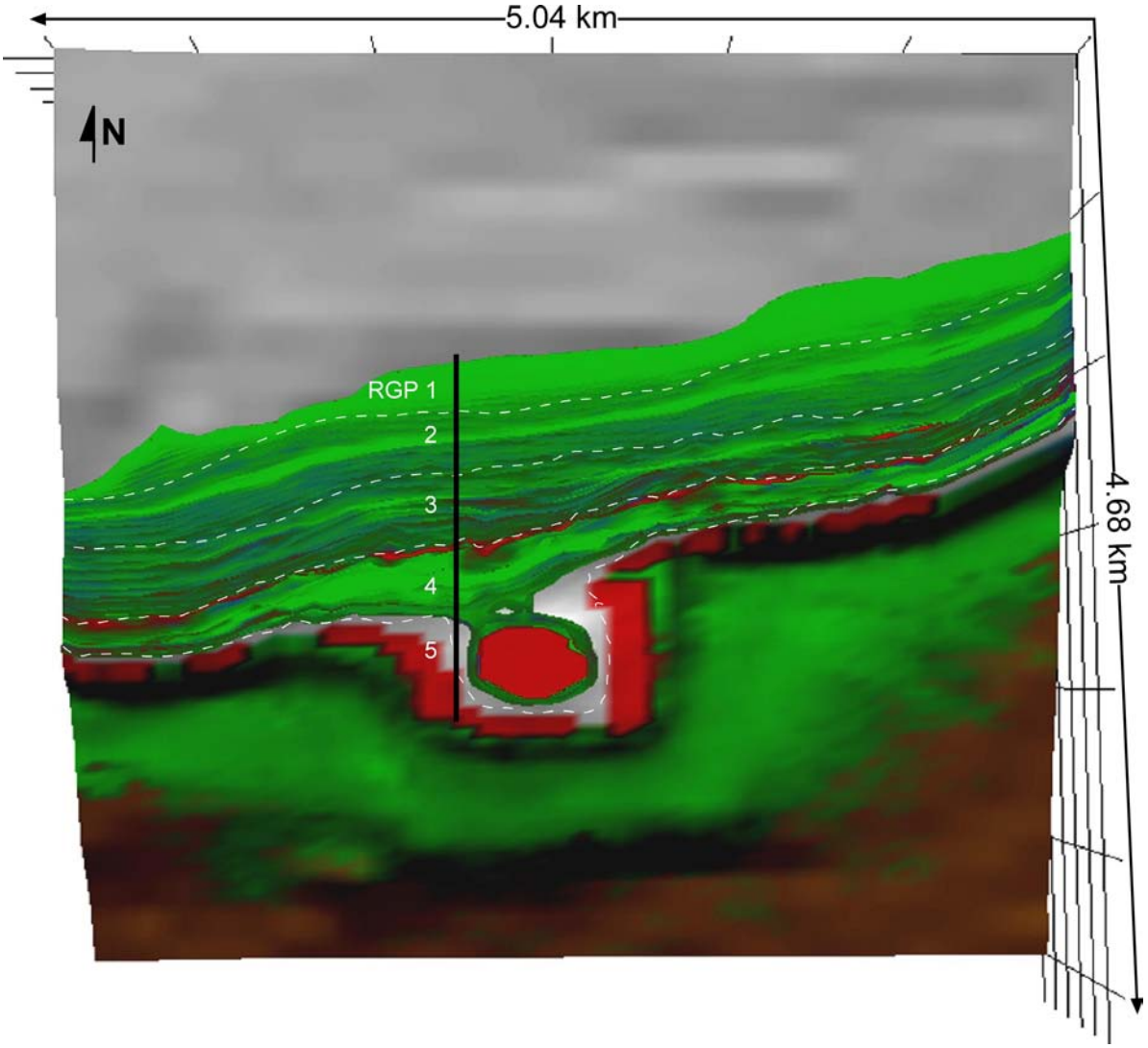

Fig. 4.9. Aerial view of the Níjar Carbonate Platform. The figure also shows the RGPs and the lateral facies distribution at the top of the platform.

RGP 4 has a more complex facies distribution, because it coincides with initiation of reef growth on top of the volcano. During the earliest stage of RGP 4 growth, the water depth over the top of the El Hoyazo volcano was around 10 m. At this stage, the preconditions for coral growth occurred at the top of this paleohigh and a small isolated reef system grew on the volcano. As a consequence, there are two reef growth domains at this stage of the platform evolution: one rims the prograding platform, the other one is an isolated patch on top of the volcano.

The main difference between the simulated platform and the facies model of the Níjar Carbonate Platform presented by Dabrio et al. (1985) is that the simulation postulates a reef patch, whereas the geological model assumes an annular reef body rimming the El

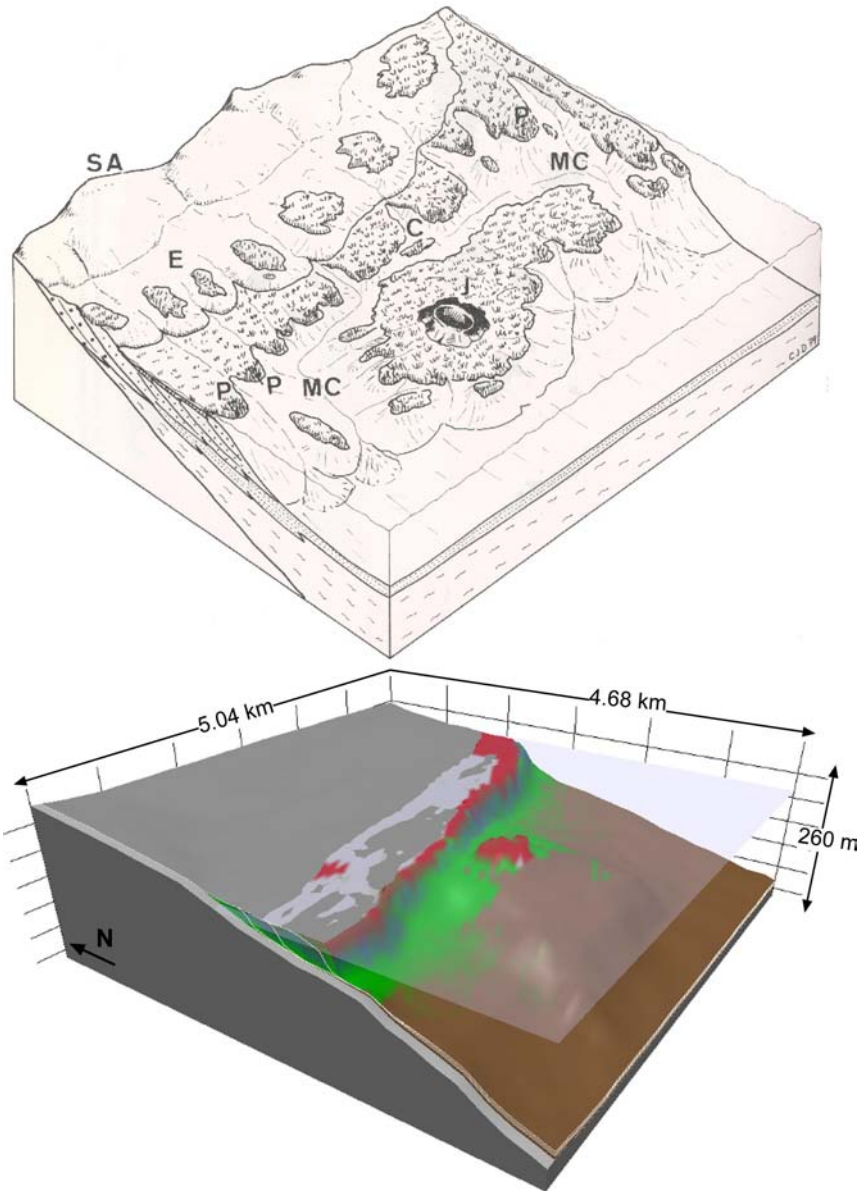

Fig. 4.10. Comparison between the geological model of the Níjar Carbonate Platform (Dabrio et al., 1985) and the 3-D computer simulation of the Níjar Carbonate Platform.

Hoyazo (Fig. 4.10). Dabrio et al. (1985) further indicate that the platform rim and the El Hoyazo reef were separated by a major water drainage channel. In the simulated Níjar Carbonate Platform, such channel geometry also occurs during the deposition of the RGP 4 (Fig. 4.10), but the channel was almost filled during the latest stage of platform evolution (RGP 5).

4.3.2 Comparison of geological and simulated cross-sections of the Níjar Carbonate Platform

The consistency of the modeling results for the Níjar Carbonate Platform is evidenced by Fig. 4.11. Two synthetic sections were reconstructed using the compiled data obtained from the facies analysis of the outcrops along ravines that cross-cut the Níjar Carbonate Platform. For each RGP, the facies distribution and the sedimentary geometries observed in the real sections compare reasonably well with the simulated sections located in approximately equivalent positions in the modeled platform.

The comparison between the real section at the El Cebollero Ravine proximity and the simulated section (Fig. 4.11 A) shows the five RGPs of the Níjar Carbonate Platform. The sediments of the RGP 1 consist of MSCF with two small patches of BBF. A downstepping of the BBF occurs below the limit between RGP 1 and 2. The RGP 2 is formed by MSCF with two small outcrops of BBF at the top of the section. The oldest sediments of the RGP are also BBF, which interfinger with MSCF. The transition between the RGP 2 and 3 is marked by downstepping of the BBF deposits occurred during the relative sea-level lowstand. The oldest part of RGP 3 is characterized by BBF deposits at the top of the section, interfingering with MSCF deposits. A downstepping of the BBF deposits, which indicates a relative sea-level fall, is observed at the top of the RGP 3 in the younger part of this RGP. The pattern of RGP 4 is similar to the one for RGP 3. The BBF outcrops in the RGP 4, however, are smaller than the BBF deposits in RGP 3. Small coral patches of *Porites* are preserved at the top of the RGP 4. RGP 5 shows a sigmoidal geometry where BBF deposits outcrop at the top of the section, interfingering with MSCF.

The second section, which dissects the El Hoyazo volcano, is located in the proximity of the El Algarrobo Ravine (Fig. 4.11 B). In this section, the first RGP extends about 150 m. The deposits of the RGP 1 and 2 are sigmoidal bodies, which consist mainly of MSCF. However, a small outcrop of BBF is preserved in the youngest part of the RGP 2, which is a remnant of the BBF downstepping, controlled by the general relative sea-level fall during the platform growth. RGP 3 is characterized by MSCF deposits in the oldest parts. A large outcrop of BBF deposits occurs in the youngest part of the RGP 3 before the initiation of RGP 4. RGP 4 consists of BBF deposits interfingering with MSCF during the early stages. During the youngest stages of the RGP 4, the most interesting feature is the

different progradational directions which are observed in the BBF and RFF deposits. The progradation landwards was caused by the inception of a small platform on the volcano. The RGP 5 shows a sigmoidal geometry, where the proximal facies (RFF and BBF) are partially preserved in the upper part of the section and interfinger with the MSCF and the pelagic deposits.

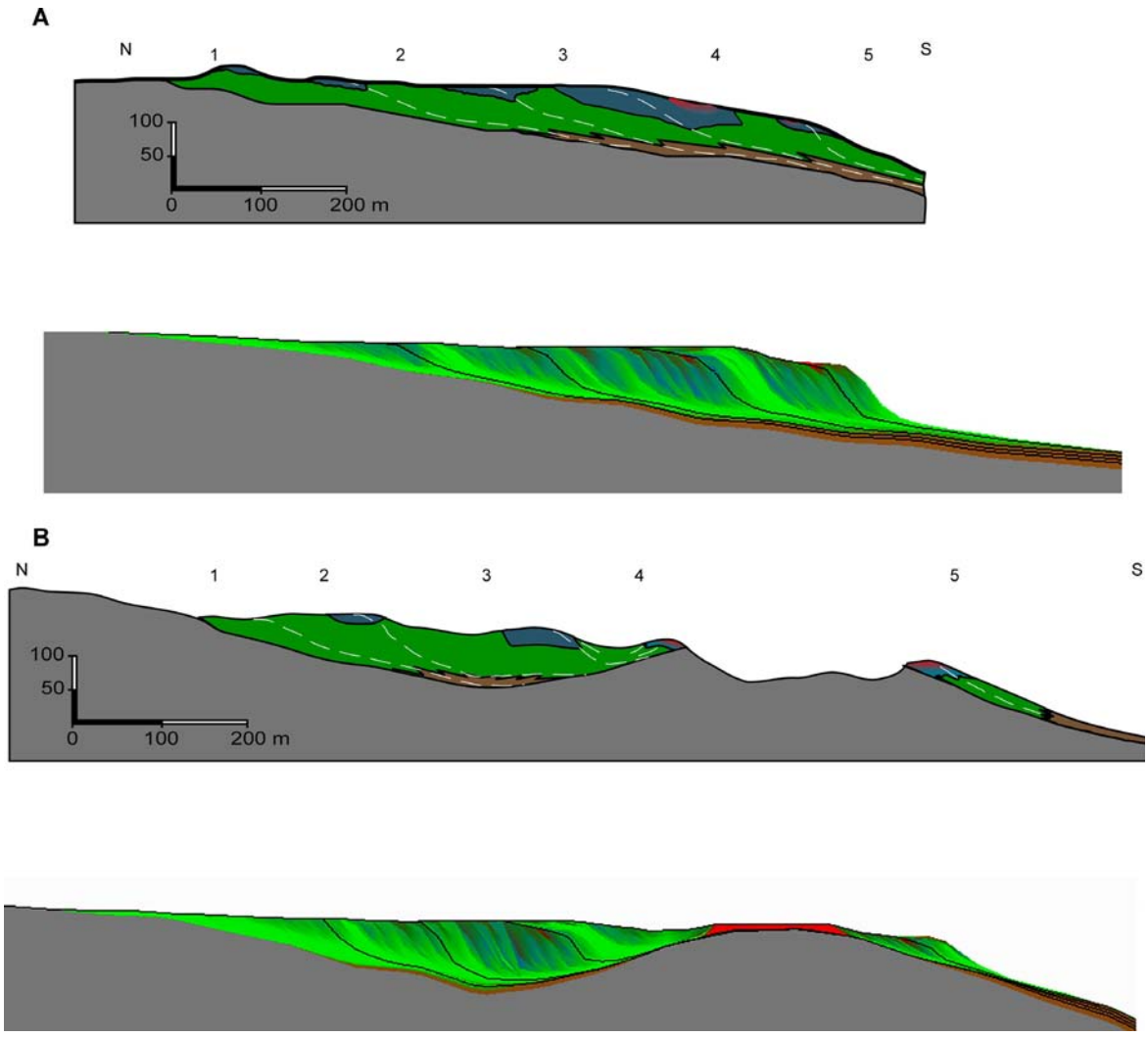

Fig. 4.11. A. Comparison between the geological cross section at the El Cebollero Ravine (upper part) and a section of the simulated platform in an equivalent position. **B.** Same for the El Algarrobo ravine.

4.3.3 Facies distribution and facies bodies in the Níjar Carbonate Platform

Erosion also played an important role during the development of the Níjar Carbonate Platform, affecting the final shape of the platform. Fig. 4.12 A shows a section of the Níjar Carbonate Platform after the deposition of the RGP 1. At this stage of platform evolution, the RGP 1 had a extension of about 800 m; there is a thin package of shallow-water facies

(BBF and RFF) forming the top of this RGP. Fig 4.12 B shows the same section after approximately 80 Ka of platform evolution. In this section, the only RFF preserved is the one deposited during RGP 4. Note that the most proximal 300 m of RGP 1 has been entirely eroded.

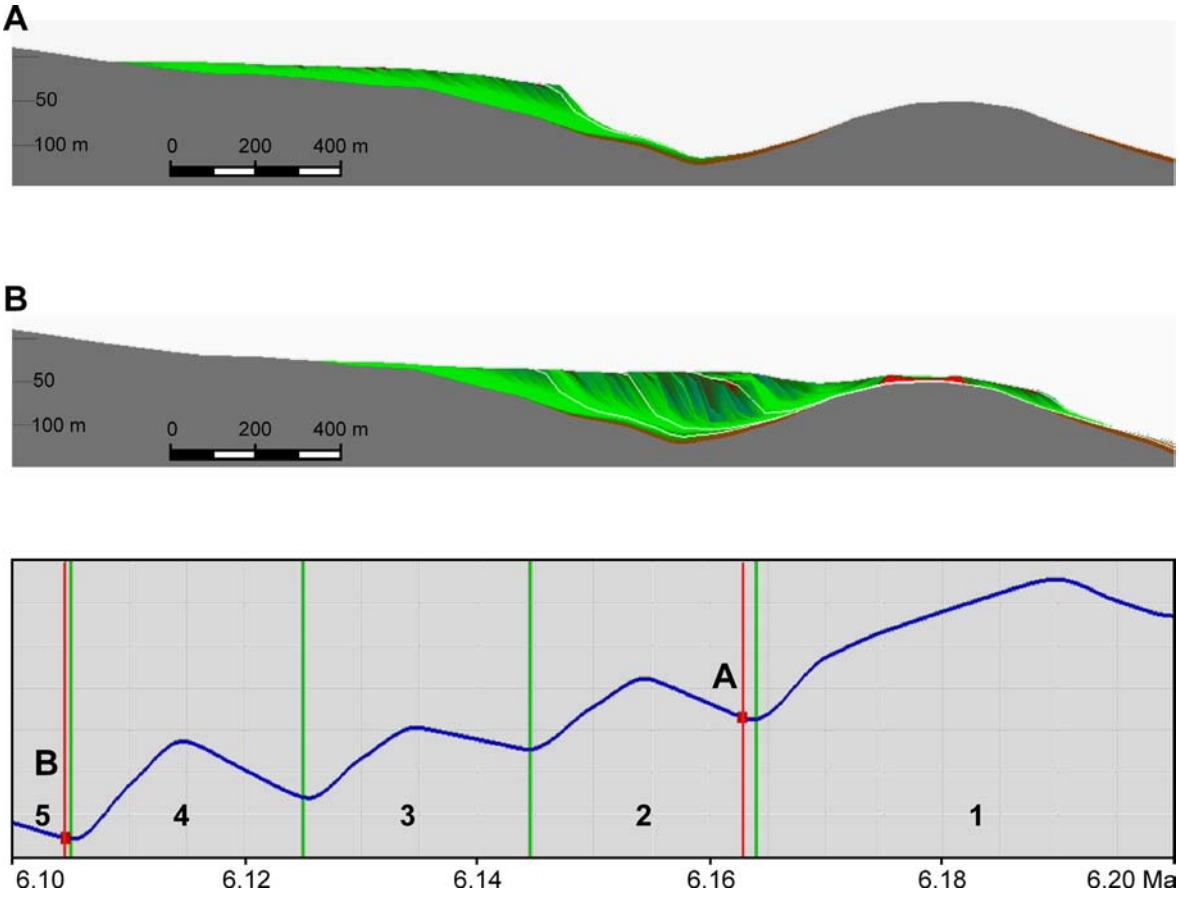

Fig 4.12. A. Section through the Níjar Carbonate Platform after deposition of the RGP 1. **B.** Same section after the major sea-level drop. Note that the shallow facies of the earliest RGP has been abraded and the El Hoyazo volcano was overlain by RFF deposits. In the lower part of the figure, the sea-level curve used for simulation of platform growth is shown. A and B designate position of time steps shown in 4.12. A and 4.12. B.

The facies distribution in the Níjar Carbonate Platform is shown in Figs 4.13 A, B, and C. The RFF distribution along two discontinuous belts, with a large isolated outcrop on the top of the EL Hoyazo Volcano, is displayed in Fig 4.13 A. The BBF deposits shown in Fig 4.13 B are heterogeneously distributed in the platform. Note that the amount of BBF deposits is reduced in the area behind the El Hoyazo volcano. Due to this, the area was relatively sheltered and the production of BBF particles from the reef framework was less significant. The MSCF deposits (Fig 4.13 C) are uniformly distributed in the Níjar

Carbonate Platform. Erosion only abraded the upper MSCF layers of the oldest RGPs deposited during the relative sea-level highstand.

Fig 4.13 D represents the sea-level curve used for the modeling of the Níjar Carbonate Platform. The color code of this curve coincides with the colors used in the facies distribution figures, and as such allow an age assignment of platform facies bodies. It results that the preserved RFF was mainly deposited during RGPs 4 and 5. Also note that most of the BBF in the Níjar Carbonate Platform belongs to RGPs 3 and 4. Only very small BBF outcrops deposited during RGP 1 are preserved in the last stage of simulated platform evolution.

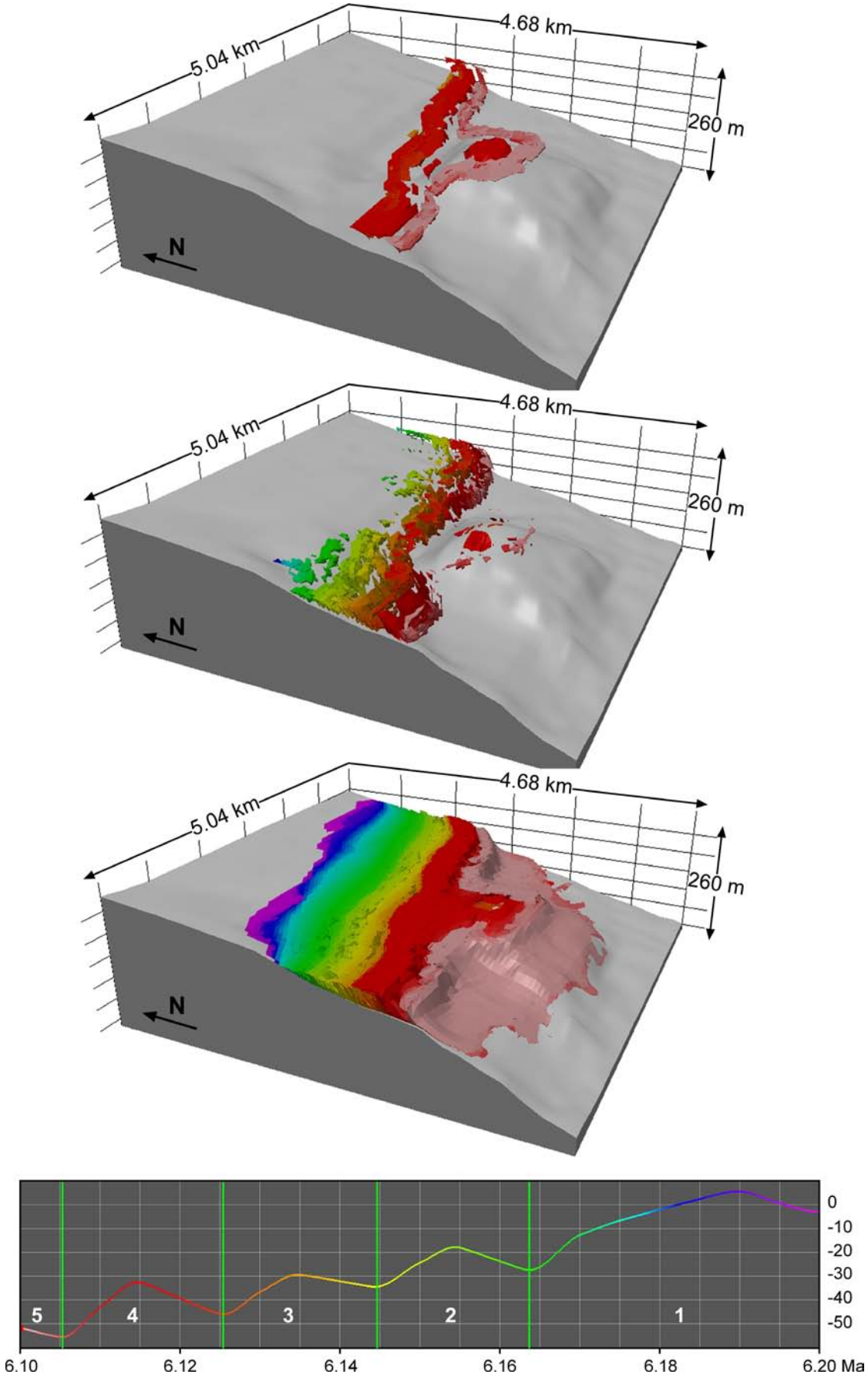

Fig. 4.13. A. RFF distribution in the Níjar Carbonate Platform. Color-to-age relationship is shown in the sea-level curve in D. **B.** Distribution of BBF deposits in the Níjar Carbonate Platform. **C.** Situation of MSCF deposits in the Níjar Carbonate Platform. **D.** Sea-level curve used for simulation of the platform. The color coding of the sea-level curve indicates the age of the corresponding interval.

4.4 Volumes of the individual facies in both carbonate platforms

REPRO provides numerical files with the accumulative volumes for the RFF, BBF and the MSCF, which were used to exhaustively analyze the volume of individual facies that compose the platform. Figs 4.14 and 4.15 show curves that represent the increment of the occupied volume for the different reef facies during the development of the Cariatiz and Níjar carbonate platforms. The simulated Cariatiz Carbonate Platform, including the pelagic sediments deposited in the basin, has a volume of around 0.8 km^3, whereas the modeled Níjar Carbonate Platform has a volume of approximately 0.62 km^3.

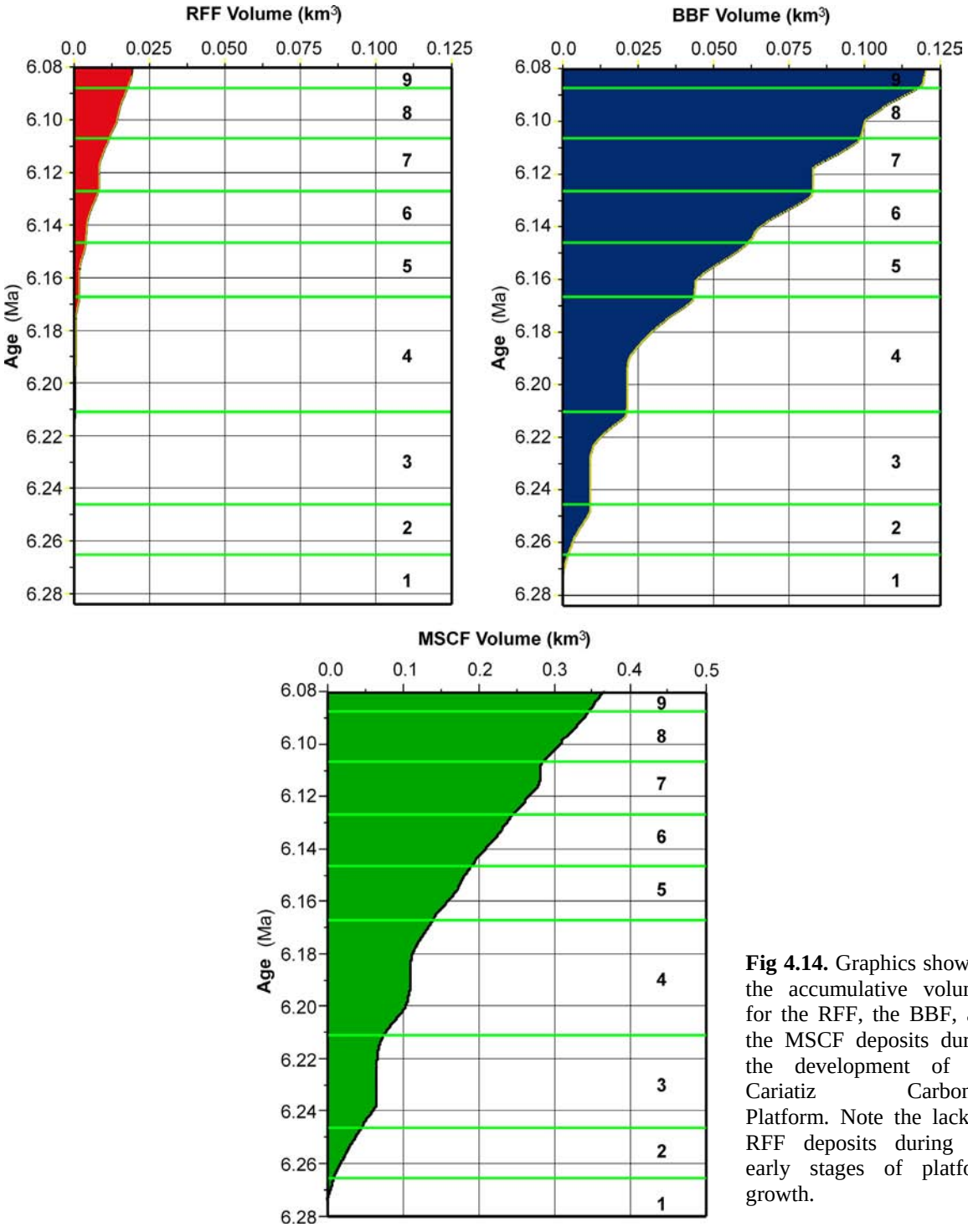

Fig 4.14. Graphics showing the accumulative volumes for the RFF, the BBF, and the MSCF deposits during the development of the Cariatiz Carbonate Platform. Note the lack of RFF deposits during the early stages of platform growth.

The Cariatiz Carbonate Platform contains 0.02 km^3 of reef deposits, 0.12 km^3 of breccias, and of 0.38 km^3 of calcarenites (Fig. 4.14). The Níjar Carbonate Platform comprises 0.0125 km^3 of reef framework, 0.085 km^3 of breccia, and 0.33 km^3 of calcarenites. The volumes of RFF deposits in both carbonate platforms represent about 2.5 % of the entire volume of the platforms. The volumes of BBF in the Cariatiz and Níjar carbonate platforms comprise approximately 15% of the total platform volume, while the MSCF volumes represent almost 50 % of it.

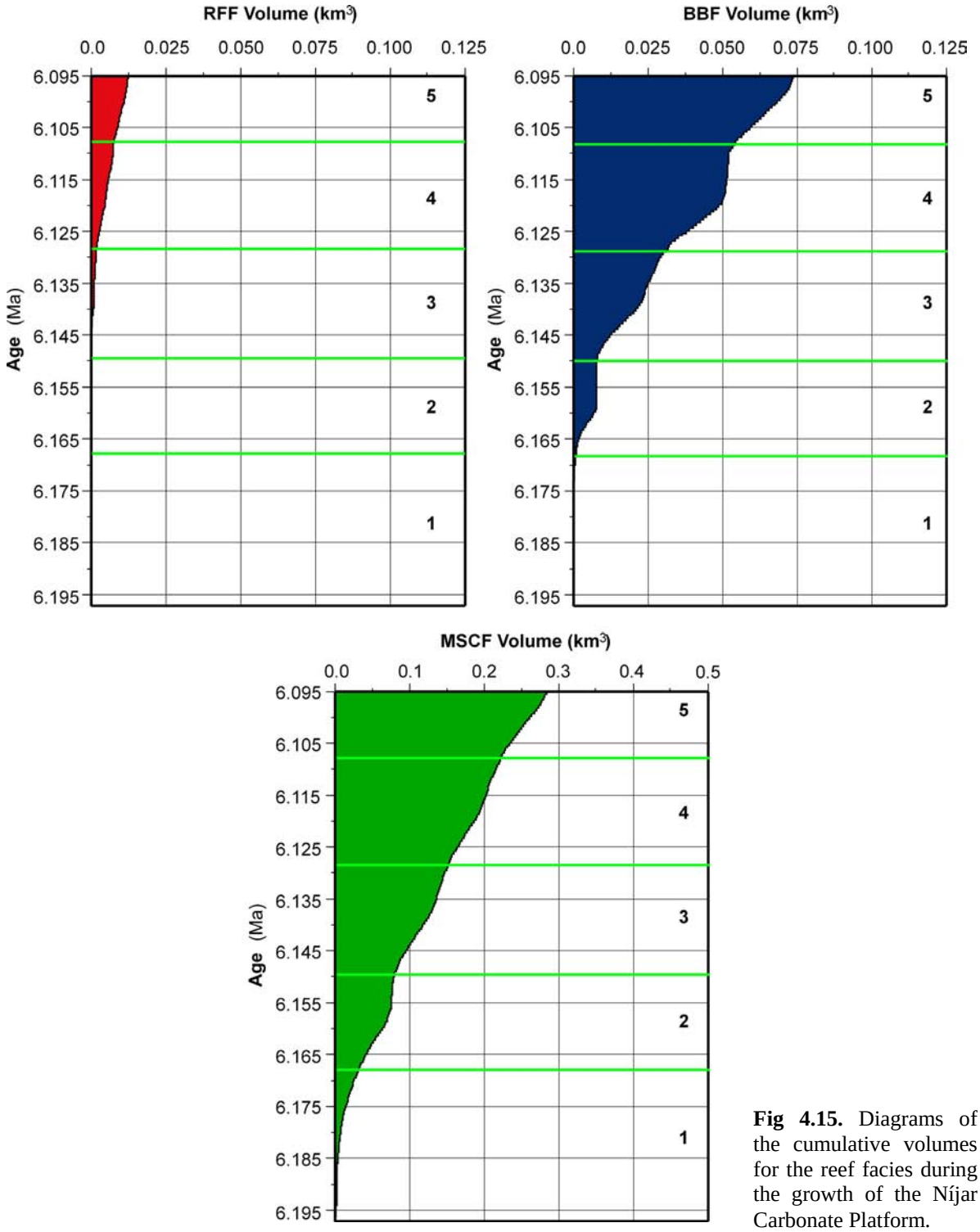

Fig 4.15. Diagrams of the cumulative volumes for the reef facies during the growth of the Níjar Carbonate Platform.

The time interval for the development of the Níjar Carbonate Platform was approximately half that for Cariatiz Carbonate Platform growth. The total volume of the Cariatiz Carbonate Platform, however, is approximately only 25 % larger than the volume of the Níjar Carbonate Platform. In order to get a good fit of the simulated and the real platforms, the reef production and debris export parameters used for the modeling of the Níjar Carbonate Platform are higher than the parameters used for the simulation of the Cariatiz Carbonate Platform. The corresponding values are listed in Tab. 1.

	CARIATIZ CARBONATE PLATFORM	NIJAR CARBONATE PLATFORM
Maximum number of BBF particles created in reef-crest per time step	3000	4520
Grain size of the BBF particles in the source point	38.2 cm	38.2 cm
Slip Factor for BBF	0.3	0.285
Maximum number of calcarenite particles created per time step	6600	6750
Grain size of the MSCF particles in the source point	0.61 cm	0.61 cm
Slip Factor for MSCF	220	900

Tab. 4.1. Comparison of the values of parameters used in the modeling of the carbonate platforms.

The combination of the graphical distribution of the different reef facies (Figs. 4.7 and 4.13) with their volumetric curves (Figs. 4.14,4.15) provides a powerful tool for the exploration of reservoir rocks formations. The lithological characteristics, assumed for the different reef facies, such as high porosity and permeability of the BBF and RFF deposits due to large sizes of the forming particles, can also be used in order to identify the potential reservoirs for oil or underground waters.

Chapter 5: Discussion and conclusions

Integration of outcrop data with the herein developed forward computer modeling and simulation of the carbonate platforms makes it possible to contribute new facets which complement existing models of the western Mediterranean carbonate platforms. These are also relevant to some ongoing discussions about different details of the stratigraphy and the controlling factors of the pre-MSC carbonate complexes. The 3-D computer models show the internal complexity of the platforms with their lateral wedging-out of individual high-frequency sequences. Modeling further proves that the distinct platforms had entirely different carbonate growth and accumulation rates. Simulation results also introduce new data about sea-level changes affecting platform evolution and the role of tectonic uplift. Finally it is shown that the correlation of neritic- with hemipelagic- to pelagic carbonate records is not straightforward.

5.1 Lateral Facies Variations

Internal complexity and laterally incomplete packages of strata are observed in modeled carbonate systems, even when the initial slope conditions are simple, as in a homoclinal slope (Burgess & Wright, 2003) for example. In the case of the simulated carbonate platforms, the initial surfaces of the platforms have complex topographies. Lateral facies changes are basically caused by the interactions between different controlling parameters implicated in the evolution of the platforms, such as the relative sea-level fluctuations, the erosion affecting the subaerial areas of the platforms, the initial topography, and parameters that manage the spreading of reef-debris. The maximum depth of the "hydrodynamic zone" parameter is another function which has a strong influence on the lateral stacking variation of the reef-debris facies because it determines the areas where breccias are generated by breakage of the reef framework.

5.2 Size of the western Mediterranean Miocene carbonate platforms

There are a series of western Mediterranean Messinian carbonate platforms which have distinct shapes and sizes. From West to East these are the Melilla-Nador platform, the Betic: Las Negras, Níjar, Cariatiz and Santa Pola platforms, and the Balearic Llucmajor Platform (Fig. 5.1).

Saint Martin et al. (1991), Cunningham et al. (1994, 1997), Saint Martin and Cornée (1996), Cornée et al. (2002), and Garcia et al. (2004) report that the Melilla-Nador Carbonate Platform prograded around 500 m in approximately 360 ka (between 6.46 and 6.10 Ma). According to the different age models this corresponds to a progradation rate of 1.4 to 1.9 km/Ma. Even though there are discrepancies in the proposed age models for the

carbonate platforms analyzed in the province of Almería (for details, see previous chapters and Mankiewicz 1987, Franseen and Mankiewicz, 1991, Martín and Braga, 1993, Mankiewicz 1996, Braga and Martín, 1996, Franseen et al., 1998, Warrlich et al., 2005), it can be assumed that the Las Negras Platform advanced 1000 m in approx. 500 ka (progradation rate of 2 km/Ma), the Níjar Carbonate Platform 1000 m during approx. 100 ka (progradation rate of 10 km/ma), and the Cariatiz Carbonate Platform 1300 m during approx. 200 Ka (progradation rate of approximately 6 km/Ma). The Santa Pola Carbonate Platform (Esteban, 1979, Feldmann and McKenzie, 1997) prograded around 4000 m during approx. 500 ka (between 6.2 and 5.7) with a progradation rate of about 8 km/Ma. Pomar (1991, 2001) analyzed the Llucmajor Carbonate Platform, which during approximately 3 Ma prograded 20 km at a rate of 7 km/Ma.

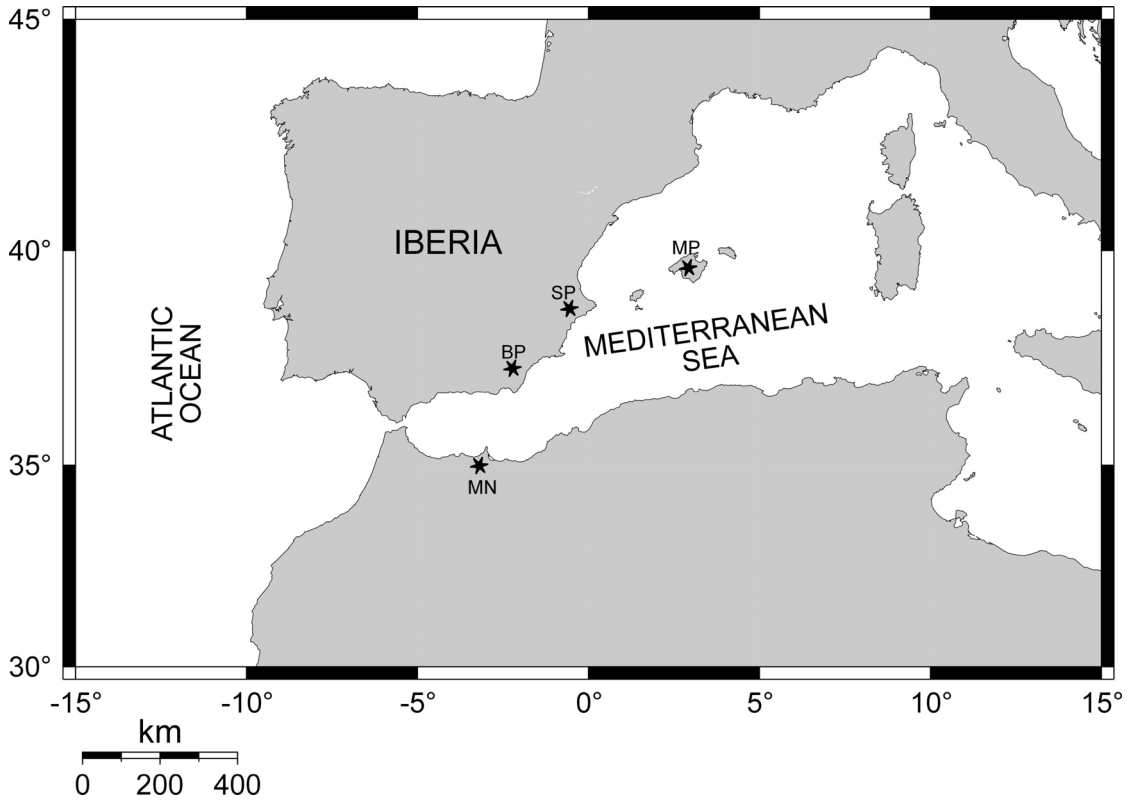

Fig. 5.1. Location of the Messinian platforms in the western Mediterranian region. MN: Melilla-Nador platform; BP: Betic platforms; SP: Santa Pola platform; MP: Majorca platform

The W-E differences of the progradation rate values, and the W-E size increment of the platforms indicate a certain palaeogeographical control on platform evolution. A possible mechanism is the inflow of cool Atlantic waters through the Rifian Corridor (Benson et al., 1991, Esteban et al., 1996), which would have reduced carbonate production rates in the western platforms.

These carbonate platforms have, however, similar thicknesses. The thickness of the Melilla-Nador platform oscillates between 50 to 70 m. Las Negras platform has a maximum thickness of about 60 to 70 m, the Níjar and the Cariatiz Platforms have thicknesses of approx. 90 m. The thickness of the Santa Pola Platform oscillates around 90 m (Feldmann and McKenzie, 1997). The Llucmajor Carbonate Platform has a maximum thickness of around 120 m according to Pomar and Ward (1995).

These data confirm the variability of parameters involved in the evolution and shape of these platforms. These parameters are related to the morphologies and angles of the platform substrates and to the conditions which were involved in the production, and deposition of the reef-facies, as well as the transport of reef debris. Ecological factors, such as reef productivity, nutrients, water temperature, currents, siliciclastic inputs, and salinity rate could also have played fundamental roles in the development of the platforms. The computer simulation of all these parameters results extremely complicated, in consequence, they have been introduced in the modeling by having a detailed control of the reef production and the generation and export of reef particles.

In the simulation of the Cariatiz and Níjar carbonate platforms, the initial topographies of the simulated platforms, as well as the angle of the substrate, are major controlling factors of platform development. On a gentle slope, progradation of the simulated reefal systems is more significant during stages of sea-level fall. This principle is corroborated by the simulation results of the platforms, which reveal that the Cariatiz Carbonate Platform progrades about 1.2 km during 200 ka and the total volume of the simulated platform was 0.8 km^3, whereas the Níjar Carbonate Platform, which grew only during the major sea-level lowering described in the Cariatiz Carbonate Platform (ca. 100 ka), shows about 1 km of progradation, and the entire volume is only 25 % smaller than the volume of the Cariatiz platform. Nevertheless, the differences in progradation rates and volumes between the platforms are not only produced because the growth of the Níjar Carbonate Platform occurred during a major sea-level lowering. Another additional reason for the size difference could also be that the Níjar platform was exposed to more agitated waters, because the Almería-Níjar Basin opens directly to the Mediterranean Sea. In the simulation, this mechanism is introduced by more elevated rates of debris export in the Níjar Platform compared to the Cariatiz Platform (Tab. 4.1).

5.3 High-frequency sea-level fluctuations

There is an ongoing discussion about the role of sea-level changes for the evolution of the western Mediterranean late Miocene carbonate platforms. Pomar (1993) discusses how reef growth packages of different sizes and geometries in the Llucmajor Platform are controlled by sea-level fluctuations. He distinguishes 5 orders of periodicity, with

amplitudes ranging between several meters and hundreds of meters. A similar model was presented by Braga and Martin (1996) for the Cariatiz Carbonate Platform, with two orders of sea-level changes. Goldstein and Franseen (1995) and Warrlich et al. (2005) propose similar mechanisms with different orders of fluctuations for the Las Negras and the Níjar platforms. In contrast, Conesa et al. (1999) and Cornée et al. (2004), exclude high-frequency sea-level fluctuations as a controlling mechanism for the growth of the western Mediterranean carbonate platforms.

The modeling results presented herein corroborate that short-term sea-level fluctuations were involved in platform formation. The curve used for modeling, which incorporates a eustatic signal, shows a pattern and trend that match well with the pattern of the curves based on the changes of the reef-crest position of the analyzed platforms. The difference of amplitudes between the global sea-level curve based on the $\delta^{18}O$ fluctuations, and the relative sea-level curves derived from the changes in position of the reef crest can be successfully explained by a regional tectonic uplift of around 110 m/Ma which affected the Sorbas basin (Braga et al., 2003) during the development of the platforms.

The same value was introduced into the Níjar model, as no uplift data have been published for this area. Nevertheless, the sea-level lowering described by Warrlich et al. (2005) widely exceeds the sea-level lowering indicated by the variations of the reef crest position and the sea-level lowering depicted in the oxygen isotope derived global sea-level curve. This mismatch between the different data sets is to a certain extent a consequence of different stratigraphic subdivisions. Whereas the northernmost calcarenites of the Níjar Carbonate Platform were assigned to DS E by Warrlich et al. (2005), it is herein proposed that these calcarenites are part of the Azagador Mb. This interpretation strongly reduces the value of relative sea-level lowering.

The sea-level curve used in the modeling of the Cariatiz and Níjar carbonate platforms shows a maximal fluctuation of about 65 m, which is slightly smaller than the maximal fluctuations of the relative sea-level curves based on changes in the reef-crest position. The curves based on the changes of reef crest position present an uncertainty because the reef crests are not preserved along the entire progradational profiles of the platforms. Nevertheless, the sea-level curve used for the simulation of the platforms is in compliance with longer-term sea level lowering which occurred between 6.5 and 6 Ma described by Abreu and Anderson (1998).

5.4 Periodicity of high-frequency sea-level changes

The pattern of the isotope-derived sea-level curve, used in the simulation of the Cariatiz and Níjar carbonate platforms, indicates that, in addition to the long-term sea-level trend which triggered formation of the Fringing Reef Unit (Braga and Martin, 1996), two periodicities of short-term sea-level changes influenced platform growth during distinct time intervals. The wavelet power spectrum (Fig. 2.17) reveals that the shorter term period occurred during the oldest RGP and during the major sea-level lowering (RGPs 5-9) in the Cariatiz Carbonate Platform, as well as during the RGPs 2 to 5 in the Níjar Carbonate Platform. This period corresponds to precession, whereas the longer term period of RGPs 3 and 4 in the Cariatiz Carbonate Platform, and the RGP 1 in the Níjar Carbonate Platform, which is correlated to the RGP 4 of the Cariatiz Carbonate Platform, corresponds to obliquity.

Late Miocene cyclic variability of the $\delta^{18}O$ record is postulated to be primarily controlled by obliquity and to a lesser degree by precession. This paradigm is an outcome of the spectral analysis of open ocean isotope records, where significant power is found in the obliquity band of the spectra and less power in the precessional band (Sierro et al., 1999). Consequently, Sierro et al. (1999), based on an analysis of the Abad Mb in the Sorbas Basin, propose that the precessional cyclicity during growth of the carbonate platforms only governed climate change, which, in turn, affected rain fall intensity and hence water salinity. Coral reefs are supposed to grow during humid phases coinciding with the deposition of sapropels in the basin. This view of a pure climatic control of precession has been recently challenged. Van der Laan et al. (2005) show that the Messinian precession component in the $\delta^{18}O$ record in the area of Ain el Beida (NW Morocco) not only bears a climatic signal, but is also influenced by glacial variability. In other terms, this means that precession-driven eustatic sea-level fluctuations were recognized in this record.

The modeling results point to a complex interaction of precession and obliquity as controlling factors of sea-level oscillations. It is proposed that the amplitudes of the sea-level changes caused by precessional cycles were modulated by obliquity during the 3rd and 4th cycles in the development of the Cariatiz Carbonate Platform, and during RGP 1 of the Níjar Carbonate Platform. This amplitude modulation of the precessional cycles by obliquity occurred during the highstand stage of the longer-term cycle, which is related to short eccentricity (Braga & Martín, 1996). The lowstands of the precessional cycles during this interval are reduced, as the obliquity fluctuations are superimposed in such a way that the precessional minima (lowstands) are compensated by rising intervals of

obliquity cycles. This assumption is a certain modification to Braga and Martín (1996), who related the RGPs of the platform exclusively to precessional cyclicity.

5.5 Correlation between neritic and pelagic records

The cyclicity of the hemipelagic sediments in the Sorbas Basin was investigated in a series of studies (Sierro et al., 1993, 1999, Krijgsman et al., 2001). The correlation between the number of pelagic cycles and the neritic cycles described herein is not straightforward. In the Sorbas Basin, there are eighteen precessional cycles in the hemipelagic deposits between PF-event 4 (Sierro et al., 1993) and the base of the Yesares Mb. (Krijgsman et al., 1999). This time interval of lithological succession encompasses the start and the demise of the Cariatiz Carbonate Platform (Braga and Martín, 1996). The cycle number in the basin, however, may be distorted by a minor slump described by Sierro et al. (2001). This slump, which is recorded 6 cycles above the position of the PF-event 4, was suggested as an indicator of the presence of an unconformity between the Bioherm and the Fringing Reef Unit (Sierro et al., 2001). This would imply that the nine RGPs of the Cariatiz Carbonate Platform correlate to twelve precessional cycles of the Upper Abad Mb.

The discrepancy between the hemipelagic and neritic cyclicity in the Messinian of the Sorbas Basin would even be more important if one takes into account the possibility that not all the neritic sediment packages have a basinal equivalent. This could be the case for RGPs 3 and 4 of the Cariatiz Carbonate Platform, which downlap onto the lower bounding unconformity of the Fringing Reef Unit (Fig. 2.9).

In conclusion, there is apparently a pronounced difference between the pelagic and the neritic sediment record in the Sorbas Basin. This could demonstrate that the neritic and the pelagic/hemipelagic realms record environmental disturbances in a distinct way.

5.6 Final remarks

Although the program REPRO produced solid results, which add new data to the ongoing discussion on periodicities in Miocene deposits, it must also be realized that these models - like any other models of natural processes - can only be an approximation of nature, where more random phenomena are involved than can be included in the modeling development. Deviations of the model realizations from observations are therefore an inherent feature.

References

Abreu V.S. and **Anderson J.B.** (1998) Glacial eustasy during the Cenozoic; sequence stratigraphic implications. *AAPG Bulletin*, **82**, 1385-1400.

Addicott, W.O., **Snavely, P.D.Jr**, **Poore, R.Z.**, and **Bukry, D.** (1979) La secuencia Neógena marina de los campos de Dalías y Níjar. *Estudios geol.*, **35**, 609-631.

Bakker, H.E., **De Jong, K.**, **Helmers, H.**, and **Biermann, C.** (1989) The geodynamic evolution of the Internal Zone of the Betic Cordilleras (south-east Spain); a model based on structural analysis and geothermobarometry. J. met. Geol. 7, 359-381.

Bellon, H., **Bordet, P.**, and **Montenat, C.** (1983) Chronology of the Neogene magmatism of the Betic Cordillera, southern Spain. *Bull. Soc. Géol. Fr.*, **25**, 205-217.

Benson, R. H., Rakic-El Bied, K., and **Bonaduce, G.** (1991) An important current reversal (influx) in the Rifian Corridor (Morocco) at the Tortonian-Messinian boundary; the end of Tethys Ocean. In: *Special section on Paleoceanography of marginal seas*. Paleoceanography, **6**, 165-192.

Billups K. (2002) Late Miocene through early Pliocene deep water circulation and climate change viewed from the sub-Antarctic South Atlantic. *Palaeogeogr. Palaeoclimatol. Palaeoecol*, **185**, 287-307.

Bosence, D. and **Waltham, D.** (1990) Computer modeling the internal architecture of carbonate platforms. *Geology*, **18**, 26-30.

Bosellini A. (1984) Progradation geometries of carbonate platforms; examples from the Triassic of the Dolomites, northern Italy. *Sedimentology*, **31** (1), 1-24.

Bosence, D.W.J., Pomar, L., Waltham, D.A. and **Lankester, T.H.G.** (1994) Computer modeling a Miocene carbonate platform, Mallorca, Spain. *AAPG Bulletin*, **78**, 247-266.

Bosscher H. and **Schlager W.** (1992) Computer simulation of reef growth. *Sedimentology*, **39**, 503-512.

Bowmann S.A. and **Vail P.R.** (1999) Interpreting the stratigraphy of the Baltimore Canyon section, offshore New Jersey with PHIL, a stratigraphic simulator. In: *Numerical experiments in stratigraphy; recent advances in stratigraphic and sedimentologic computer simulations*. *SEPM Spec. Publ.*, **62**, 117-138. Tulsa, Oklahoma, USA.

Braga, J.C. and **Martín, J.M.** (1992) Messinian carbonates of the Sorbas basin: sequence stratigraphy, cyclicity and facies. In: *Late Miocene Carbonate Sequences of Southern Spain*: A Guidebook for Las Negras and Sorbas area, in conjunction with the SEPM/IAS Research Conference on Carbonate Stratigraphic Sequences: Sequences Boundaries and Associated Facies, August 30-September 3, La Seu, 78-108.

Braga, J.C. and **Martín, J.M.** (1996) Geometries of reef advance in response to relative sea-level changes in a Messinian (uppermost Miocene) fringing reef (Cariatiz Reef, Sorbas Basin, SE Spain). *Sediment. Geol.*, **107**, 61-81.

Braga, J.C., Martín, J.M. and **Quesada, C.** (2003) Patterns and average rates of late Neogene-Recent uplift of the Betic Cordillera, SE Spain. *Geomorphology*, **50**, 3-26.

Braga, J.C., Martín, J.M. and **Riding, R.** (1996) Internal structure of segment reefs; Halimeda algal mounds in the Mediterranean Miocene. *Geology (Boulder)*, **24**, 35-38.

Braga, J.C., Jiménez A.P., Martín, J.M. and **Rivas, P.** (1993) Bioconstrucciones de corallinaceas profundas y someras en secuencias deltaico-arrecifales en el Messiniense de la cuenca de Sorbas (Almeria, SE España). *Comunicaciones IX Jornadas de Paleontología*, Málaga, 65-69.

Burgess, P.M. and **Wright, V.P.** (2003) Numerical forward modeling of carbonate platform dynamics; an evaluation of complexity and completeness in carbonate strata. *J. Sediment. Res.*, **73**, 637-652.

Chalker, B.E., Barnes, D.J., Dunlop, W.C. and **Jokiel, P.L.** (1988) Light and reef-building corals. *Interdisc. Sci. Rev.*, **13**, 222-237.

Civis, J., Martinell, J. and **De Porta, J.** (1977) Precision sobre la edad del Miembro Zorreras (Sorbas, Almeria). In: *Messinian Seminar*, Málaga, Abst., vol. 3, 31-32.

Conesa, G., Martin, J.P.S., Cornée, J.J. and **Muller, J.P.** (1999) Nouvelles contraintes sur la crise de salinite messinienne par l'etude d'une plate-forme carbonatee marginale (bassin de Sorbas, Espagne), *CR. Acad. SCI. II A*, **328** (2), 81-87.

Cornée, J. J., Roger, S., Muench, P., Saint Martin, J. P., Feraud, G., Conesa, G., and **Pestrea-Saint Martin, S.** (2002) Messinian events: new constraints from sedimentological investigations and new (super 40) Ar/ (super 39) Ar ages in the Melilla-Nador Basin (Morocco). *Sediment. Geol.* **151**, 127-147.

Cornée J.J., Saint Martin J.P., Conesa G., Munch P., André J.P., Saint Martin S. and **Roger S.** (2004) Correlations and sequence stratigraphic model for Messinian carbonate platforms of the western and central Mediterranean. *Int. J. Earth Sci.(Geol. Rundsch.)*, **93**, 621-633.

Cunningham, K. J., Farr, M. R., and **Rakic-El Bied, K.** (1994) Magnetostratigraphic dating of an upper Miocene shallow-marine and continental sedimentary succession in northeastern Morocco. *Earth Planet. Sci. Lett.*, **127**, 77-93.

Cunningham, K. J., Benson, R. H., Rakic-El Bied, K., and **McKenna, L. W. (1997)** Eustatic implications of late Miocene depositional sequences in the Melilla Basin, norteastern Morocco. *Sediment. Geol.*, **107**, 147-165.

Dabrio, C. B., Martín, J. M. (1978) The Messinian reefs of Almería, southeastern Spain. *Cuar. Geol. Univ. Granada*, **8-9**, 83-100.

Dabrio, C., Esteban, M. and **Martín, J.M.** (1981) The coral reef of Níjar, Messinian (Uppermost Miocene), Almería Province, S.E. Spain. *J. sedim. Petrol.*, **51**, 521-539.

Dabrio, C.J., Martín, J.M. and **Megias, A.G.,** (1985) The tectosedimentary evolution of Mio-Pliocene reefs in the Province of Almería. In: *6th European Regional Meeting of Sedimentologists*, Excursion Guidebook *(Eds. Milá M.D. and Rosell J.),* Lleida, pp.269-305.

Di Ballestini, G., **Toscani, L.**, **Iaccarino, S.**, and **Villa, I.M.** (1987) K/Ar ages and the geological setting of calc-alkaline volcanic rocks from Sierra de Gata, SE Spain. *Neues Jahrb. Mineral. Monatsh.*, **8**, 369-383.

Doligez, B., Granjeon, D., Joseph, P., Eschard, R. (1999) How can stratigraphic modeling help constrain geostatistical reservoir simulations?. In: *Numerical experiments in stratigraphy; recent advances in stratigraphic and sedimentologic computer simulations. SEPM Spec. Publ.*, **62**, 239-244. Tulsa, Oklahoma, USA.

Duggen, S., **Hoernle, K.**, **van den Bogaard, P.**, and **Harris, C.** (2004) Magmatic evolution of the Alboran region; the role of subduction in forming the western Mediterranean and causing the Messinian salinity crisis. *Earth Planet. Sci. Lett.*, **218**, 91-108.

Eberli, G.P. and **Ginsburg, R.N.** (1989) Cenozoic progradation of northwestern Great Bahama Bank, a record of lateral platform growth and sea-level fluctuations. In: *Controls on carbonate platform and basin development* (Eds. Crevello, P.D., Wilson, J.L., Sarg, J.F., and Read, J.F.). *SEPM* Spec. Publ. **44**, 339-351.

Egeler, C. G. and **Simon, O. J.** (1969). Sur la tectonique de la Zone Bétique (Cordillères Bétiques, Espagne). *Koninklijke Nederlandse Akademie van Wetenschappen, Natuurkunde, Verhandelingen 1st serie,* **XXV**(3), 1–90.

Esteban, M. (1979) Significance of the upper Miocene coral reefs of the western Mediterranean. *Palaeogeogr. Palaeoclimatol. Palaeoecol.*, **29**, 169-188.

Esteban, M. (1996) An overview of Miocene reefs from Mediterranean areas; general trends and facies models. In: *Models for Carbonate Stratigraphy from Miocene Reef Complexes of Mediterranean Regions*. Concepts in Sedimentology and Paleontology Series. *Soc. Econ. Paleont. Miner.*, Tulsa, **5**, 3-53.

Esteban, M. and **Gíner, J.** (1980) Messinian coral reefs and erosion surfaces in Cabo de Gata (Almería, SE Spain). *Acta geol. Hisp.*, **15**, 97-104.

Fairbanks, R.G. and **Matthews, R.K.** (1978) The marine oxygen isotope record in Pleistocene coral, Barbados, West Indies. *Quaternary Res.*, **10**, 181-196.

Feldmann, M., and **McKenzie, J. A.** (1997) Messinian stromatolite-thrombolite associations, Santa Pola, SE Spain; an analogue for the Palaeozoic?. *Sedimentology*, **44**, 893-914.

Fernandez Soler, J.M.F. (1992) *El volcanismo calco-alcalino de Cabo de Gata (Almería)* [Ph.D. thesis]. *Est. Vulcanol. Petrol., Univ. de Granada.*

Fisher, R.A. (1936) The wave of advance of advantageous genes. *Ann. Of Eugen*, **7**, pp. 355-369.

Fortuin, A.R. and **Krijgsman, W.** (2003) The Messinian of the Níjar Basin (SE Spain): sedimentation, depositional environments and paleogeographic evolution. *Sed. Geol.*, **160**, 213-242.

Franseen, E. K., **Mankiewicz, C.**, and **Pray, L. C.** (1988) Depositional sequences and correlation of middle to upper Miocene reef complexes, Nijar and Las Negras areas, southeastern Spain. Abstract *AAPG Bull.*, **72**, 186-187.

Franseen, E.K. and **Goldstein, R.H.** (1992) Sequence stratigraphy of Miocene strata, Las Negras area, southeastern Spain: implications for quantification of relative change in sea level. In: *Late Miocene Carbonate Sequences of Southern Spain*: A Guidebook for Las Negras and Sorbas area, in conjunction with the SEPM/IAS Research Conference on Carbonate Stratigraphic Sequences: Sequences Boundaries and Associated Facies, August 30-September 3, La Seu, 1-77.

Franseen, E.K. and **Goldstein, R.H.** (1996) Palaeoslope, sea-level, and climate controls on Upper Miocene platform evolution, Las Negras area, southeastern Spain. In: *Models for Carbonate Stratigraphy from Miocene Reef Complexes of Mediterranean Regions*. Concepts in Sedimentology and Paleontology Series. *Soc. Econ. Paleont. Miner.*, Tulsa, **5**, 159-176.

Franseen, E.K. and **Mankiewicz, C.** (1991) Depositional sequences and correlation of middle (?) to late Miocene carbonate complexes, Las Negras and Níjar areas, southeastern Spain. *Sedimentology*, **38**, 871–898.

Franseen, E.K. and **Mankiewicz, C.** (1993) Depositional Sequences and Correlation of Middle(?) to Late Miocene Carbonate Complexes, Las Negras and Nijar Areas, Southeastern Spain: Reply. *Sedimentology*, **40**, 353-356.

Franseen, E. K., Goldstein, R. H., and **Farr, M. R.** (1998) Quantitative controls on location and architecture of carbonate depositional sequences; upper Miocene, Cabo de Gata region, SE Spain. *J. Sed. Res* , 68, 283-298.

Garcia, F., Conesa, G., Muench, P., Cornee, J. J., Saint Martin, J. P., and **Andre, J. P.** (2004) Evolution of the Melilla-Nador Basin (northeastern Morocco) coastal environment during upper Messinian between 6.0 and 5.77 Ma. *Geobios*, **37**, 23-36.

Gautier, F., Clauzon, G., Suc, J.P., Cravatte, J. and **Violanti, D.** (1994) Age et duree de la crise de salinite messinienne; Age and duration of the Messinian salinity crisis. *CR. Acad. SCI. II A*, **318**, 1103-1109.

Goldstein, R.H. and **Franseen, E.K.** (1995) Pinning points; a method providing quantitative constraints on relative sea-level history. *Sediment. Geol.*, **95** (1-2), 1-10.

Goubert, E., Néraudeau, D., Rouchy, J.M. and **Lacour, D.** (2001) Foraminiferal record of environmental changes; Messinian of the Los Yesos area (Sorbas Basin, SE Spain). *Palaeogeogr. Palaeoclimatol. Palaeoecol*, **175** (1-4), p. 61-78.

Hilgen, F.J., Krijgsman, W., Langereis, C.G., Lourens, L.J., Santarelli, A. and **Zachariasse, W.J.** (1995) Extending the astronomical (polarity) time scale into the Miocene. *Earth Planet. Sc. Lett.*, **136**, 495-510.

Hodell, D.A., Benson, R.H., Kent, D.V., Boersma, A., and **Rakic-El Bied, K.**, (1994) Magnetostratigraphic, biostratigraphic, and stable isotope stratigraphy of an Upper Miocene drill core from the Salé Briqueterie (northwestern Morocco): a high-resolution chronology for the Messinian stage. *Paleoceanography*, **9**, 835-855.

Hsü, K.J., **Montadert, L.**, **Bernouilli, D.**, **Cita, M.B.**, **Erickson, A.**, **Garrison, R.E.**, **Kidd, R.B.**, **Melieres, F.**, **Müller, C.**, and **Wright, R.** (1977) History of the Mediterranean salinity crisis. *Nature*, **267**, 399-403.

Huessner, H. and **Roessler, J.** (1996) Modeling of reef growth in a 3-dimensional space. *Goettinger Arbeiten zur Geologie und Palaeontologie*. Sonderband, SB2, 397-404.

Huessner, H. , Roessler, J., Betzler, C., Petschick, R. and **Peinl, M.** (2001) Testing 3D computer simulation of carbonate platform growth with REPRO; the Miocene Llucmajor carbonate platform (Mallorca*). Palaeogeogr. Palaeoclimatol. Palaeoecol*, **175**, 239-247.

Iaccarino, **S. Borlotti**, **E., Papani**, **G., Pelosio**, **G.** and **Raffi,S.** (1975) Lithostratigrafia e biostratigrafia di alcune serie Neogeniche della provinca di Almeria (Andalusia orientale,Spagna). *Ateneo Parmenje, Acta Nat.* 11, 237-313.

Jiménez, A.P., **and Braga, J.C.** (1993) Occurrence and taphonomy of bivalves from the Níjar reef (Messinian, Late Miocene, SE Spain). *Palaeogeogr., Palaeoclimatol., Palaeoecol.,* **102**, 239-251.

Keigwin, L.D., (1987) Pliocene stable-isotope record of Deep Sea Drilling Project Site 606: sequential events of ^{18}O enrichment beginning at 3.1. *Init. Repts. DSDP*, **94**, 911-920.

Kendall, C.G.ST.C. and **Schlager, W.** (1981) Carbonates and relative changes in sea level. *Mar. Geol.*, **44** (1-2), 181-212.

Kendall, C.G.St.C., Whittle, G.L., Ehrlich, R., Moore, P.D., Cannon, R.L. and Hellmann, D.R. (1993) Computer sedimentary simulation models sequence stratigraphy. *Oil and Gas J.*, **91**, 46-51.

Krijgsman, W., Hilgen, F.J., Fortuin A. and **Sierro, F.J.** (2001) Astrochronology for the Messinian Sorbas basin (SE Spain) and orbital (precessional) forcing for evaporite cyclicity. *Sediment. Geol.*, **140,** 43-60.

Krijgsman, W., Hilgen, F.J., Raffi, I., Sierro, F.J. and **Wilson, D.S.** (1999) Chronology, causes and progression of the Messinian salinity crisis. *Nature* (London), **400**, 652-655.

López-Ruiz, J. and **Rodríguez-Badiola, E.** (1980) La región volcánica Neógena del sureste de España. *Est. Geol.*, **36**, 5-63.

Lough, J.B. and **Barnes, D.J.** (2000) Environmental controls on growth of the massive coral Porites. *J. Exp. Mar. Biol. Ecol.,* **245**, 225-243.

Mankiewicz, C. (1987) *Sedimentology and calcareous algal paleoecology of middle and upper Miocene reef complexes near Fortuna (Murcia Province) and Níjar (Almería Province), southeastern Spain.* PhD thesis, University of Wisconsin-Madison, USA.

Mankiewicz, C. (1996) The middle to upper Miocene carbonate complex of Nijar, Almeria Province, southeastern Spain. In: *Models for Carbonate Stratigraphy from Miocene Reef Complexes of Mediterranean Regions*. Concepts in Sedimentology and Paleontology Series. *Soc. Econ. Paleont. Miner.*, Tulsa, **5**, 141-157.

Martín, J.M. and **Braga, J.C.** (1990) Arrecifes messinienses de Almería. Tipologías de crecimiento, posición estratigráfica y relación con las evaporitas. *Geogaceta*, **7**, 66-68.

Martín, J.M. and **Braga, J.C.** (1993) Discussion (of Franseen E. K., Mankiewicz C., (1991) Depositional sequences and correlation of Middle (?) to Late Miocene carbonate complexes, Las Negras and Níjar areas, southeastern Spain). *Sedimentology*, **40**, 351−356.

Martín, J.M. and **Braga, J.C.** (1994) Messinian events in the Sorbas Basin in southeastern Spain and their implications in the Recent history of the Mediterranean. *Sediment. Geol.*, **90**, 257-268.

Martín, J.M. and **Braga, J.C.** (2001) Shallow marine sedimentation. In: A Field Guide to the Neogene Sedimentary Basins of the Almeria Province, South-East Spain. Blackwell Science Ed.

Martín, J.M., Braga, J.C. and **Riding, R.** (1993) Siliciclastic stromatolites and thrombolites, late Miocene, S.E. Spain. *J. sedim. Petrol.*, **63**, 131-139.

Martín, J.M., Braga, J.C. and **Riding, R.** (1997) Late Miocene Halimeda alga-microbal segment reefs in the marginal Mediterranean Sorbas Basin, Spain. *Sedimentology*, **44**, 441-456.

Martín, J.M., **Braga, J.C.**, and **Rivas, P.** (1989) Coral successions in upper Tortonian reefs in SE Spain. *Lethaia*, 22, 271-286.

Martín, J.M., **Braga, J.C.**, **Betzler, C.**, and **Brachert, T**. (1996) Sedimentary model and high-frequency cyclicity in a Mediterranean, shallow-shelf, temperate-carbonate environment (uppermost Miocene, Agua Amarga Basin, southern Spain). *Sedimentology*, **43** 263-277.

Megías, A.G. (1985) Tectosedimentary relationships between Mio-Pliocene reefs and evaporites in Almería and Sorbas Basins, SE Iberian Peninsula. In: *Int. Ass. Sedimentologists 6th Ann. Meeting*, 292-295.

Miller, K.G., Fairbanks, R.G. and **Thomas, E.** (1987) Benthic foraminiferal carbon isotopic records and the development of abyssal circulation in the eastern North Atlantic. *Initial Rep. Deep Sea*, **94**, 981-996.

Montgomery, P., **Farr, M.R.**, **Franseen, E.K.** and **Goldstein, R.H.** (2001) Constraining controls on carbonate sequences with high-resolution chronostratigraphy: Upper Miocene, Cabo de Gata region, SE Spain. *Palaeogeogr. Palaeoclimatol. Palaeoecol.*, **176**, 11−45.

Nordlund, U. (1999a) Stratigraphic modeling using common-sense rules. In: *Numerical experiments in stratigraphy; recent advances in stratigraphic and sedimentologic computer simulations. SEPM Spec. Publ.,* **62**, 245-251. Tulsa, Oklahoma, USA.

Nordlund, U. (1999b) FUZZIM; forward stratigraphic modeling made simple. In: *Freeware and shareware in the geosciences* (ed. Butler, J.C.*), Computers & Geosciences*, **25**, 449-456.

Ott D´Estevou, P. (1980) Evolution dynamique du bassin Néogene de Sorbas (Cordillères Bétiques Orientales, Espagne). Doc. Et Trav. IGAL, Paris, 1.

Ott d´Estevou, P. and **Montenat, C.** (1990) Le bassin de Sorbas-Tebarnas. *Doc. Trav. IGAL*, 12-13: p. 101-128.

Pomar, L. (1991) Reef geometries, erosion surfaces and high-frequency sea-level changes, upper Miocene reef complex, Mallorca, Spain. Sedimentology, **38**, 243-269.

Pomar, L. (1993) High-resolution sequence stratigraphy in prograding Miocene carbonates; application to seismic interpretation. In: *Carbonate sequence stratigraphy; recent developments and application*, AAPG bulletin, **57**, 389-407.

Pomar, L. (2001) Ecological control of sedimentary accommodation; evolution from a carbonate ramp to rimmed shelf, upper Miocene, Balearic Islands. In: *Paleoceanology of reefs and carbonate platforms; Miocene to modern*. *Palaeogeogr. Palaeoclimatol. Palaeoecol,* **175**, 249-272.

Pomar, L. and **Ward, W.C.** (1991) Caracteristicas de las secuencias deposicionales de alta frecuencia en el sistema arrecifal del Mioceno superior de Mallorca; Characteristics of the high-frequency depositional sequences in the upper Miocene reef complex of Majorca. *Acta Geologica Hispanica*, **26**, 181-194.

Pomar, L. and **Ward, W.C.** (1994) Response of a late Miocene Mediterranean reef platform to high-frequency eustasy. *Geology*, **22**, 131-134.

Pomar, L. and **Ward, W.C.** (1995). Sea-level Changes, Carbonate Production and Platform Architecture: The Llucmajor Platform, Mallorca, Spain. In: *Sequence Stratigraphy and Depositional Response to Eustatic, Tectonic and Climatic Forcing* (Ed. Haq, B.) 87-112. Kluwer Academic Press.

Pomar, L., Ward, W.C., Green, D.G. (1996) Upper Miocene reef complex of the Llucmajor area, Mallorca, Spain. In: *Models for Carbonate Stratigraphy from Miocene Reef Complexes of Mediterranean Regions*. Concepts in Sedimentology and Paleontology Series. *Soc. Econ. Paleont. Miner.*, Tulsa, **5**, 191-225.

Prentice, M.L. and **Matthews R.K.** (1988) Cenozoic ice-volume history: Development of a composite oxygen isotope record. *Geology* **16**, 963-966. Abstr.

Riding, R., Martín, J.M. and **Braga, J.C.** (1991) Coral-stromatolite reef framework, upper Miocene, Almeria, Spain. *Sedimentology*, **38**, 799-818.

Roep, T. B. and **Van Harten, D.**, (1979) Sedimentological and ostracodological observations on Messinian post-evaporite deposits of some southeastern Spanish basins Anonymous. VIIth international congress on Mediterranean Neogene, Annales Geologiques des Pays Helleniques, Tome hors serie, p. 1037-1044. Meeting: VIIth international congress on Mediterranean Neogene, Athens, Greece.

Roessler, J. and **Huessner, H.** (1997) Numerical solution of the 1+2 dimensional Fisher´s equation by Finite Elements and the Galerkin method. *Math. Comput. Modelling*, **3**, 57-67.

Rouchy, J. M., **Orszag-Sperber, F.**, **Blanc-Valleron, M. M.**, **Pierre, C.**, **Riviere, M.**, **Combourieu-Nebout, N.**, and **Panayides, I.** (2001) Paleoenvironmental changes at the Messinian-Pliocene boundary in the eastern Mediterranean (southern Cyprus basins); significance of the Messinian Lago-Mare. *Sed. Geol.*, **145**, 93-117.

Ruegg, G.J.H. (1964) Geologische Onderzoekingen in Het Bekken Van Sorbas, S Spanje. Amsterdam Geological Institute, University of Amsterdam, The Netherlands.

Saint Martin, J. P., and **Cornee, J.J.** (1996) The Messinian reef complex of Melilla, northeastern Rif, Morocco. In: *Models for Carbonate Stratigraphy from Miocene Reef Complexes of Mediterranean Regions*. Concepts in Sedimentology and Paleontology Series. *Soc. Econ. Paleont. Miner.*, Tulsa, **5**, 227-237.

Saint Martin, J. P., Cornee, J. J., Muller, J., Camoin, G., Andre, J. P., Rouchy, J. M., and **Benmoussa, A.** (1991) Global versus regional controls during the development of a Messinian carbonate platform (Melilla Basin, Morocco); sequence stratigraphy and tectonics. *CR Somm. Soc. Géol. Fr.*, **312** , 1573-1579.

Serrano, F. (1979) *Los foraminíferos planctónicos del Mioceno superior de la cuenca de Ronda y su comparación con los de otras áreas de las Cordilleras Béticas*. PhD thesis, University of Malaga, Spain.

Serrano, F. (1990) El Mioceno Medio en el área de Níjar (Almería, España). Rev. Soc. Geol. España, **3**, 65-77.

Shackleton, N.J. and **Crowhurst, S.** (1997) Sediment fluxes based on an orbitally tuned time scale 5 Ma to 14 Ma, Site 926. In *Proceedings of the Ocean Drilling Program, Scientific Results* (Eds. Shackleton, N.J., Curry, W.B., Richter, C., et al.), **154**, 69-82.

Shackleton, N.J. and **Hall, M.A.** (1997) The late Miocene stable isotope record, Site 926. In *Proceedings of the Ocean Drilling Program, Scientific Results* (Eds. Shackleton, N.J., Curry, W.B., Richter, C., et al.), **154**, 367-373.

Shackleton, N.J. and **Kennett, J.P.** (1975) Paleotemperature history of the Cenozoic and the initiation of Antarctic glaciation; oxygen and carbon isotope analyses in DSDP sites 277, 279, and 281. *Initial Rep. Deep Sea*, **29**, 743-755.

Siciliano, D., Potts, D.C. and **Maragos, J.E.** (2002) Modeling reef accretion at Kure atoll, Northwestern Hawaiian Island, using remote sensing techniques and field measurements. *ASLO-AGU Ocean Sciences Meeting*. Honolulu. 11-15 February.

Sierro, F. J., Hilgen, F. J., Krijgsman, W. and **Flores, J. A.** (2001) The Abad composite (SE Spain); a Messinian reference section for the Mediterranean and the APTS. *Palaeogeogr. Palaeoclimatol. Palaeoecol*, **168** (1-2), p. 141-169

Sierro, F.J., Flores, J.A., Civis, J., Gonzalez Delgado, J.A. and **Frances, G.** (1993) Late Miocene globorotaliid event-stratigraphy and biogeography in the NE-Atlantic and Mediterranean. *Mar. Micropaleontol.*, **21**, 143-168.

Sierro, F.J., Flores, J.A., Zamarreno, I., Vazquez, A., Utrilla, R., Frances, G., Hilgen, F.J. and **Krijgsman, W.** (1999) Messinian pre-evaporite sapropels and precession-induced oscillations in western Mediterranean climate. *Mar. Geol.*, **153** (1-4), 137-146.

Spezzaferri, S., Mckenzie, J.A. and **Isern, A.** (2002) Linking the oxygen isotope record of late Neogene eustasy to sequence stratigraphic patterns along the Bahamas margin; results from a paleoceanographic study of ODP Leg 166, Site 1006 sediments. *Mar. Geol.*, **185**, 95-120.

Torrence, C. and **Compo G.P.** (1998) A practical guide to wavelet analysis. *Bull. Amer. Met. Soc.*, **79**, 61-78.

Troelstra, S.R., Van De Poel, H.M., Huisman, C.H.A., Geerlings, L.P.A. and **Dronkert, H**. (1980) Paleoecological changes in the lastest Miocene of the Sorbas Basin, SE Spain. *Géol. Méditerranée* **7**, 115-126.

Van de Poel, H.M. (1991) Messinian stratigraphy of the Níjar Basin (S.E. Spain) and the origin of its gypsum-ghost limestones. *Geol. Mijnb*. **70**, 215-234.

Van der Laan, E., Hilgen, F.J., Lourens, L.J., and **Gaboardi, S.** (2005) Regional climate and glacial control on high-resolution oxygen records from Ain el Beida (latest Miocene, NW Morocco): A cyclostratigraphic analysis in the depth and time domain. *Paleoceanography*, **20**, PA1001.

Vidal, L., Bickert, T., Wefer, G. and **Roehl, U.** (2002) Late Miocene stable isotope stratigraphy of SE Atlantic ODP Site 1085; relation to Messinian events. *Mar. Geol.*, **180**, 71-85.

Völk H. R. (1967) *Zur Geologie und Stratigraphie des Neogenbeckens von Vera, Südost-Spanien*. PhD Thesis. Municipal University of Amsterdam.

Völk, H.R. and **Rondeel, H.E.** (1964) Zur gliederung des Jungtertiärs im Becken von Vera, Südost Spanien. *Geol. Mijnb.* **43**, 310-315.

Warrlich, G.M.D., Waltham, D.A. and **Bosence, D.W.J.** (2002) Quantifying the sequence stratigraphy and drowning mechanisms of atolls using a new 3-D forward stratigraphic modelling program (CARBONATE 3D). In: *Numerical and physical experimental stratigraphy* (Eds. Burgess, P.M., Paola, C.). *Basin Research*, **14**, 379-400.

Warrlich, G., Bosence, D., and **Waltham, D.** (2005) 3D and 4D controls on carbonate depositional systems: sedimentological and sequence stratigraphic analysis of an attached carbonate platform and atoll (Miocene, Níjar Basin, SE Spain). *Sedimentology*, **52**, 363-389.

Whitaker, F.W., Smart, P., Hague, Y., Waltham, D. and **Bosence, D.** (1997) Coupled two-dimensional diagenetic and sedimentological modeling of carbonate platform evolution. *Geology*, **25**, 175-178.

Whitaker, F., Smart, P., Hague, Y., Waltham, D. and **Bosence, D.** (1999) Structure and function of a coupled two-dimensional diagenetic and sedimentological model of carbonate platform evolution. In: *Numerical experiments in stratigraphy; recent advances in stratigraphic and sedimentologic computer simulations*. *SEPM Spec. Publ.*, **62**, 337-355. Tulsa, Oklahoma, USA.

Williams, T., Kroon, D., and **Spezzaferri, S.** (2002) Middle and Upper Miocene cyclostratigraphy of downhole logs and short- to long-term astronomical cycles in carbonate production of the Great Bahama Bank. *Mar. Geol.*, **185**, 75-93.

Zeck, H.P. (1970) An erupted migmatite from Cerro del Hoyazo, SE Spain. *Contrib. Mineral. Petrol.*, **26**, 225-246.

Zeck, H.P. and **Williams, I.S.** (2002) Inherited and magmatic zircon from Neogene Hoyazo cordierite dacite, SE Spain - anatectic source rock provenance and magmatic evolution. *J. Petrol.*, **43**, 1089-1104.

Appendix 1: Parameter files

Explanation of the parameters used in the parameter files

Main Modelling Parameters	Definition
1	Coral growth rate used in the Fisher-eq.
2	Light extinction coeff. according to Bosscher/Schlager.
3	Light intensity ratio according to Bosscher/Schlager.
4	Diffusion coeff. for the coral used in the Fisher-eq.
5	Thickness of the living layer in the reef crest
15	N° of debris BBF particles
16	Grain size of BBF particles
17	Slip factor for BBF particles
19	N° of debris MSCF particles
20	Grain size of MSCF particles
21	Slip factor for MSCF particles
31	Max. pelagic rain per time step
32	Change coeff. for the hyperbolic tangent of the pelagic rain
33	Depth of the inflection point of the hyperbolic tangent profile
35	Growth strength of reef in Lagoon
36	Diffusion strength of reef in Lagoon
38	Same that 35 for BBF
39	Same that 36 for BBF
72	Erosion rate per time step
73	Factor for reef growth coeff. on salien fore-reef points
74	Depth of reef growth during initial conditions
81	Depth up to which reef can be abraded by wave action
82	Same that 81 for lagoon
83	Depth up to which the zoning routine divides into lagoon, reef crest and fore reef
85	Parameter controlling river input in the basin

The other parameters are used to control the error margin of the program and the tolerance for different factors. From the parameter 117, eventually storm event affecting the basin could be supplied.

Note: the numerical values for distance or depth are always expressed in km.

PARAMETER FILE USED FOR THE MODELING OF THE CARIATIZ CARBONATE PLATFORM

noecfil
nogrfil
repro28.r469
noutfiltg
cnew2.dat
sea17.dat
nosubfil

600.	1)	growth coeff. reef (rkk_1)
160.	2)	light extinction coeff. reef (rl_1)
2.6	3)	light int.rat. reef (rli_1);(small:near/large:below light ext.prf.)
2.5	4)	diffusion coeff. reef (dxx_1)
0.45e-3	5)	strength of biologic active reef layer (v_lim_1)
2.e-1	6)	
0.	7)	growth coeff. inv.wedge (rkk_2)
0.	8)	light extinction coeff. inv.wedge (rl_2)
10.	9)	light int.rat. inv.wedge (rli_2);(small:near/large:below light ext.prf.)
.02	10)	diffusion coeff. reef inv.wedge (dxx_2)
8.e-3	11)	strength of biologic active wedge layer (v_lim_2)
40.	12)	initial time step for lagoon growth (lagstart)
12345.	13)	random seed no for reef crest PS (idum3)
.0	14)	
3000.	15)	reef debris iterations brecc (iitrc_1)
3.82e-4	16)	reef debris load brecc (redist00_1)
.30	17)	reef debris slip factor brecc (slf0_1)
.0	18)	
6600.	19)	reef debris iterations calc (iitrc_2)
6.1e-6	20)	reef debris load calc (redist00_2)
220.	21)	reef debris slip factor calc (slf0_2)
.0	22)	
0.	23)	reef debris iterations cong (iitrc_3)
1.e-3	24)	reef debris load cong (redist00_3)
5.	25)	reef debris slip factor cong (slf0_3)
0.	26)	
0.	27)	IVW debris iterations (iitrc_4)
1.e-3	28)	IVW debris load (redist00_4)
0.	29)	IVW debris slip factor (slf0_4)
.0	30)	
.27e-4	31)	max. pelagic rain (p00)
83.	32)	change rate tanh pelagic rain (p11)
.09	33)	inflection point tanh pelagic rain (tnhi)
.0	34)	
1.08	35)	reef growth factor in lagoon (rgfl)
1.03	36)	reef diffusion factor in lagoon (rdfl)
2.e-1	37)	
1.2	38)	reef growth factor in brecc (rgfb)
1.2	39)	reef diffusion factor in brecc (rdfb)
2.	40)	
0.7	41)	reef growth factor in calc (rgfc)
0.7	42)	reef diffusion factor in calc (rdfc)
2.	43)	
1.	44)	reef growth factor in cong (rgfg)
1.	45)	reef diffusion factor in cong (rdfg)
2.e-1	46)	
0.	47)	reef growth factor in IVW (rgfw)
0.	48)	reef diffusion factor in IVW (rdfw)
.0	49)	
0.	50)	reef growth factor in pelag (rgfp)
0.	51)	reef diffusion factor in pelag (rdfp)
2.	52)	
.0	53)	
.0	54)	IVW growth factor in lagoon (wgfl)
.0	55)	IVW diffusion factor in lagoon (wdfl)

```
.0          56)
1.          57)  IVW growth factor in brecc (wgfb)
1.          58)  IVW diffusion factor in brecc (wdfb)
.0          59)
1.          60)  IVW growth factor in calc (wgfc)
1.          61)  IVW diffusion factor in calc (wdfc)
.0          62)
1.          63)  IVW growth factor in cong (wgfg)
1.          64)  IVW diffusion factor in cong (wdfg)
.0          65)
1.          66)  IVW growth factor in reef (wgfr)
1.          67)  IVW diffusion factor in reef (wdfr)
.0          68)
1.          69)  IVW growth factor in pelag (wgfp)
1.          70)  IVW diffusion factor in pelag (wdfp)
.0          71)
.125e-3     72)  er_fct(1) erosion rate per step
12.3        73)  er_fct(2) salient node factor
.0035       74)  er_fct(3) IC depth
.067        75)  er_fct(4) IC factor
1.          76)  er_fct(5) distribution factor: near 0 => uniform / larger => towards grad.
1.          77)
0.          78)
1.          79)  change rate for ec-parameter (ec_cr)
.2          80)  threshold value for ec-parameter (ec_tw)
.009        81)  depth of reef action zone (raz)
.003        82)  depth of hydrodyn. action zone  (haz)
.009        83)  zoning threshold depth (ztd)
.0          84)
.110e3      85)  river sed. iterations (iit)
.70         86)  river redistribution unit (redistv0)
2.5         87)  river slip factor (slfv0)
48.         88)  river inv. dispersion factor: near 0 => uniform / larger => towards grad. (wgt_rv)
.185        89)  row/vert.fraction of river source (prs)
.465        90)  col/hor. fraction of river source (prc)
.0          91)  the following 4 are calculation precision parameters for reef growth eq.
1.e-5       92)  init. relative error tolerance for RKF45_1 (relerr_1)
1.e-5       93)  init. absolute error tolerance for RKF45_1 (abserr_1)
1.e-3       94)  max. relative error tolerance for RKF45_1 (relmx_1)
1.e-3       95)  max. absolute error tolerance for RKF45_1 (absmx_1)
.0          96
.0          97
.0          98
.0          99
.0         100  !!!!!     do not reset parameters with XXX prefix    !!!!!
0.         101) XXX switch random (0.) <-> coords.(1.) IC input (icrc)
4.         102) XXX no. of ICs (max.=25 for coord. input)  (nric)
2345.           103) random generator seed no. for reef debris (idum0)
5.e-5           104) XXX max. IC value for random setting  (vp)
5.e-5           105) XXX max. IC value for random reseeding (vpres)
1.         106) XXX fraction of newly flooded nodes to be reseeded (fres)
0.         107
1.         108) XXX output interpol.(ioint): =0.=> 'x-dir.' ; =1.=> 'hexagon'
1.         109) XXX output format (iofmt): =0.=> binary ; =1.=> formatted
-627.5     110) init. time (tin)
400.       111) no. of steps  (nots)
-607.3     112) final time  (tmax)
1.         113) XXX s.lev.&subs. interp.(methint): 0.=>spline ; 1.=>akima
0.         114
0.         115
0.         116
10.        117) XXX no. of storm events (max.10) (nev)
0.         118
```

0. 119 !!! do not reset rest of parameters !!!
4. 120) 1.) time step w. storm (dto. following entries) (jst(1))
0.9 121) remaining fraction (dto. following entries) (srd(1))
0. 122
22. 117) 2.) time step
0.95 118) remaining fraction
0. 119
30. 120) 3.) time step
0.9 121) remaining fraction
0. 122
22. 123) 4.) time step
0.95 124) remaining fraction
0. 125
26. 126) 5.) time step
0.9 127) remaining fraction
0. 128
3. 129) 6.) time step
0.9 130) remaining fraction
0. 131
7. 132) 7.) time step
0.3 133) remaining fraction
0. 134
90. 135) 8.) time step
0.7 136) remaining fraction
0. 137
22. 138) 9.) time step
0.95 139) remaining fraction
0. 140
36. 141) 10.) time step
0.7 142) remaining fraction
0. 143
0. 144
0.1 145) 1. x.coord. (xcd(1))
0.88 146) y.coord. (ycd(1))
0.005 147) IC (v_1)
0. 148
0.2 149) 2. x.coord.
0.87 150) y.coord.
0.005 151) IC
0. 152
0.3 153) 3. x.coord.
0.89 154) y.coord.
0.005 155) IC
0. 156
0.4 157) 4. x.coord.
0.88 158) y.coord.
0.005 159) IC
0. 160
0.5 161) 5. x.coord.
0.87 162) y.coord.
0.005 163) IC
0. 164
0.6 165) 6. x.coord.
0.89 166) y.coord.
0.0 167) IC
0. 168
0.7 169) 7. x.coord.
0.88 170) y.coord.
0.005 171) IC
0. 172
0.8 173) 8. x.coord.
0.89 174) y.coord.
0.005 175) IC

0. 176
0.9 177) 9. x.coord.
0.87 178) y.coord.
0.005 179) IC
0. 180
0.15 181) 10.x.coord.
0.88 182) y.coord.
0.005 183) IC
0. 184
0.25 185) 11.x.coord.
0.89 186) y.coord.
0.005 187) IC
0. 188
0.35 189) 12.x.coord.
0.88 190) y.coord.
0.005 191) IC
0. 192
0.45 193) 13.x.coord.
0.87 194) y.coord.
0.005 195) IC
0. 196
0.55 197) 14.x.coord.
0.87 198) y.coord.
0.005 199) IC
0. 200
0.65 201) 15.x.coord.
0.88 202) y.coord.
0.005 203) IC
0. 204
0.75 205) 16.x.coord.
0.87 206) y.coord.
0.005 207) IC
0. 208
0.85 209) 17.x.coord.
0.88 210) y.coord.
0.005 211) IC
0. 212
0.95 213) 18.x.coord.
0.89 214) y.coord.
0.005 215) IC
0. 216
0.1 217) 19.x.coord.
0.88 218) y.coord.
0.005 219) IC
0. 220
0.23 221) 20.x.coord.
0.89 222) y.coord.
0.005 223) IC
0. 224
0.37 225) 21.x.coord.
0.87 226) y.coord.
0.005 227) IC
0. 228
0.44 229) 22.x.coord.
0.88 230) y.coord.
0.005 231)IC
0. 232
0.53 233) 23.x.coord.
0.87 234) y.coord.
0.005 235) IC
0. 236
0.66 237) 24.x.coord.
0.88 238) y.coord.

0.005 239) IC
0. 240
0.77 241) 25.x.coord.
0.88 242) y.coord.
0.007 243) IC
0. 244
.0 245
.0 246
.0 247
.0 248
.0 249
.0 250
==========
Comments:

PARAMETER FILE USED FOR THE MODELING OF THE NIJAR CARBONATE PLATFORM
noecfil
nogrfil
repro29.r247
noutfiltg
nisur25.dat
sea18.dat
nosubfil

500.	1)	growth coeff. reef (rkk_1)
130.	2)	light extinction coeff. reef (rl_1)
4.5	3)	light int.rat. reef (rli_1);(small:near/large:below light ext.prf.)
3.15	4)	diffusion coeff. reef (dxx_1)
5.5e-4	5)	strength of biologic active reef layer (v_lim_1)
2.e-1	6)	
0.	7)	growth coeff. inv.wedge (rkk_2)
0.	8)	light extinction coeff. inv.wedge (rl_2)
10.	9)	light int.rat. inv.wedge (rli_2);(small:near/large:below light ext.prf.)
.02	10)	diffusion coeff. reef inv.wedge (dxx_2)
8.e-3	11)	strength of biologic active wedge layer (v_lim_2)
198.	12)	initial time step for lagoon growth (lagstart)
12345.	13)	random seed no for reef crest PS
.0	14)	
4520.	15)	reef debris iterations brecc (iitrc_1)
3.82e-4	16)	reef debris load brecc (redist00_1)
.285	17)	reef debris slip factor brecc (slf0_1)
.0	18)	
6750.	19)	reef debris iterations calc (iitrc_2)
6.1e-6	20)	reef debris load calc (redist00_2)
900.	21)	reef debris slip factor calc (slf0_2)
.0	22)	
0.	23)	reef debris iterations cong (iitrc_3)
1.e-3	24)	reef debris load cong (redist00_3)
5.	25)	reef debris slip factor cong (slf0_3)
0.	26)	
0.	27)	IVW debris iterations (iitrc_4)
1.e-3	28)	IVW debris load (redist00_4)
0.	29)	IVW debris slip factor (slf0_4)
.0	30)	
.46e-4	31)	max. pelagic rain (p00)
89.	32)	change rate tanh pelagic rain (p11)
.085	33)	inflection point tanh pelagic rain (tnhi)
.0	34)	
2.68	35)	reef growth factor in lagoon (rgfl)
2.63	36)	reef diffusion factor in lagoon (rdfl)
2.e-1	37)	
1.2	38)	reef growth factor in brecc (rgfb)
1.2	39)	reef diffusion factor in brecc (rdfb)
2.	40)	
0.7	41)	reef growth factor in calc (rgfc)
0.7	42)	reef diffusion factor in calc (rdfc)
2.	43)	
1.	44)	reef growth factor in cong (rgfg)
1.	45)	reef diffusion factor in cong (rdfg)
2.e-1	46)	
0.	47)	reef growth factor in IVW (rgfw)
0.	48)	reef diffusion factor in IVW (rdfw)
.0	49)	
0.	50)	reef growth factor in pelag (rgfp)
0.	51)	reef diffusion factor in pelag (rdfp)
2.	52)	
.0	53)	
.0	54)	IVW growth factor in lagoon (wgfl)
.0	55)	IVW diffusion factor in lagoon (wdfl)

```
.0          56)
1.          57)  IVW growth factor in brecc (wgfb)
1.          58)  IVW diffusion factor in brecc (wdfb)
.0          59)
1.          60)  IVW growth factor in calc (wgfc)
1.          61)  IVW diffusion factor in calc (wdfc)
.0          62)
1.          63)  IVW growth factor in cong (wgfg)
1.          64)  IVW diffusion factor in cong (wdfg)
.0          65)
1.          66)  IVW growth factor in reef (wgfr)
1.          67)  IVW diffusion factor in reef (wdfr)
.0          68)
1.          69)  IVW growth factor in pelag (wgfp)
1.          70)  IVW diffusion factor in pelag (wdfp)
.0          71)
1.255e-4    72)  er_fct(1) erosion rate per step
11.8        73)  er_fct(2) salient node factor
.004        74)  er_fct(3) IC depth
.068        75)  er_fct(4) IC factor
1.          76)  er_fct(5) distribution factor: near 0 => uniform / larger => towards grad.
1.          77)
0.          78)
1.          79)  change rate for ec-parameter (ec_cr)
.2          80)  threshold value for ec-parameter (ec_tw)
.007        81)  depth of reef action zone (raz)
.003        82)  depth of hydrodyn. action zone  (haz)
.0067       83)  zoning threshold depth (ztd)
.0          84)
.0          85)  river sed. iterations (iit)
.0          86)  river redistribution unit (redistv0)
0.          87)  river slip factor (slfv0)
0.          88)  river inv. dispersion factor: near 0 => uniform / larger => towards grad. (wgt_rv)
.0          89)  row/vert.fraction of river source (prs)
.0          90)  col/hor. fraction of river source (prc)
.0          91)  the following 4 are calculation precision parameters for reef growth eq.
1.e-5       92)  init. relative error tolerance for RKF45_1 (relerr_1)
1.e-5       93)  init. absolute error tolerance for RKF45_1 (abserr_1)
1.e-3       94)  max. relative error tolerance for RKF45_1 (relmx_1)
1.e-3       95)  max. absolute error tolerance for RKF45_1 (absmx_1)
.0          96
.0          97
.0          98
.0          99
.0         100  !!!!!     do not reset parameters with XXX prefix    !!!!!
0.         101) XXX switch random (0.) <-> coords.(1.) IC input (icrc)
4.         102) XXX no. of ICs (max.=25 for coord. input)  (nric)
2345.           103) random generator seed no. for reef debris (idum0)
5.e-5           104) XXX max. IC value for random setting  (vp)
5.e-5           105) XXX max. IC value for random reseeding (vpres)
1.         106) XXX fraction of newly flooded nodes to be reseeded (fres)
0.         107
1.         108) XXX output interpol.(ioint): =0.=> 'x-dir.' ; =1.=> 'hexagon'
1.         109) XXX output format (iofmt): =0.=> binary ; =1.=> formatted
-619.79    110) init. time (tin)
200.       111) no. of steps  (nots)
-609.53    112) final time  (tmax)
1.         113) XXX s.lev.&subs. interp.(methint): 0.=>spline ; 1.=>akima
0.         114
0.         115
0.         116
10.        117) XXX no. of storm events (max.10) (nev)
0.         118
```

0. 119 !!! do not reset rest of parameters !!!
4. 120) 1.) time step w. storm (dto. following entries) (jst(1))
0.9 121) remaining fraction (dto. following entries) (srd(1))
0. 122
22. 117) 2.) time step
0.95 118) remaining fraction
0. 119
30. 120) 3.) time step
0.9 121) remaining fraction
0. 122
22. 123) 4.) time step
0.95 124) remaining fraction
0. 125
26. 126) 5.) time step
0.9 127) remaining fraction
0. 128
3. 129) 6.) time step
0.9 130) remaining fraction
0. 131
7. 132) 7.) time step
0.3 133) remaining fraction
0. 134
90. 135) 8.) time step
0.7 136) remaining fraction
0. 137
22. 138) 9.) time step
0.95 139) remaining fraction
0. 140
36. 141) 10.) time step
0.7 142) remaining fraction
0. 143
0. 144
0.1 145) 1. x.coord. (xcd(1))
0.88 146) y.coord. (ycd(1))
0.005 147) IC (v_1)
0. 148
0.2 149) 2. x.coord.
0.87 150) y.coord.
0.005 151) IC
0. 152
0.3 153) 3. x.coord.
0.89 154) y.coord.
0.005 155) IC
0. 156
0.4 157) 4. x.coord.
0.88 158) y.coord.
0.005 159) IC
0. 160
0.5 161) 5. x.coord.
0.87 162) y.coord.
0.005 163) IC
0. 164
0.6 165) 6. x.coord.
0.89 166) y.coord.
0.0 167) IC
0. 168
0.7 169) 7. x.coord.
0.88 170) y.coord.
0.005 171) IC
0. 172
0.8 173) 8. x.coord.
0.89 174) y.coord.
0.005 175) IC

0. 176
0.9 177) 9. x.coord.
0.87 178) y.coord.
0.005 179) IC
0. 180
0.15 181) 10.x.coord.
0.88 182) y.coord.
0.005 183) IC
0. 184
0.25 185) 11.x.coord.
0.89 186) y.coord.
0.005 187) IC
0. 188
0.35 189) 12.x.coord.
0.88 190) y.coord.
0.005 191) IC
0. 192
0.45 193) 13.x.coord.
0.87 194) y.coord.
0.005 195) IC
0. 196
0.55 197) 14.x.coord.
0.87 198) y.coord.
0.005 199) IC
0. 200
0.65 201) 15.x.coord.
0.88 202) y.coord.
0.005 203) IC
0. 204
0.75 205) 16.x.coord.
0.87 206) y.coord.
0.005 207) IC
0. 208
0.85 209) 17.x.coord.
0.88 210) y.coord.
0.005 211) IC
0. 212
0.95 213) 18.x.coord.
0.89 214) y.coord.
0.005 215) IC
0. 216
0.1 217) 19.x.coord.
0.88 218) y.coord.
0.005 219) IC
0. 220
0.23 221) 20.x.coord.
0.89 222) y.coord.
0.005 223) IC
0. 224
0.37 225) 21.x.coord.
0.87 226) y.coord.
0.005 227) IC
0. 228
0.44 229) 22.x.coord.
0.88 230) y.coord.
0.005 231)IC
0. 232
0.53 233) 23.x.coord.
0.87 234) y.coord.
0.005 235) IC
0. 236
0.66 237) 24.x.coord.
0.88 238) y.coord.

0.005 239) IC
0. 240
0.77 241) 25.x.coord.
0.88 242) y.coord.
0.007 243) IC
0. 244
.0 245
.0 246
.0 247
.0 248
.0 249
.0 250
==========
Comments: